Stochastic Models of Atom-Photon Dynamics with Applications to Cooling Quantum Gases

by

Josh W. Dunn

B.A., University of Colorado, Boulder, 2002

A thesis submitted to the

Faculty of the Graduate School of the

University of Colorado in partial fulfillment

of the requirements for the degree of

Doctor of Philosophy

Department of Physics

2007

This thesis entitled:
Stochastic Models of Atom-Photon Dynamics with Applications to Cooling Quantum Gases
written by Josh W. Dunn
has been approved for the Department of Physics

Chris H. Greene

John L. Bohn

Date

The final copy of this thesis has been examined by the signatories, and we find that both the content and the form meet acceptable presentation standards of scholarly work in the above mentioned discipline.

Dunn, Josh W. (Ph.D., Physics)

Stochastic Models of Atom-Photon Dynamics with Applications to Cooling Quantum Gases

Thesis directed by Professor Chris H. Greene

Through the years, stochastic physics has provided important insight into natural phenomena that possess an inherently random nature. From its foundations in the study of Brownian motion up through its myriad present applications, a stochastic description of nature has yielded an elegant theoretical understanding, as well as providing practical and efficient simulation techniques. One particularly important application is to the field of quantum optics, in which the interaction of light and matter is treated in a fundamentally quantum-mechanical manner. The work presented here utilizes the methods of stochastic physics to understand a variety of quantum-optical phenomena involving the dynamics of atoms interacting with photons. A solid theoretical understanding of such phenomena is often necessary to describe laser cooling of atoms, and many such applications are discussed here. A detailed model of atoms with complex internal structure interacting with three-dimensional laser fields is presented, as well as the rich dynamics of three-level atoms interacting with two lasers. Applications to cavity cooling of atoms and molecules are discussed, and a method for describing non-Markovian dynamics using relaxation techniques is presented. A novel cooling scheme utilizing Feshbach resonances in the scattering of two atoms is also treated.

Acknowledgements

I would like to thank Chris Greene for his many years of guidance and support during my graduate career. His passion for physics is contagious and it inspires those who interact with him strive for a deeper understanding of nature. His curiosity extends over a very broad range, and he is often willing to tackle projects outside of his main expertise in order to expand his understanding of physics. I appreciate his willingness to allow me to pursue a study of quantum optics and stochastic physics even given his limited experience in these fields. I believe that our collaboration has been very fruitful. Combining my day-to-day learning about quantum optics with Chris's comprehensive understanding of traditional atomic physics has allowed us to develop models of atom-photon dynamics with unprecedented attention to an accurate treatment of atomic internal degrees of freedom. Our collaboration has often led to the realization of parallels between quantum-optical concepts and the many theories developed by Fano, which Chris knows so well. For me, this conceptual bridge has been very useful, illuminating tough subjects and often revealing an elaborate and scattered collection of methodologies to be unified under a simple physical picture. I am proud to be a part of this scientific lineage.

I am grateful to the many physicists at JILA who helped me during my time here. Jun Ye has been kind enough to provide me with many opportunities to put theory to use in describing various aspects of his vast array of cold-atom and cold-molecule experiments. Over the years, Jinx Cooper has been a helpful and reliable fountain of

physics knowledge. He was always willing to utilize his lifetime of experience to help me understand the tricky and subtle aspects of quantum optics. Robin Santra, during his time as a post doc in Chris's group, was patient and willing to answer my many questions involving atomic structure.

I would also like to thank various other collaborators that made my work possible. Jan Thomsen from Denmark and Flavio Cruz from Brazil provided the experimental background and the impetus for our joint project that led to a better understanding of multilevel atomic dynamics as well as a cooling scheme that they are currently implementing. Ben Lev's strong knowledge of cavity QED led to many interesting discussions between us about the dynamics of atoms and molecules in an optical cavity.

Finally, I would like to thank the National Science Foundation for funding my research as a graduate student.

Contents

Chapter

Tables

Table

Figures

Figure

Chapter 1

Introduction

The beginnings of the stochastic description of nature can be traced back to Einstein's 1905 work [4] concerning the observation of Brownian motion, in which small particles immersed in water follow erratic, seemingly random trajectories. Einstein's analysis, performed concurrently and independently by Smoluchowski [5], seems quite simple, yet it contains many of the elements of modern stochastic physics such as an idea later called the Markov approximation and a precursor to the Fokker-Planck equation [6]. Einstein's idea, that a physical theory could contain aspects that are random at a fundamental level, was revolutionary at the time, going beyond the traditional deterministic equations with which physicists had been primarily concerned prior to that. His equations employed diffusion physics, the nature of which could be determined by the microscopic interaction properties of the observed particle with atoms in the liquid. Inspired by Einstein's theory, Langevin [7] later developed an equivalent theory which, instead of a diffusion term, utilized the idea of a random fluctuating force. Langevin was able to work out the basic properties of such forces, and equations of this type bear his name today. Through the years, many physicists have built on these foundations to describe a large spectrum of stochastic problems. The work presented in this thesis continues humbly along these lines, modeling various physical phenomena using stochastic equations of motion and hopefully adding useful knowledge to the canon.

Quantum optics, another venerable branch of physics, explores the quantum-

mechanical nature of the interaction of light and matter. This encompasses a diverse and rich set of phenomena, from the nature of spontaneous emission to the scattering of intense, coherent electromagnetic waves provided by a laser to the use of an optical cavity to modify the properties of the photon vacuum as observed by an atom. The field of quantum optics contains its own set of unique concepts, techniques, and tools. Quantum opticians like to reduce the complex internal structure of an atom down to a simple two-level system whenever possible. This system can be mapped onto a spin-1/2 system for which powerful conceptual tools like the Bloch sphere can be employed. Laser interactions with the system can then be thought of as rotating a vector in a certain way around the Bloch sphere. Quantum optics also often intersects with the field of stochastic physics. Most of the work in this thesis involves light-matter interactions and thus can be classified under the heading of quantum optics.

Contained in the example of Brownian motion are the elements of the theory of system-reservoir interactions [8]. The particle's erratic motion in the liquid can be qualitatively separated into two unique influences. Over a long time scale, one type of force acts to gradually change the course of the particle's motion. On a much shorter time scale, another type of force induces the sharp motions that give the trajectory its random appearance. Treating the particle's interaction with individual atoms in the liquid as interaction with a reservoir, a detailed equation of motion can be written down. Formal solutions of this equation can be manipulated by viewing progression of time to be in discrete steps of length greater than the short time scale but shorter than the longer time scale, a procedure known as coarse-graining. In this manner, the effects of the frequently occurring collisions with atoms in the liquid can be wrapped up into an average effect. Such an equation, termed a master equation, is useful because it removes the difficulty of explicitly treating the overwhelmingly large number of microscopic processes that contribute to the particle's overall motion.

Generally speaking, a master equation is obtained from the differential Chapman-

Kolmogorov equation by setting the drift and diffusion terms to zero. The master equation describes evolution of the probability density with stochastic jumps that can occur at random intervals, in addition to any deterministic evolution. In the context of quantum optics, the master equation is useful for describing a system of one or more atoms, perhaps coupled to a laser, interacting with the ever-present vacuum photon reservoir. The system undergoes a deterministic evolution due to its own internal interactions, as well as a stochastic evolution manifested by jumps that occur due to interactions with the vacuum photon field. The quantum-optical master equation is useful because its solutions yield the density operator (often called, less generally, the density matrix) for the system at any time. The density operator can then be used to obtain average system properties by taking its product with quantum-mechanical operators and tracing over the system degrees of freedom. In this thesis, quantum-optical systems are almost exclusively modeled using master equations, as in Chapters 3 through 6.

Another aspect of the utility of the quantum-optical master equation is its amenability to stochastic Monte Carlo techniques [9, 10, 11, 12, 13, 14, 15]. The system-reservoir-interaction portion of the master equation can be unraveled and interpreted as a sum over an infinite number of individual trajectories for wave functions rather than density matrices. These trajectories each execute a random walk in phase space with randomly spaced jumps occurring due to the interaction with vacuum photon states. Besides offering an elegant fundamental interpretation of system-reservoir interactions, this unraveling can be put to use as a simulation technique. A set of wave functions can be independently propagated with jump processes occurring according to a numerical pseudo-random number generator. Although the exact master-equation evolution is only obtained in the limit of an infinite number of such trajectories, a rather small number of trajectories can provide a very good approximation of the dynamics. Moreover, the error involved in using a finite number instead of an infinite number of trajectories is implicitly determined by the technique. For systems with a large number of degrees

of freedom N, the propagation of wave functions of size N rather than a density matrix of size N^2 offers extensive numerical advantages, both in terms of computational speed and storage. This actually understates the problem, since the master equation for a density operator cannot be phrased as a linear $N \times N$ matrix equation. Only by going to a space of $N^2 \times N^2$ can the problem be expressed in a form for which a numerical linear matrix solver can be used. In this thesis, stochastic-trajectory techniques are utilized in Chapters 3 and 5. This subject is formalized by the concept of Liouville space, which is discussed in detail in Chapters 3 and 4, as well as Appendix A.

A good theoretical understanding of cooling processes is of practical use as well as being fundamentally intriguing. Cooling is basically a means of decreasing a system's footprint in phase space, and as such, it makes use of many ideas in thermodynamic theory. Ideas for cooling schemes are continually surfacing, and it can be an enlightening exercise to test them against the rigors of the second law of thermodynamics. Once such idea is presented here in Chapter 2. From a practical standpoint, cooling is tremendously important in the today's field of atomic, molecular, and optical physics. The variety of quantum phenomena observed and employed in current experiments is made possible primarily when the system, often a gas of atoms, is cooled to very low temperatures. Such temperature regimes reduce the noise associated with higher temperature systems, as in experiments involving atomic clocks and precision standards. In addition, they can allow for quantum degeneracy to be obtained, as in the Bose-Einstein condensates and degenerate Fermi gases common to experiments now.

Of all the various cooling methods, one particular type — laser cooling — has been perhaps the most influential. The idea of scattering detuned laser light off an ensemble of atoms to reduce their kinetic energy has contributed in some way to just about every experiment involving cold atoms. A thorough understanding of the physics of laser cooling [16, 17, 18], developed throughout the 1980's and 1990's, paved the way to a Nobel Prize for its major contributors in 1997. Laser cooling comes in a variety of

forms and complexities, and Chapters 3, 4, and 5 discuss the theoretical modeling of a few of these.

The main themes of the work presented here are stochastic quantum mechanics and cooling. Although a physical model that describes a cooling process often involves some sort of stochastic element, this will not be the case in Chapter 2, in which a cooling idea for two trapped interacting atoms is explored. This process will be modeled using deterministic (in the sense that quantum mechanics is deterministic for the wave function) scattering models. Thus, this chapter is connected to the others only by the subject of cooling. At the other end of the spectrum, Chapter 6 discusses the application of relaxation techniques to the field of nonlinear optical spectroscopy for understanding non-Markovian scattering phenomena in recent experiments. This chapter utilizes the stochastic physics developed earlier in the thesis, but the subject has really nothing to do with cooling. Nevertheless, the progression of chapters is intended to offer a somewhat continuous train of thought.

Chapter 2 presents a novel cooling technique that makes use of Feshbach resonances in the scattering of two atoms. A few types of basic scattering models, using one or more channels and different descriptions of the interaction, are first developed. After a brief example of using these models to describe molecular photodissociation, details of the cooling scheme are presented. The scattering models are employed to simulate the workings of the cooling scheme, and the results yield an understanding of how effective the scheme is. The work discussed here was published in Ref. [1].

Chapter 3 develops the master equation for an atom with complicated internal structure interacting with a three-dimensional polarization-gradient laser field. Details of the derivation of the relaxation operator for this system are relegated to Appendix B, and a thorough derivation of the semiclassical optical Bloch equations for the system are presented in Appendix C. The method of stochastic trajectories is presented, and then applied to the system at hand. This yields numerical results for the cooling dynamics

of the fermionic alkaline-earth atoms ^{25}Mg and ^{87}Sr. These results are compared to the cooling behavior of atoms with simpler internal structure. The work presented here has been published in Ref. [2].

The laser cooling of three-level systems using two lasers is presented in Chapter 4. The equations of motion are derived in one dimension for this system, and a sparse-matrix method is used to obtain direct and exact solutions, bypassing the use Monte Carlo techniques for this problem. A rich variety of phenomena is observed, the interpretation of which leads to an understanding of the cooling technique in terms of electromagnetically induced transparency. The dynamical effects of scattering light off atoms with asymmetric Fano lineshapes is discussed, and it is shown that such scattering can lead to lower temperatures than would be expected using a more simplistic analysis with Lorentzian lineshapes. The work presented here has been submitted for publication and a preprint version can be found in Ref. [3].

The master-equation models from the previous chapters are extended to include an optical cavity in Chapter 5, with the goal of calculating cavity-cooling dynamics for molecules. The full master equation is then manipulated to yield a master equation for just the molecule system, coupled to a Langevin equation for the cavity mode. The cavity mode operator is then approximated as a classical field, which will be valid in the limit of large photon numbers in the cavity. The set of coupled equations is then solved to illustrate the effects of cooling on the population distribution, and the validity of the semiclassical approximation is tested.

Lastly, Chapter 6 illustrates a possible idea for modeling non-Markovian dynamics in the interparticle scattering of an atomic gas. A relaxation-type theory of atomic collisions, originally applied to understanding static pressure broadening in gases, is extended for use the framework of nonlinear optical spectroscopy. The use of relaxation theory should provide detailed and accurate scattering information and may lead to a new method for modeling the cutting-edge transient four-wave mixing experiments

being performed today.

Chapter 2

Feshbach-Resonance Cooling

2.1 Introduction

The achievement in 1995 [19, 20] of quantum degeneracy in an atomic gas, known as Bose-Einstein condensation (BEC) for bosonic constituents, was the result of years of development of various cooling techniques. In the end, this feat required not a single cooling method, but a series of methods, each particularly suited to traversing a certain temperature range of the gas. In the first condensate, a relatively hot gas of rubidium atoms was first cooled by basic Doppler laser cooling, after which more sophisticated polarization-gradient laser-cooling schemes produced further cooling, and finally a creative series of evaporative-cooling trajectories did the trick.

Although many well-developed cooling schemes exist and have been successful for a variety of atoms, there is always a desire for new cooling ideas. An atom's internal structure might make laser cooling ineffective, or the details of the interatomic scattering properties of an atom might not yield a favorable ratio of elastic to inelastic collisions, something that evaporative cooling requires. The scheme presented in this chapter is in the spirit of the search for novel cooling techniques that may potentially find success in systems where other techniques have failed. It also tells a somewhat entertaining story about those who attempt to defy the second law of thermodynamics.

For completeness, this chapter begins with a brief summary of the elements of collision theory necessary to understand the following development. The next section

develops the quantum-defect theory of two particles in a harmonic trap, which will be used to model the Feshbach-resonance cooling scheme. This section explores the single-channel as well as the two-channel scattering models, utilizing a zero-range-potential to describe the interparticle interactions. In order to provide more general insight, the following section develops a two-channel square-well-potential version of the two-particle theory. An example of using the previously developed theories for a perturbative treatment of molecular photodissociation is briefly illustrated. Next, the Feshbach-resonance cooling scheme is described, the results of calculations are presented, and the efficacy of the scheme is assessed.

Parts of this chapter are developed from research by this author which has been published in Ref. [1], and some of the text and figures have been adapted from the work therein.

2.2 Collision-theory basics

The purpose of this section is to provide a summary overview of the basic concepts and results of two-particle collision theory. Once introduced, these concepts will be useful in understanding the terminology used in developing the scattering models of various sophistication later in the chapter. The general theory of potential scattering theory is first presented, followed by a treatment of the so-called cold-collision regime, in which a great deal of simplifications can be made for the low-energy collisions which occur in the quantum-gas experiments found in many of today's laboratories.

2.2.1 Potential scattering theory

In understanding the physics of the collision of two particles, it is equivalent and simpler to study the problem of a single particle colliding with a potential $V(\mathbf{r})$. The

time-dependent Schrödinger equation for this situation is

$$\left[-\frac{\hbar^2}{2m}\nabla^2 + V(\mathbf{r})\right]\Psi(\mathbf{r},t) = i\hbar\frac{\partial}{\partial t}\Psi(\mathbf{r},t) \tag{2.1}$$

where m is the mass of the particle, $\hbar$ is a constant related to Planck's constant h by $\hbar = \frac{h}{2\pi}$, and $\Psi(\mathbf{r},t)$ is the wave function representing the particle. For $V(\mathbf{r})$ real and independent of time, an assumption that is typically valid, stationary state wave functions $\psi(\mathbf{r})$ can be found which are solutions to the time-independent Schrödinger equation,

$$\left[-\frac{\hbar^2}{2m}\nabla^2 + V(\mathbf{r})\right]\psi(\mathbf{r}) = E\psi(\mathbf{r}). \tag{2.2}$$

Here, the particle's energy E is defined as

$$E = \frac{p^2}{2m} = \frac{\hbar^2 k^2}{2m}, \tag{2.3}$$

where $\mathbf{k}$ is the wave vector, defined in terms of the particle's momentum $\mathbf{p}$ as

$$\mathbf{k} = \frac{\mathbf{p}}{\hbar}. \tag{2.4}$$

If $V(\mathbf{r})$ goes to zero faster than $1/r$ for large r, then outside of a certain range Eq. (2.2) describes a free particle. In this region, the wave function $\psi_{\mathbf{k}_\mathrm{i}}$ for a given initial wave number $\mathbf{k}_\mathrm{i}$, can be written as the sum of an incoming plane wave and an outgoing scattered spherical wave,

$$\psi_{\mathbf{k}_\mathrm{i}}(\mathbf{r}) \underset{r\to\infty}{\sim} A\left[\mathrm{e}^{i\mathbf{k}_\mathrm{i}\cdot\mathbf{r}} + f(k,\theta,\phi)\frac{\mathrm{e}^{ikr}}{r}\right]. \tag{2.5}$$

where $f(k,\theta,\phi)$, called the scattering amplitude and which is a function of the incoming wave vector k and the spherical coordinates θ and ϕ, describes the amplitude of the outgoing wave as a function of the direction and momentum of the incoming wave. It can be shown that the differential cross-section is related to the scattering amplitude by the expression

$$\frac{d\sigma}{d\Omega} = |f(k,\theta,\phi)|^2, \tag{2.6}$$

with the total cross-section then given by integrating the differential cross section over all solid angles,

$$\sigma_{\text{tot}} = \int \frac{d\sigma}{d\Omega} d\Omega = \int |f(k,\theta,\phi)|^2 \, d\Omega. \tag{2.7}$$

If $V(\mathbf{r})$ is spherically symmetric,

$$V(\mathbf{r}) \to V(r), \tag{2.8}$$

then $\psi_{\mathbf{k_i}}$ can be expanded in a series of products of Legendre polynomials and radial functions,

$$\psi_{\mathbf{k_i}}(k,r,\theta) = \sum_{l=0}^{\infty} R_l(k,r) P_l(\cos\theta), \tag{2.9}$$

where $R_l(k,r)$ is a radial function, independent of angle, and $P_l(\cos\theta)$ is the lth Legendre polynomial. This series is referred to as a partial wave expansion, with each term of the expansion representing an individual partial wave, parameterized by a single value of angular momentum l. It will be useful to redefine the radial functions as

$$u_l(k,r) \equiv r R_l(k,r). \tag{2.10}$$

Then the separated Schrödinger equation for the u_l radial functions, which is called the radial equation, is

$$\left[\frac{d^2}{dr^2} - \frac{l(l+1)}{r^2} - U(\mathbf{r}) + k^2\right] u_l(k,r) = 0, \tag{2.11}$$

where

$$U(\mathbf{r}) = \frac{2\mu}{\hbar^2} V(\mathbf{r}) \tag{2.12}$$

is the rescaled interaction potential. The asymptotic solutions to the radial equation are

$$u_l(k,r) \underset{r\to\infty}{\sim} \frac{A_l(k)}{k} \sin\left[kr - l\pi/2 + \delta_l(k)\right], \tag{2.13}$$

where A_l and δ_l are constants (with respect to r), and δ_l is referred to as the phase shift for the lth partial wave. In the partial-wave formalism, various scattering properties

can be expressed as sums of partial-wave contributions. For example, the scattering amplitude is

$$f(k,\theta) = \frac{1}{2ik}\sum_{l=0}^{\infty}(2l+1)\left\{e^{2i\delta_l(k)}-1\right\}P_l(\cos\theta), \tag{2.14}$$

and the total cross-section is equal to the sum of all partial wave cross-sections,

$$\sigma_{\text{total}}(k) = \sum_{l=0}^{\infty}\sigma_l(k), \tag{2.15}$$

where the partial wave cross-sections are

$$\sigma_l(k) = \frac{4\pi}{k^2}(2l+1)\sin^2\delta_l(k). \tag{2.16}$$

2.2.2 Cold collisions

In the radial equation for $u_l(k,r)$, Eq. (2.11), the l-dependent term can be added to the bare potential $U(r)$ and the two treated as an effective potential,

$$U_{\text{eff}}(r) = U(r) + \frac{l(l+1)}{r^2}. \tag{2.17}$$

The second term, called the centrifugal barrier, will cause the effective potential to increase with increasing values of l. For small collision energies, this centrifugal barrier will become insurmountable for partial waves beyond a certain value of l. For collisions of low enough energy, only the $l = 0$ partial waves will contribute to the scattering; the others will be prevented from colliding. Collisions occurring in this low energy range are termed cold collisions. Since only s-wave ($l = 0$) collisions occur in this regime, the number of partial waves that need to be considered is reduced, and many of the scattering properties simplify. This reduction of the partial-wave series given in Eq. (2.9) to include only the first term is very useful as it can allow scattering properties to often be determined analytically when working in the cold-collisions regime.

If a quantity called the scattering length is defined as the low energy limit of the tangent of the phase shift for an s-wave collision,

$$a = -\lim_{k\to 0}\frac{\tan\delta_0(k)}{k}, \tag{2.18}$$

then the scattering properties reduce to simple expressions involving a. In particular, the scattering amplitude becomes

$$f \underset{k\to 0}{\to} -a, \tag{2.19}$$

the differential cross section becomes

$$\frac{d\sigma}{d\Omega} \underset{k\to 0}{\to} a^2, \tag{2.20}$$

and the total cross section reduces to

$$\sigma_{\text{tot}} \underset{k\to 0}{\to} 4\pi a^2. \tag{2.21}$$

A positive scattering length indicates that the interactions between the particles are repulsive, while a negative scattering length indicates that the interactions are attractive.

2.2.3 Feshbach resonances

Feshbach resonances have had an enormous impact on the study of cold quantum gases in recent years, as have been extensively utilized experimentally to control the interaction strength between atoms in these gases [**?**, 21, 22, 23, 24]. Controlled by adjusting the magnetic field applied to the gas, Feshbach resonances amount to a knob by which experimentalists can tune the interparticle interactions. Such control, when applied to, for example, optical lattices containing one or more atoms at each site, can allow unprecedented insight into the physics of condensed matter systems.

A Feshbach resonance [25, 26, 27], as opposed to a shape resonance, is fundamentally a multichannel phenomenon, as it occurs for two atoms when their collision energy becomes degenerate with a bound state in a closed collision channel, producing brief transitions into and out of this state. It is primarily in order to describe such a resonance that motivates the use of various multichannel models in the following sections.

2.3 Zero-range-potential model for two particles in a harmonic trap

To describe the dynamics of the Feshbach-resonance cooling scheme, it is necessary to utilize a quantum-mechanical model for two particles interacting in a harmonic trap. Drawing from the basic collision theory presented in the preceding section, a theory with both a single channel as well as a two-channel theory will be presented. The single-channel theory is simpler, and provides a good starting point, while the introduction of a second channel allows for a more accurate description of the scattering by allowing inelastic phenomena to take place. Many papers have addressed the issue of the applicability of the single-channel model for various types of resonances, from narrow to broad. Such details are beyond the scope of the present discussion, and a two-channel theory will be the primary tool utilized to model the Feshbach-resonance cooling scheme.

Although a variety of methods can be used to solve the zero-range-potential problem in a harmonic trap, this section will utilize a quantum-defect-theory approach.

2.3.1 One channel

In the past, a single-channel quantum-defect-theory model of two interacting trapped particles has been successfully used to describe the coherent atom-molecule quantum beats produced in an atomic gas with a Feshbach resonance, which has been subjected to magnetic-field ramps [28]. The development of this model is outlined here to provide a basis for understanding the subsequent development of a two-channel theory.

The interaction between the two harmonically trapped particles is described by an energy-independent regularized zero-range potential [28, 29, 30],

$$V(r) = \frac{4\pi\hbar^2 a}{m}\delta^{(3)}(\mathbf{r})\frac{\partial}{\partial r}r, \tag{2.22}$$

where $\mathbf{r}$ is the (vector) interparticle coordinate and a is the two-particle scattering

length. The Hamiltonian for the system is separable into center-of-mass and relative (interparticle) parts. This is due to the fact that the interaction potential given above depends only on the relative coordinate, while the free-space kinetic energy operator for a pair of particles can always be written as the sum of a relative and a center-of-mass term. The center-of-mass degree of freedom exhibits a trivial simple-harmonic-oscillator spectrum, so only the relative motion is considered in the following. Also, since the zero-range interaction in Eq. (2.22 affects only s-wave interactions, the equation can be restricted to consider only $l = 0$. Defining the reduced mass, $\mu = m/2$, the time-independent Schrödinger equation for the relative-coordinate wave function $\psi(r)$ of two atoms interacting in a harmonic-oscillator trap is given by

$$\left(-\frac{\hbar^2}{2\mu}\frac{d^2}{dr^2} + V(r) + \frac{1}{2}\mu\omega^2 r^2\right)\psi(r) = E\psi(r). \tag{2.23}$$

Defining the dimensionless units of length $x = r/L_{\text{osc}}$, where $L_{\text{osc}} = \sqrt{\hbar/(\omega m/2)}$ is the reduced-mass oscillator length, and of energy $\epsilon = E/\hbar\omega$, rescaling the s-wave eigenfunction as

$$\psi_{\epsilon,l=0} = \frac{u(x)}{x}\frac{1}{\sqrt{4\pi}}, \tag{2.24}$$

and noting that Eq. (2.22) is nonzero only at the origin, Eq. (2.23) becomes

$$\left(-\frac{1}{2}\frac{d^2}{dx^2} + \frac{1}{2}x^2\right)u(x) = \epsilon u(x), \tag{2.25}$$

with the zero-range potential interaction imposing the boundary condition on $u(x)$ at the origin of

$$\frac{u'(0)}{u(0)} = -\frac{L_{\text{osc}}}{a}. \tag{2.26}$$

The solutions to Eq. (2.25), regular and irregular at the origin, can then be found and cast in terms of the effective quantum number $\nu = \epsilon/2 - 3/4$. Applying the techniques of quantum defect theory, the quantization condition for the scaled energy ϵ in terms of the quantum defect β is obtained,

$$\epsilon = 2(n - \beta) + \frac{3}{2}, \tag{2.27}$$

where $n = 0, 1, 2, 3, \ldots$. Enforcing the boundary condition on the logarithmic derivative of $u(x)$ at the origin, given in Eq. (2.26), yields the quantum-defect equation

$$\tan \pi\beta = -\frac{a}{L_{\text{osc}}} \frac{2\Gamma\left(\frac{\epsilon}{2} + \frac{3}{4}\right)}{\Gamma\left(\frac{\epsilon}{2} + \frac{1}{4}\right)}. \tag{2.28}$$

Equation (2.28) along with Eq. (2.27) can be solved self consistently to obtain the energy eigenvalues ϵ for a specified scattering length a. The eigenenergies ϵ obtained are illustrated in Fig. 2.1 as a function of the scattering length in oscillator units a/L_{osc}. Note that the energy levels undergo a shift as the inverse of the scattering length goes through zero, or equivalently, the scattering length goes through infinity. This effect is due to the introduction of a new bound state, and the characteristics of these level shifts will provide the basic motivation for the Feshbach resonance cooling scheme presented later in this chapter.

Note that a somewhat different approach to solving this problem is given in Ref. [29], yielding the transcendental equation

$$\frac{2\Gamma\left(\frac{-\epsilon}{2} + \frac{3}{4}\right)}{\Gamma\left(\frac{-\epsilon}{2} + \frac{1}{4}\right)} = \frac{L_{\text{osc}}}{a}, \tag{2.29}$$

which can be shown to be equivalent to the system of equations specified by Eq. (2.27) and Eq. (2.28).

2.3.2 Two channels

In order to later model the effects of the magnetic field ramps for the Feshbach-resonance cooling scheme, a two-channel Feshbach resonance model is now developed, based on the single-channel model described in Ref. [28]. Both of these models describe a two-atom Feshbach resonance for a harmonic trap, and utilize a zero-range potential to describe the interaction between the two atoms. The two-channel model has the advantage of allowing for a field-dependent resonance state. In the two-channel problem, the s-wave radial solutions for the relative coordinate r of the atom pair satisfy the

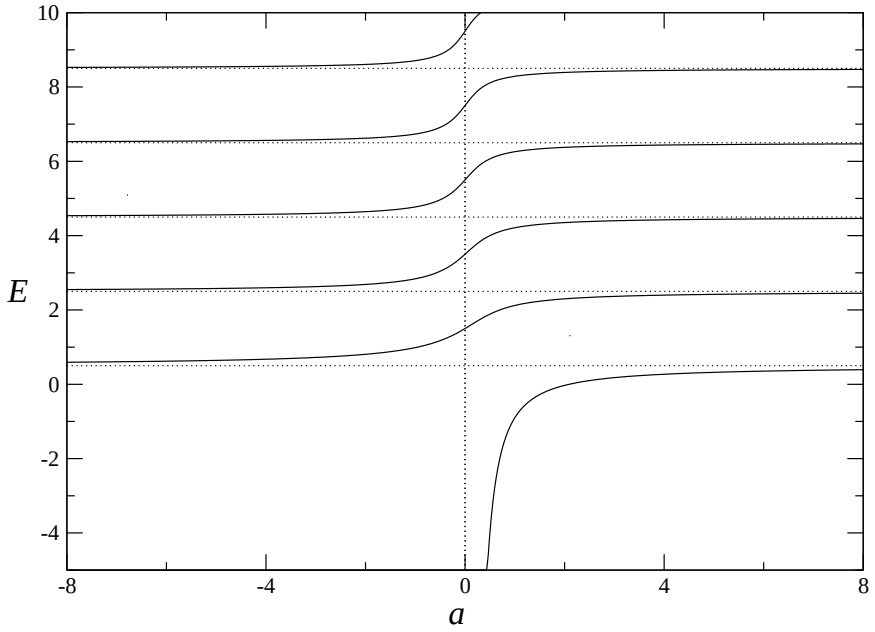

Figure 2.1: Eigenspectrum in oscillator units $\hbar\omega$ for two particles in a harmonic trap, as a function of the two-particle scattering length a in units of the reduced-mass oscillator length $L_{\rm osc}$.

matrix equation

$$\underline{H}\psi(r) = E\psi(r), \tag{2.30}$$

where the Hamiltonian matrix $\underline{H}$ is defined as

$$\underline{H} = -\frac{\hbar^2}{2\mu}\underline{1}\frac{d^2}{dr^2} + \underline{V}(\mathbf{r}) + \underline{E}^{th}, \tag{2.31}$$

and $\psi(r)$ is a two-component wave-function vector with components $\psi_i(r)$ corresponding to the ith channel. In Eq. (2.30), the first term on the right hand side is the two-channel kinetic energy operator, where $\underline{1}$ is the identity matrix. The matrix $\underline{V}$ represents the two-particle interactions, with diagonal elements describing single-channel scattering and the off-diagonal elements describing channel coupling. The matrix $\underline{E}^{th}$ is a diagonal matrix that describes the bare (zero interaction) splitting of the thresholds of the two channels. As such, it will be a diagonal matrix, and in most cases the zero of energy will be chosen so that only one element is nonzero. Here it will be written as

$$\underline{E}^{th} = \begin{pmatrix} 0 & 0 \\ 0 & \Delta\epsilon \end{pmatrix}, \tag{2.32}$$

where $\Delta\epsilon$ is the energy shift of the second channel from the first channel.

Along the lines of the single-channel model developed above, the interactions within each channel will be described by independent zero-range potentials, and a parametric channel coupling will be introduced. Using the same scaled length and energy parameters from the single channel model, this results in decoupled time-independent Schrödinger equations for the two channels,

$$\left(-\frac{1}{2}\frac{d^2}{dx^2} + \frac{1}{2}x^2\right) u_1(x) = \epsilon u_1(x) \tag{2.33}$$

$$\left(-\frac{1}{2}\frac{d^2}{dx^2} + \frac{1}{2}x^2\right) u_2(x) = (\epsilon - \Delta\epsilon)\, u_2(x), \tag{2.34}$$

where u_i for $i = 1, 2$ is the wave function for the ith channel, scaled as in Eq. (2.24). The zero-range potential imposes a boundary condition at the origin, which is written

here as

$$\frac{d}{dx}\begin{pmatrix} u_1(x) \\ u_2(x) \end{pmatrix}_{x=0} = \begin{pmatrix} -\frac{1}{a_1} & \zeta \\ \zeta & -\frac{1}{a_2} \end{pmatrix} \begin{pmatrix} u_1(x) \\ u_2(x) \end{pmatrix}_{x=0} . \tag{2.35}$$

Equation (2.35) contains the in-channel scattering physics in the diagonal terms, with a_i being the single-channel scattering length for the ith channel, and with the channel coupling represented in the off-diagonal elements by the parameter ζ.

Again applying a quantum-defect-theory treatment, along the lines of Ref. [28] for a single-channel model, a transcendental equation is obtained [31],

$$\left(\frac{2\Gamma\left(-\frac{\epsilon}{2}+\frac{3}{4}\right)}{\Gamma\left(-\frac{\epsilon}{2}+\frac{1}{4}\right)} - \frac{1}{a_1}\right)\left(\frac{2\Gamma\left(-\frac{\epsilon-\Delta\epsilon}{2}+\frac{3}{4}\right)}{\Gamma\left(-\frac{\epsilon-\Delta\epsilon}{2}+\frac{1}{4}\right)} - \frac{1}{a_2}\right) - \zeta^2 = 0, \tag{2.36}$$

the solutions of which, for specified values of a_1, a_2, ζ, and $\Delta\epsilon$, are the eigenenergies of the interacting system.

The aggregate scattering length for the full two-channel problem predicted by this model, in the low-collision-energy limit when $\omega \to 0$, is

$$a(E,B) = \left(\frac{1}{a_1} + \frac{|\zeta|^2}{\sqrt{2\mu\Delta\epsilon(B)/\hbar^2 - 2\mu E/\hbar^2} - 1/a_2}\right)^{-1} . \tag{2.37}$$

This expression can be compared to the known scattering length, determined from either experiment or more detailed scattering calculations, to determine the values of the parameters a_1, a_2, and ζ. The parameters also affect the magnetic-field dependence of the adiabatic energy states for the interacting system, and can also be fitted to. Although it is often found that a given set of parameters will not provide accurate scattering predictions over all regimes, they can be chosen to suitably describe the scattering over a certain range of interest.

2.4 Square-well-potential model for two particles in free space

In this section, the theory will be generalized to describe interactions between the two particles described by square-well potentials, which, although not usually as

analytically appealing as zero-range potentials, can provide a better description of short-range interaction physics when such a thing is important. The theory presented here is based on a model developed by Chris Greene [32].

The two-channel Hamiltonian will be written as Eq. (2.31) in the previous section, with the constant potential in the inner region given by

$$\underline{V}(r) = \begin{pmatrix} -V_1 & V_{12} \\ V_{12} & -V_2 \end{pmatrix} \theta(r_0 - r), \tag{2.38}$$

and the upper threshold specified by

$$\underline{E}^{th} = \begin{pmatrix} 0 & 0 \\ 0 & E_2^{th} \end{pmatrix}. \tag{2.39}$$

The solution matrix, given by $\underline{u}(r)$, obeys $\underline{u}(0) = 0$.

Define the matrix

$$\underline{W} = \left(-\frac{2m}{\hbar^2}\right)\left(\underline{V}(r) + \underline{E}^{th} - \epsilon\underline{1}\right) = \left(\frac{2m}{\hbar^2}\right)\begin{pmatrix} \epsilon + V_1 & -V_{12} \\ -V_{12} & \epsilon - E_2^{th} + V_2 \end{pmatrix}. \tag{2.40}$$

The eigenvector and eigenvalue matrices corresponding to $\underline{W}$ are $\underline{X}$ and $\underline{w}^2$, respectively: $\underline{WX} = \underline{Xw}^2$. Two uncoupled single-channel equations for $\underline{y}(r) = \underline{X}^T\underline{u}(r)$ are then obtained. The regular solutions at the origin that satisfy these uncoupled equations are simply

$$\underline{y}(r) = \begin{pmatrix} \sin w_1 r & 0 \\ 0 & \sin w_2 r \end{pmatrix}. \tag{2.41}$$

2.5 Digression: application to molecular dissociation

As an example of the utility of the theory developed earlier in this chapter, this section applies two-channel scattering models to the problem of molecular dissociation induced by an oscillating magnetic field of perturbative amplitude. For the present purpose, only processes in free-space will be considered, and the scattering equations will be used neglecting the harmonic-oscillator trapping potential.

2.5.1 Zero-range potential

The model consists of two scattering channels, each with a zero-range potential at the origin. The radial wave function satisfies the following free-space coupled equations,

$$-\frac{\hbar^2}{2m}\frac{d^2}{dx^2}u_1 = Eu_1, \tag{2.42}$$

$$-\frac{\hbar^2}{2m}\frac{d^2}{dx^2}u_2 = (E - \Delta\epsilon(B))\, u_2, \tag{2.43}$$

where E is the two-channel energy, $\Delta\epsilon(B)$ is the channel energy separation and is a function of the magnetic field, and u_1 and u_2 are the lower and upper channel radial wave functions, respectively. The effects of the true potentials in the channels are enforced by a boundary condition at the origin that fixes the log derivative of the radial wave function at that point. With the exception of the origin, the wave functions everywhere satisfy the free-particle Schrödinger equations given above. The boundary condition at the origin is given in Eq. (2.35).

Molecular dissociation consists of transitions from states below the lower-channel threshold (both channels closed) to states in which one or both of the channels are open. Thus, it is necessary to consider two separate cases: (a) the lower channel open and the upper channel closed, and (b) both channels closed. Dissociation processes consist of transitions from the bound case (b) to the continuum case (a). The two cases will be considered individually.

(a) For $\Delta\epsilon > E > 0$ (lower channel open, upper channel closed), the energy-normalized solutions are

$$\begin{pmatrix} u_{1\mathrm{a}}(x) \\ u_{2\mathrm{a}}(x) \end{pmatrix} = \sqrt{\frac{2m}{\pi k_{1\mathrm{a}}\hbar^2}} \begin{pmatrix} \sin(k_{1\mathrm{a}}x + \delta) \\ D_a e^{-\kappa_{2\mathrm{a}}x} \end{pmatrix}, \tag{2.44}$$

where D_a is a constant. From the differential equations,

$$E_a = \frac{\hbar^2 k_{1\mathrm{a}}^2}{2m} = \Delta\epsilon - \frac{\hbar^2\kappa_{2\mathrm{a}}^2}{2m}. \tag{2.45}$$

The boundary condition at the origin gives

$$\begin{pmatrix} k_{1\mathrm{a}}\cos\delta \\ -\kappa_{2\mathrm{a}}D_a \end{pmatrix} = \begin{pmatrix} -1/a_1 & \zeta \\ \zeta^* & -1/a_2 \end{pmatrix} \begin{pmatrix} \sin\delta \\ D_a \end{pmatrix}, \tag{2.46}$$

or

$$\begin{pmatrix} -1/a_1 - \frac{k_{1\mathrm{a}}}{\tan\delta} & \zeta \\ \zeta^* & -1/a_2 + \kappa_{2\mathrm{a}} \end{pmatrix} \begin{pmatrix} \sin\delta \\ D_a \end{pmatrix} = 0. \tag{2.47}$$

This equation has a non-trivial solution if

$$\begin{vmatrix} -1/a_1 - \frac{k_{1\mathrm{a}}}{\tan\delta} & \zeta \\ \zeta^* & -1/a_2 + \kappa_{2\mathrm{a}} \end{vmatrix} = 0. \tag{2.48}$$

Using the solution to this equation, and defining the energy-dependent scattering length to be $a(E_a) = -\tan\delta(k_{1\mathrm{a}})/k_{1\mathrm{a}}$,

$$\frac{1}{a(E_a)} = \frac{1}{a_1} + \frac{|\zeta|^2}{\sqrt{\frac{2m}{\hbar^2}(\Delta\epsilon - E_a)} - 1/a_2}. \tag{2.49}$$

Going back to Eq. (2.47) closed-channel amplitude is determined to be

$$\begin{aligned} D_a &= -\frac{\sin\delta}{\zeta}\left(\frac{1}{a_1} + \frac{k_{1\mathrm{a}}}{\tan\delta}\right) \\ &= \frac{\sin\delta}{\zeta}\left(\frac{1}{a(E_a)} - \frac{1}{a_1}\right). \end{aligned} \tag{2.50}$$

(b) For $E - \Delta\epsilon < 0$ (both channels closed), the solutions are

$$\begin{pmatrix} u_{1\mathrm{b}}(x) \\ u_{2\mathrm{b}}(x) \end{pmatrix} = \sqrt{\frac{2m}{\pi\kappa_{1\mathrm{b}}\hbar^2}} \begin{pmatrix} e^{-\kappa_{1\mathrm{b}}x} \\ D_b e^{-\kappa_{2\mathrm{b}}x} \end{pmatrix}. \tag{2.51}$$

From the differential equations,

$$E_b = -\frac{\hbar^2\kappa_{1\mathrm{b}}^2}{2m} = \Delta\epsilon - \frac{\hbar^2\kappa_{2\mathrm{b}}^2}{2m}. \tag{2.52}$$

The boundary condition at the origin gives

$$\begin{pmatrix} -\kappa_{1\mathrm{b}}\cos\delta \\ \kappa_{2\mathrm{b}}D_b \end{pmatrix} = \begin{pmatrix} -1/a_1 & \zeta \\ \zeta^* & -1/a_2 \end{pmatrix} \begin{pmatrix} 1 \\ D_b \end{pmatrix}, \tag{2.53}$$

or

$$\begin{pmatrix} -1/a_1 + \kappa_{1\mathrm{b}} & \zeta \\ \zeta^* & -1/a_2 + \kappa_{2\mathrm{b}} \end{pmatrix} \begin{pmatrix} 1 \\ D_b \end{pmatrix} = 0. \tag{2.54}$$

This equation has a non-trivial solution if

$$\begin{vmatrix} -1/a_1 + \kappa_{1\mathrm{b}} & \zeta \\ \zeta^* & -1/a_2 + \kappa_{2\mathrm{b}} \end{vmatrix} = 0. \tag{2.55}$$

Using Eq. (2.54), the upper-channel amplitude is found to be

$$D_b = \frac{1}{\zeta}\left(\kappa_{1\mathrm{b}} - \frac{1}{a_1}\right), \tag{2.56}$$

or equivalently,

$$D_b = \frac{\zeta^*}{\kappa_{2\mathrm{b}} - 1/a_2}. \tag{2.57}$$

2.5.1.1 Dissociation rate

At this point, time-dependent perturbation theory will be used to determine the rate of transitions from case (b), where a true bound state exists, to case (a), where the lower channel is open, and the states of the coupled system are all continuum.

The perturbation being applied is a magnetic field, oscillating with frequency ν_{pert}, with amplitude B_{pert}, and with an envelope of length t_{pert}, as used, for example, in experiments at JILA [33]. This type of oscillating field pulse is shown in Fig. 2.2. This oscillation can be represented by

$$B(t) = B_{\mathrm{ini}} + B_{\mathrm{pert}} \sin\left(\pi \frac{t}{t_{\mathrm{pert}}}\right) \sin\left(2\pi\nu_{\mathrm{pert}} t\right), \tag{2.58}$$

where B_{ini} is the magnetic field at which the pulse is centered, and B_{pert} is the amplitude of the oscillations.

The first-order transition amplitude in time-dependent perturbation theory is

$$c_n^{(1)}(t) = \frac{-i}{\hbar} \int_{t_0}^{t} dt' e^{i\omega_{ni}t'} V_{ni}(t'), \tag{2.59}$$

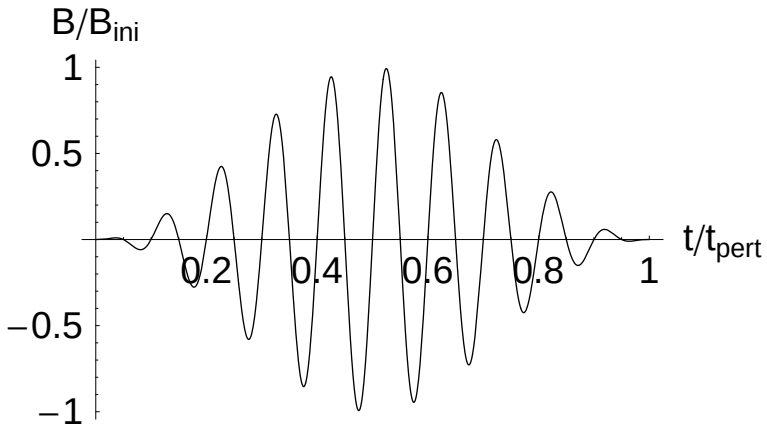

Figure 2.2: An example of the type of magnetic field pulse used in molecular-dissociation experiments. This pulsed magnetic field is used here as a perturbation in a in a two-channel model of dissociation. The amplitude of the pulse is $B_{\rm ini}$, the width of the envelope is $t_{\rm pert}$, and the frequency of oscillation is $\nu_{\rm pert}$. In this plot, $\nu_{\rm pert} = 10/t_{\rm pert}$.

where V_{ni} is the transition matrix element between the state $|i\rangle$ and the state $|n\rangle$. The perturbation that considered here is of the form

$$\begin{aligned} V(t) &= \begin{pmatrix} 0 & 0 \\ 0 & \Delta\epsilon(B(t)) - \Delta\epsilon(B_{\text{ini}}) \end{pmatrix}, \\ &= \begin{pmatrix} 0 & 0 \\ 0 & \mu\left(B(t) - B_{\text{ini}}\right) \end{pmatrix}, \end{aligned} \tag{2.60}$$

where μ is the slope of $\Delta\epsilon$ with respect to B.

The transition matrix element for each of the two cases will now be considered.

2.5.1.2 Bound-bound transitions

Transitions that occur between case (b) and case (b) are bound-bound transitions. The transition matrix element is

$$\begin{pmatrix} u_{1\text{b}}(x) & u_{2\text{b}}(x) \end{pmatrix} V(t) \begin{pmatrix} u_{1\text{b}'}(x) \\ u_{2\text{b}'}(x) \end{pmatrix} = u_{2\text{b}}(x) B_{\text{pert}} \sin\left(\pi \frac{t}{t_{\text{pert}}}\right) \sin\left(2\pi\nu_{\text{pert}} t\right) u_{2\text{b}'}(x). \tag{2.61}$$

The transition amplitude is then given by

$$\begin{aligned} c^{(1)}_{EE'}(t) &= \frac{2m\mu B_{\text{pert}}}{\pi\sqrt{\kappa_{1\text{b}}\kappa_{1\text{b}'}}\hbar^2} D_b D_{b'} \int_0^\infty dx e^{-(\kappa_{2\text{b}}+\kappa_{2\text{b}'})x} \\ &\qquad \times \int_{t_0}^t dt' e^{i(E-E')t/\hbar} \sin\left(\pi \frac{t}{t_{\text{pert}}}\right) \sin\left(2\pi\nu_{\text{pert}} t\right) \\ &= \frac{2m\mu B_{\text{pert}}}{\pi\sqrt{\kappa_{1\text{b}}\kappa_{1\text{b}'}}\hbar^2} \frac{\zeta^{*2}}{\left(\kappa_{2\text{b}} - 1/a_2\right)\left(\kappa_{2\text{b}'} - 1/a_2\right)} \frac{1}{\kappa_{2\text{b}} + \kappa_{2\text{b}'}} f(E - E', \nu_{\text{pert}}, t), \end{aligned} \tag{2.62}$$

where

$$f(E - E', \nu_{\text{pert}}, t) = \int_{t_0}^t dt' e^{i(E-E')t/\hbar} \sin\left(\pi \frac{t}{t_{\text{pert}}}\right) \sin\left(2\pi\nu_{\text{pert}} t\right). \tag{2.63}$$

The bound-bound transition rate is then

$$\begin{aligned}
R_{EE'}(t) &= \left|c^{(1)}_{EE'}(t)\right|^2 \\
&= \left(\frac{2m\mu B_{\text{pert}}}{\pi\hbar^2}\right)^2 \frac{1}{\kappa_{1\text{b}}\kappa_{1\text{b}'}} \left(\frac{1}{\kappa_{2\text{b}}+\kappa_{2\text{b}'}}\right)^2 \left(\frac{|\zeta|^2}{(\kappa_{2\text{b}}-1/a_2)\,(\kappa_{2\text{b}'}-1/a_2)}\right)^2 \\
&\qquad\qquad \times f^2(E-E',\nu_{\text{pert}},t) \\
&= \left(\frac{\mu B_{\text{pert}}}{\pi}\right)^2 \frac{1}{\sqrt{EE'}} \left(\frac{1}{\sqrt{\Delta\epsilon-E}+\sqrt{\Delta\epsilon-E'}}\right)^2 \\
&\quad \times \left(\frac{|\zeta|^2}{\left(\sqrt{\frac{2m}{\hbar^2}\,(\Delta\epsilon-E)}-1/a_2\right)\left(\sqrt{\frac{2m}{\hbar^2}\,(\Delta\epsilon-E')}-1/a_2\right)}\right)^2 \\
&\qquad\qquad \times f^2(E-E',\nu_{\text{pert}},t).
\end{aligned} \tag{2.64}$$

2.5.1.3 Bound-free transitions

Transitions that occur between case (b) and case (a) are bound-free transitions. The transition matrix element is

$$\begin{pmatrix} u_{1\text{a}}(x) & u_{2\text{a}}(x) \end{pmatrix} V(t) \begin{pmatrix} u_{1\text{b}}(x) \\ u_{2\text{b}}(x) \end{pmatrix} = u_{2\text{a}}(x) B_{\text{pert}} \sin\left(\pi\frac{t}{t_{\text{pert}}}\right) \sin\left(2\pi\nu_{\text{pert}}t\right) u_{2\text{b}}(x). \tag{2.65}$$

The transition amplitude is then given by

$$\begin{aligned}
c^{(1)}_{ba}(t) &= \frac{2m\mu B_{\text{pert}}}{\pi\sqrt{k_{1\text{a}}\kappa_{1\text{b}}}\hbar^2} D_a D_b \int_0^\infty dx e^{-(\kappa_{2\text{a}}+\kappa_{2\text{b}})x} \\
&\qquad\qquad \times \int_{t_0}^t dt' e^{i(E_a-E_b)t/\hbar} \sin\left(\pi\frac{t}{t_{\text{pert}}}\right) \sin\left(2\pi\nu_{\text{pert}}t\right) \\
&= \frac{2m\mu B_{\text{pert}}}{\pi\sqrt{k_{1\text{a}}\kappa_{1\text{b}}}\hbar^2} \frac{\zeta^* \sin\delta}{\zeta} \left(\frac{1}{a(E_a)}-\frac{1}{a_1}\right) \frac{1}{\kappa_{2\text{b}}-1/a_2} \frac{1}{\kappa_{2\text{a}}+\kappa_{2\text{b}}} f(E_b-E_a,\nu_{\text{pert}},t).
\end{aligned} \tag{2.66}$$

The transition rate is then calculated to be

$$\begin{aligned}
R_{ba}(t) &= \left|c_{ba}^{(1)}(t)\right|^2 \\
&= \left(\frac{2m\mu B_{\text{pert}}}{\pi\sqrt{k_{1\text{a}}\kappa_{1\text{b}}}\hbar^2}\right)^2 \sin^2\delta \left(\frac{1}{a(E_a)} - \frac{1}{a_1}\right)^2 \left(\frac{1}{\kappa_{2\text{b}} - 1/a_2}\right)^2 \left(\frac{1}{\kappa_{2\text{a}} + \kappa_{2\text{b}}}\right)^2 \\
&\qquad \times f^2(E_b - E_a, \nu_{\text{pert}}, t) \\
&= \left(\frac{2m\mu B_{\text{pert}}}{\pi\hbar^2}\right)^2 \frac{\sin^2\delta}{k_{1\text{a}}\kappa_{1\text{b}}} \left(\frac{1}{\kappa_{2\text{a}} + \kappa_{2\text{b}}}\right)^2 \left(\frac{|\zeta|^2}{\sqrt{\frac{2m}{\hbar^2}(\Delta\epsilon - E_a)} - 1/a_2}\right)^2 \left(\frac{1}{\kappa_{2\text{b}} - 1/a_2}\right)^2 \\
&\qquad \times f^2(E_b - E_a, \nu_{\text{pert}}, t) \\
&= \left(\frac{\mu B_{\text{pert}}}{\pi}\right)^2 \frac{\sin^2\delta}{\sqrt{-E_a E_b}} \left(\frac{1}{\sqrt{\Delta\epsilon - E_a} + \sqrt{\Delta\epsilon - E_b}}\right)^2 \\
&\quad \times \left(\frac{|\zeta|}{\sqrt{\frac{2m}{\hbar^2}(\Delta\epsilon - E_a)} - 1/a_2}\right)^2 \left(\frac{|\zeta|}{\sqrt{\frac{2m}{\hbar^2}(\Delta\epsilon - E_b)} - 1/a_2}\right)^2 \\
&\qquad \times f^2(E_b - E_a, \nu_{\text{pert}}, t).
\end{aligned} \tag{2.67}$$

In the above equation, the expression for the energy-dependent scattering length given in Eq. (2.49) has been inserted. From Eq. (2.48),

$$\tan\delta = \frac{k_{1\text{a}}}{\frac{|\zeta|^2}{\kappa_{2\text{a}} - 1/a_2} - 1/a_1}, \tag{2.68}$$

so, using the fact that $\sin^2(\arctan x) = \frac{x^2}{1+x^2}$,

$$\sin^2\delta = \frac{k_{1\text{a}}^2}{\left(\frac{|\zeta|^2}{\kappa_{2\text{a}} - 1/a_2} - 1/a_1\right)^2 + k_{1\text{a}}^2}. \tag{2.69}$$

For $t > t_{\text{pert}}$, the function f^2 will be a sharply peaked function of ν_{pert} centered on the transition energy.

At this point, it would also be possible to calculate the dissociation properties taking into account interference between the two possible pathways of bound-bound-free indirect and bound-free direct dissociation. This would yield behavior characterized by Fano lineshapes [34], originally developed in the context of autoionization theory.

2.5.2 Square-well potential

Since both channels are closed, the solutions for $r > r_0$ must decay exponentially,

$$\vec{\psi}^{phys}(r) = \begin{pmatrix} N_1 e^{-q_1 r} \\ \\ N_2 e^{-q_2 r} \end{pmatrix}. \tag{2.70}$$

Smoothly matching the solution and its derivative at r_0 requires

$$\vec{\psi}^{phys}(r_0) = \underline{X}\underline{y}(r_0)\vec{z}, \tag{2.71}$$

$$\vec{\psi}'^{phys}(r_0) = \underline{X}\underline{y}'(r_0)\vec{z}, \tag{2.72}$$

or

$$\underline{X}\underline{y}(r_0)\vec{z} = \underline{D}(r_0)\vec{s}, \tag{2.73}$$

$$\underline{X}\underline{y}'(r_0)\vec{z} = \underline{D}'(r_0)\vec{s}, \tag{2.74}$$

with

$$\underline{D}(r) = \begin{pmatrix} e^{-q_1 r} & 0 \\ \\ 0 & e^{-q_2 r} \end{pmatrix}, \tag{2.75}$$

and

$$\vec{s} = \begin{pmatrix} N_1 \\ \\ N_2 \end{pmatrix}. \tag{2.76}$$

Eliminating z and defining the R-matrix gives

$$\left(\underline{RD}(r_0) - \underline{D}'(r_0)\right)\vec{s} = 0, \tag{2.77}$$

which has a non-trivial solution when

$$\det\left(\underline{RD}(r_0) - \underline{D}'(r_0)\right) = 0, \tag{2.78}$$

or

$$\begin{vmatrix} \left(R_{11} - q_1\right) e^{-q_1 r_0} & R_{12} e^{-q_2 r_0} \\ \\ R_{21} e^{-q_1 r_0} & \left(R_{22} - q_2\right) e^{-q_2 r_0} \end{vmatrix} = 0. \tag{2.79}$$

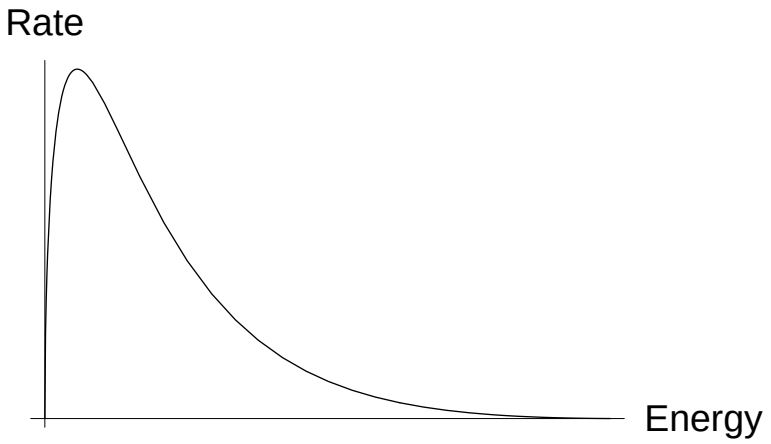

Figure 2.3: An example of a typical molecular photodissociation spectrum obtained using the two-channel square-well model. Plotted is the photodissociation rate as a function of energy, both in arbitrary units.

This gives the quantization condition

$$e^{-(q_1+q_2)r_0}\left[(R_{11}-q_1)(R_{22}-q_2)-R_{12}R_{21}\right]=0. \tag{2.80}$$

The normalization condition requires

$$\begin{aligned}1 &= \int_0^{r_0} dr \begin{pmatrix}\sin w_1 r & B^\dagger \sin w_2 r\end{pmatrix} \underline{X}^T \underline{X} \begin{pmatrix}\sin w_1 r \\ B \sin w_2 r\end{pmatrix} + \int_{r_0}^{\infty} dr \left|\vec{\psi}^{phys}(r)\right|^2 \\ &= \int_0^{r_0} dr \sin^2 w_1 r + |B|^2 \int_0^{r_0} dr \sin^2 w_2 r + |N_1|^2 \int_{r_0}^{\infty} dr e^{-2q_1 r} + |N_2|^2 \int_{r_0}^{\infty} dr e^{-2q_2 r}.\end{aligned} \tag{2.81}$$

Square-well calculations of the dissociation rate utilizing this model and to find bound-bound and bound-free transition rates using Mathematica yield spectra of the form shown in Fig. 2.3. The shape of this spectrum agrees with the predictions of more sophisticated scattering models, and comparison with such models or with experimentally obtained spectra can be used to determine the correct model parameters.

2.6 The cooling scheme

In this section, the workings of the Feshbach-resonance cooling scheme are presented. This scheme makes use of the unique characteristics of a Feshbach resonance to reduce the energy of pairs of externally confined atoms. It will be shown how this method can be used to cool pairs of atoms taken from a thermal distribution. The basis of the cooling scheme originates from observing, as shown in Fig. 2.1 that the quantum-mechanical energy levels of two atoms in a harmonic trap shift by an energy of approximately two trap quanta as the scattering length is adjusted through the resonance. If the scattering length is a function of some control parameter, then as the control parameter is swept in one direction across the resonance, it will induce this energy shift. Throughout this section, the particular control parameter considered will be the magnetic field B, which here is used to manipulate the atom-atom scattering length a in the vicinity of a pole. However, it is important to note that, in other contexts, the shift of the energy levels could be induced by varying the detuning of an off-resonant dressing laser, or by varying an electric field strength. The cooling scheme that is presented here in terms of the control parameter B can be extended to those other contexts in a straightforward manner. In the following, the basic mechanism of the Feshbach resonance cooling process is first developed. After that, the method of simulating the cooling, utilizing the two-body scattering models developed earlier in this chaper, will be presented. Next, the feasibility and effectiveness of the proposed cooling scheme are then illustrated through an application to a system of two atoms in a trap, as would be encountered in a realistic experimental setup. Finally, the possibility of applying the scheme to atoms in optical traps or lattices will be discussed.

As mentioned earlier in this chapter, the Schrödinger equation for two identical, interacting mass m atoms under spherical harmonic trapping potential of frequency ν can be decoupled into two equations: one involving the three relative coordinates of

the pair of atoms, and another involving the three center-of-mass coordinates [29, 30]. In the Schrödinger equation for the relative coordinate of two trapped atoms, a central potential is used. It is assumed for the time being that the center-of-mass coordinate can be neglected, which will be the case if the system is translationally cold. An applied external magnetic field B is introduced and its effect is described in a QDT context as a B-dependent quantum defect $\beta_{El}(B)$. Then, the energy levels $E_{nl}(B)$ for the relative motion of an atom pair are given by [30]

$$E_{nl}(B) = (2n - 2\beta_{El}(B) + l + 3/2)\,\hbar\omega, \tag{2.82}$$

where $\omega = 2\pi\nu$. Note that the quantum defect $\beta_{El}(B)$ depends strongly on the relative orbital angular momentum l of the pair but it varies only weakly as the radial oscillator quantum number n is changed. The defect $\beta_{El}(B)$ has only a weak dependence on the energy when considered on the scale of an oscillator quantum. Explicitly, this can be written as $|\mathrm{d}\beta_{El}(B)/\mathrm{d}E_{nl}| \ll 1/\hbar\omega$.

It will be shown later that the quantum defect for one relative partial wave l for an atom pair (for example, the s wave, p wave, or d wave) must change by approximately unity across the energy range $k_{\mathrm{B}}\Delta T$ of interest, and across the accessible range of the control parameter, ΔB. The Feshbach resonance, which causes the scattering phaseshift to change by a value of π is the result of this unit variation of $\beta_{El}(B)$. A simple closed-form expression can be derived for the quantum defect β_{El}, as is shown in Refs. [30] and [35]. This expression can be simplified when considering energies that are higher than the energy of first few trap states to become

$$\beta_{El}(B) \approx \arctan\left(\frac{a\,(E_{nl}, B)\,\hbar\omega}{2L_{\mathrm{osc}}E_{nl}\sqrt{e}}\right), \tag{2.83}$$

where $a(E_{nl}, B)$ is the energy- and field-dependent scattering length and $L_{\mathrm{osc}} = \sqrt{\hbar/\,(\mu\omega)}$ is the characteristic oscillator length for the system, with the reduced mass $\mu = m/2$ defined.

For simplicity, the present development is constrained to consider only an s-wave resonance. However, the ideas described could be easily extended to higher partial-wave resonances. The limiting low-energy scattering phaseshift is proportional to the wavenumber $k = (2\mu E/\hbar^2)^{1/2}$ for an s-wave Feshbach resonance. The E- and B-dependent scattering length, along the lines of Section 1.3, (dropping the subscript l for notational efficiency, and because only the s wave is being considered) is then given by

$$a(E_n, B) = a_{\rm bg} + \frac{\Gamma_E \sqrt{\hbar^2/(8\mu E_n)}}{E_n + (B - B_{\rm res})E'_{\rm res}(B)}, \tag{2.84}$$

where $a_{\rm bg}$ is the background scattering length. A zero-energy bound state is created when the the magnetic field strength is equal to $B_{\rm res}$, the resonance magnetic field . The width Γ_E in energy of the resonance is related to the width Δ in the control parameter β_{El} by the relation $\Gamma_E = 2ka_{\rm bg}E'_{\rm res}(B)\Delta$, where $E'_{\rm res}$ signifies the rate at which the resonance energy $E_{\rm res}$ changes as a function of the control parameter [36]. Figure 2.4 provides a plot of the characteristic s-wave energy levels E_n for the relative coordinate of two atoms in a spherical harmonic-oscillator trapping potential, as functions of the applied magnetic field B for the particular case of a magnetic Feshbach resonance in the scattering of $^{85}{\rm Rb}(2,-2)+^{85}{\rm Rb}(2,-2)$. A somewhat large and perhaps unrealistic trapping frequency of $\nu = 1\,{\rm MHz}$ is used in this in order to accentuate the field dependence of the energy levels for visualization purposes. The idea for using such a setup for cooling involves ramping the magnetic field B slowly from B_1 to B_2 and then quickly back to B_1. A magnetic-field ramp for a more realistic situation encountered in an experiment would likely cross more level shifts (that is, it would cover a larger range of magnetic field). The quantum-mechanical state that undergoes an energy-level shift for for the field value of $B = B_2$ (which will be defined by $n = Q$ later in this chapter) is indicated by a dashed line. In the example illustrated in Fig. 2.4, the model resonance parameters considered are $B_{\rm res} = 155.2\,{\rm G}$, $E'_{\rm res} = -3.5\,{\rm MHz/G}$, $\Gamma_B = 10\,{\rm G}$,

and $a_{\rm bg} = -380\,a_0$, where a_0 is the Bohr radius.

The particular choice of parameters affects the magnetic-field dependence of the adiabatic energy states. These parameters can thus be adjusted to provide satisfactory agreement with experimental data in the regions presently of interest. For example, for ^{85}Rb, empirically determined parameters are found to be $a_1 = -435\,a_0$, $a_2 = 1.49\,a_0$, and $\zeta = 0.00116\,a_0^{-1}$. Simulations of the field ramps can then be performed by specifying an initial state of the system and numerically solving the Schrödinger equation.

The basic idea of cooling with a Feshbach resonance involves ramping the magnetic field through the region in which the energy levels shift by a value of approximately $2\hbar\omega$. Figure 2.4 denotes the internal energy eigenvalues for the pair of atoms as a function of magnetic field B. If the pair of atoms is initially in an eigenstate at the field strength of $B = B_1$, then a sufficiently slow field ramp from B_1 to B_2 will decrease the internal energy of the pair by approximately $2\hbar\omega$ if the energy level undergoes a shift in that field range (see inset of Fig. 2.4). More precisely, a slow ramp here is meant to mean an adiabatic ramp. A fast ramp from B_2 back to B_1 would seem, ideally, to project the wave function of the atom pair onto an eigenstate $|n(B_2)\rangle$ with the same energy as $|n(B_1)\rangle$. This type of ramp is more precisely defined as a nonadiabatic ramp. The result of the projection is to induce a net decrease in energy of approximately $2\hbar\omega$. Once this set of field ramps is finished, additional ramps can then be performed. Ideal cooling is described in a diagrammatic manner by arrows in the inset of the figure, which has the same axes as the main figure. This diagram illustrates a process by which population is transferred from point a to point b during the adiabatic (slow) field ramp and from point b to back to point c during the nonadiabatic (fast) field ramp.

Figure 2.5 illustrates the application of diabatic vs adiabatic changes in terms of a quantum particle in a box. For a particle initially in a one-dimensional box, the wave function of the particle is depicted on the left side of the top and bottom of the figure. In the upper portion of the figure, the box is rapidly expanded to a larger size. In this

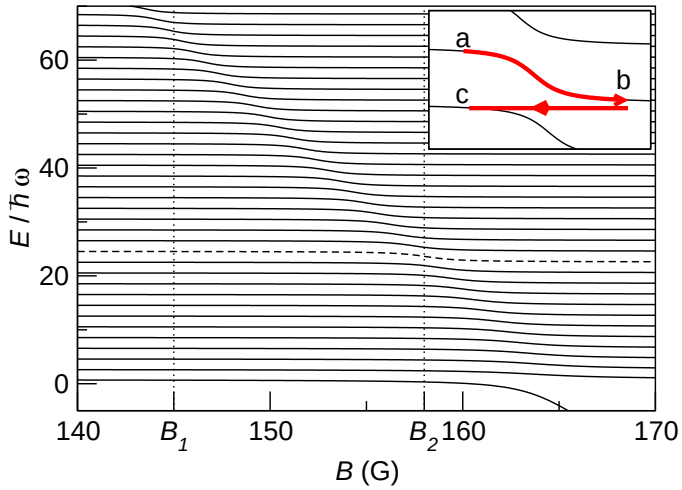

Figure 2.4: Eigenenergies of an interacting two-atom system in a harmonic trap near a Feshbach resonance, as a function of the magnetic field. The shift in the energies as the resonance is traversed can be seen, as well as the energy dependence of the location of the shift in magnetic field. The inset illustrates an ideal series of population transfers induced by magnetic field ramps for the Feshbach-resonance cooling scheme. This figure is adapted from Ref. [1].

case, assuming that the change in box size is fast enough to be in the diabatic limit, the initial wave function will project onto the eigenstates of the new system, and the wave function will be unchanged. In the bottom portion of the figure, the box is slowly expanded to a larger size. If this change is slow enough to be in the adiabatic limit, the wave function will slowly track the corresponding eigenfunction of the box, resulting in the displayed wave function. This difference of projection for fast changes and adiabatic following for slow ramps is an important concept for understanding Feshbach-resonance cooling.

The dynamics of the cooling scheme can be modeled by specifying an initial state of the system and then integrating the time-dependent Schrödinger equation,

$$i\hbar\frac{\partial}{\partial t}\left|\psi(B,t)\right\rangle = H(B)\left|\psi(B,t)\right\rangle. \tag{2.85}$$

The system state vector can be expanded in a set of eigenkets of the the system Hamiltonian for a given magnetic field,

$$\left|\psi(B_i,t)\right\rangle = \sum_{\nu_i} a_{\nu_i}^{(i)}(t)\left|\nu_i\right\rangle, \tag{2.86}$$

where the $a_{\nu_i}^{(i)}(t)$ is the expansion coefficient of the $|\nu_i\rangle$ energy eigenstate for the system with a magnetic field of B_i, which has eigenvalue $\hbar\omega_{\nu_i}$,

$$H(B_i)\left|\nu_i\right\rangle = \hbar\omega_{\nu_i}\left|\nu_i\right\rangle. \tag{2.87}$$

Consider propagating the system from an initial magnetic field value of B_1 at time t_1 to a final value of B_2 at time t_2. Using the expansion in Eq. (2.86) for the value of the initial magnetic field, Eq. (2.85) implies that

$$\frac{d}{dt}a_{\nu_1}^{(1)}(t) = -i\omega_{\nu_1}a_{\nu_1}^{(1)}(t). \tag{2.88}$$

It has already been illustrated in Fig. 2.4 how the eigenvalues ω_{ν_1} change as a function of magnetic field. This time dependence, $\omega_{\nu_i} = \omega_{\nu_i}(t)$, by way of the time-varying

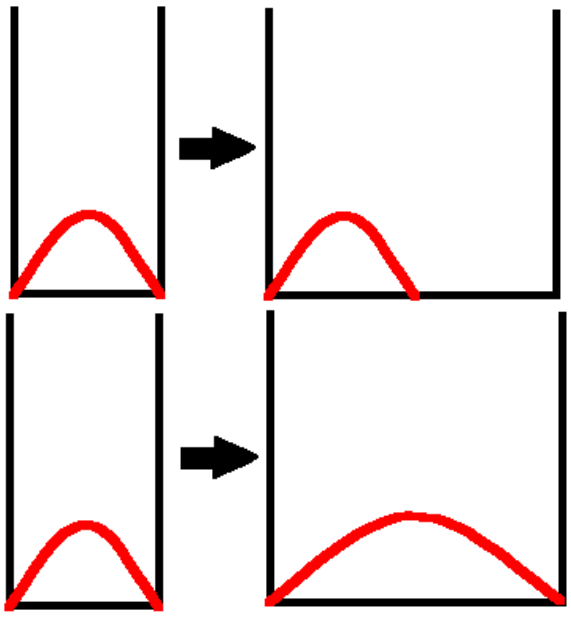

Figure 2.5: Upper figure: Wave function in a box before and after rapidly (diabatically) expanding the box. Lower plot: Wave function in a box before and after slowly (adiabatically) expanding the box.

magnetic field, yields a solution to Eq. (2.88) of

$$a_{\nu_1}^{(1)}(t_2) = a_{\nu_1}^{(1)}(t_1) e^{-i\int_{t_1}^{t_2} dt\, \omega_{\nu_1}(t)}. \tag{2.89}$$

Putting things in terms of the eigenstates of the system for the new magnetic field B_2,

$$a_{\nu_2}^{(2)}(t_2) = \sum_{\nu_i} \langle \nu_f | \nu_i \rangle \, a_{\nu_1}^{(1)}(t_1) e^{-i\int_{t_1}^{t_2} dt\, \omega_{\nu_1}(t)}, \tag{2.90}$$

where the overlap matrix $\langle \nu_2 | \nu_1 \rangle$ is defined by

$$a_{\nu_j} = \sum_{\nu_i} \langle \nu_j | \nu_i \rangle \, a_{\nu_i}, \tag{2.91}$$

and can be determined in a straightforward manner from the QDT development of two-channel model presented in Section 2.3.2. If the system is initially diagonalized over a range of magnetic-field values of interest for the problem at hand, these eigenenergies can be used to perform numerical integrations in Eq. (2.90) and, supplying initial values of the expansion coefficients and the appropriate overlap matrices, the time evolution can be determined.

2.7 Results and experimental possibilities

Upon performing simulations of the cooling using the numerical propagation technique presented in the preceding section, the effect of the adiabatic and nonadiabatic field ramps can be determined. Initially it is assumed that the atom pair is in a pure quantum state at a magnetic field of $B = B_1$. As predicted by the above qualitative discussion, the adiabatic field ramp (B_1 to B_2 and shown in Fig. 2.4) decreases the energy of the atom pair regardless of the initial eigenstate chosen. A nonadiabatic ramp (B_2 to B_1 and also shown in Fig. 2.4) for a state which is initially at a field value of B_2 and assuming that this initial state is not degenerate with the resonance state, causes the system to project onto a state at $B = B_1$ having roughly the same energy as the initial state at B_2. If, however, the pair is initially in a state that is degenerate with the

resonance state for the field value of $B = B_2$, the fast ramp is found to result in a strong projection of the initial state onto the resonance state. This is to be expected since the character of the dressed state of the interacting system having the same energy as the bare resonance state is very similar to the character of this bare resonance state. The projection between these two states is thus very effective. In this case, the atom pair must gain energy due to the fact that the resonance state at $B = B_1$ has a energy that is larger than that of the initial state at $B = B_2$.

It is now possible to generalize the above argument to allow an initial quantum state that is in a mixed state. From this, it can be shown how cooling can be performed for a more realistic ensemble of atom pairs instead of a pure state. If an atom pair is taken from a thermal distribution of pairs, the probability of occupying a level with relative-motion energy E_n is given in terms of a Boltzmann factor by $e^{-E_n/\tau}/Z(\tau)$ with $\tau = k_{\mathrm{B}}T$, where k_{B} is Boltzmann's constant, $Z(\tau) = \sum_i e^{-E_i/\tau}$ is the partition function, noting that the sum runs over all states of the system, and T is the temperature of the source distribution from which the two atoms were taken. Based on the conclusions for field ramps applied to pure states above, the application of a cooling cycle, defined as a slow field ramp from $B = B_1$ to $B = B_2$, followed by a fast ramp back to $B = B_1$, will exhibit two different types of behavior when applied to a mixed state. The first behavior is to decrease by approximately $2\hbar\omega$ the energy of the population in states which happen to undergo a full shift in the energy level between the field strengths of $B = B_1$ and $B = B_2$. The second behavior is to increase the energy of the population that happens to be the state that is degenerate with the resonance state, in other words, the state which is undergoing an energy shift at $B = B_2$. This happens because the population is moved to the state or states that are degenerate with the resonance at $B = B_1$. The state from which the population is heated originates will be denoted from this point by $n = Q$.

Figure 2.6 illustrates the results of a numerical simulation of a single cooling cycle

applied to a mixed, thermal distribution of s-wave states initial state of the system. The same model Feshbach-resonance parameters were used as the example shown in Fig. 2.4. The black line in Fig. 2.6 represents an initial s-wave relative-coordinate probability distribution for the the atom pair in a harmonic trap, again with frequency $\nu = 1\,\mathrm{MHz}$, and for a temperature $T = 1\,\mathrm{mK}$ of the source. The red line denotes the same s-wave probability distribution after the application of a slow and a fast magnetic field ramp, for a value of the cooling parameter $Q = 15$. It is clear that the application of a single cooling cycle transfers the population of the $n = Q$ state to states with much larger energy. In the example in the figure, this state is $n \approx 88$, as is evidenced by the spike seen in Fig. 2.6. As can also been seen, the field ramps transfer the population of each state with $n > Q$, states higher in energy than the Q state, each to the state next-lowest in energy, which has approximately $2\hbar\omega$ less energy than the initial state. The numerical simulations reveal that the net result of these two types of processes is to increase the overall average energy of the system. That is, the energy increase from the few cases where the pair gains a large amount of energy overwhelms the total energy decrease due to the many cases where the pair loses a small amount of energy. It turns out though, that this behavior is not entirely unexpected, as can be seen in Ref. [37] which discusses the general nature of cooling processes based on time-dependent Hamiltonians. However, it is important to note that, since the atoms gaining energy can be displaced to an arbitrarily high energy state, as determined by the values of the extremum of the field ramp ($B = B_1$ in Fig. 2.4), it should be possible to remove these atoms by utilizing methods similar to those used for atom removal in evaporative cooling.

At this point, it is interesting to observe the comparison of the Feshbach-resonance cooling scheme with the well-known evaporative cooling technique by which the most energetic atoms in a gas are allowed to escape, resulting in a colder remaining gas. The process described here is similar to a conceptual "fractional" evaporative cooling experiment, whereby the parameter Q is equivalent to the evaporative-cooling cutoff

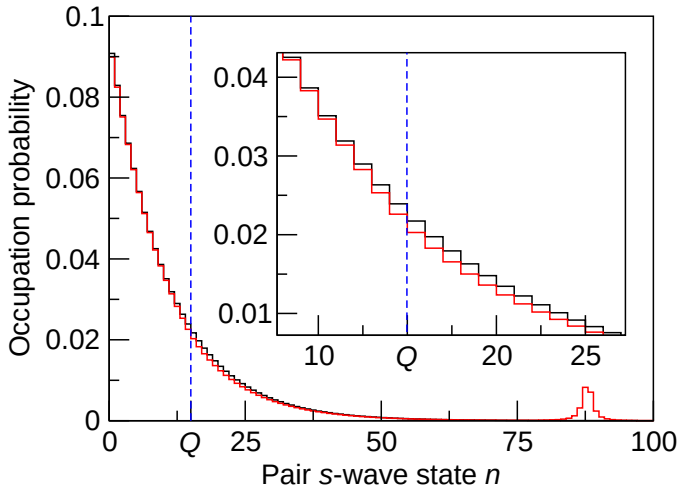

Figure 2.6: Illustration of the effect of a single Feshbach resonance cooling cycle for an atom pair taken from a thermal distribution with $T = 1\,\mathrm{mK}$ and trapped with frequency $\nu = 1\,\mathrm{MHz}$. The black (red) line represents the population distribution before (after) application of one slow and one fast magnetic field ramp. The state Q (here $Q = 15$) is indicated. This figure is adapted from Ref. [1].

parameter and, instead of all the population with $n > Q$ being removed, only a fraction of this population is skimmed off and removed from the trap. The similarity between the two methods can be clearly seen in Fig. 2.6. The nature of the cooling scheme are more explicitly shown in Fig. 2.7. Note, however, that cooling with a Feshbach-resonance scheme is differentiated from evaporative cooling by the fact that it is not fundamentally of a statistical nature. The more that is known about the atom pair's initial state, the more effectively the pair can be cooled. In fact, if the initial state of the pair is known with exact precision, not pulled from a thermal reservoir (as is the case for a pure state), it is possible to design a sequence of field-ramp that will allow the transition of an atom pair to the ground state of the trap 100% of the time in principle.

As with evaporative cooling, the requirement of atom removal leads to considerations of efficiency. An estimate of the efficiency can be made by assuming that the population of the state Q is removed from the trap, while the population of all states with $n > Q$ are moved to the next-lowest state, that is, to states with $n - 1$. This assumes that the range of the field ramps is such that the heated fraction ($n = Q$) ends up at an energy corresponding to negligible thermal population (as in Fig. 2.6), and that all population above a specified energy can be removed. If the level energies at $B = B_1$ are approximated by $E_n(B_1) \approx 2n\hbar\omega$, the probability to remove an atom pair during a cycle is

$$P_{\mathrm{rem}}(Q,\tau) = \frac{e^{-2\hbar\omega Q/\tau}}{Z(\tau)}. \tag{2.92}$$

The average energy decrease in a cooling cycle is due to the energy of the $n \approx Q$ population removed from the trap, plus the energy loss for states $n > Q$:

$$\Delta E(Q,\tau) = \left(2\hbar\omega Q + \langle E_{\mathrm{CM}}\rangle\right)\frac{e^{-2\hbar\omega Q/\tau}}{Z(\tau)} + \sum_{n=Q+1}^{\infty} 2\hbar\omega \frac{e^{-2\hbar\omega n/\tau}}{Z(\tau)}. \tag{2.93}$$

Noting that $\langle E_{\mathrm{CM}}\rangle = 3\tau$ (since $\langle E_{\mathrm{tot}}\rangle = 3\tau$ for a single atom in a harmonic trap), and with $\sum_{n=Q+1}^{\infty} e^{-2\hbar\omega n/\tau} \approx e^{-2\hbar\omega Q/\tau}\tau/2\hbar\omega$, Eq. (2.93) becomes

$$\Delta E(Q,\tau) = \frac{e^{-2\hbar\omega Q/\tau}}{Z(\tau)}\left(2\hbar\omega Q + 4\tau\right). \tag{2.94}$$

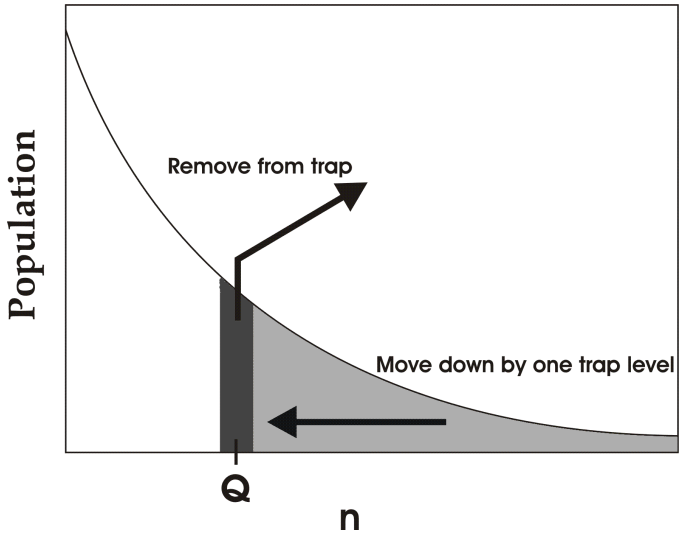

Figure 2.7: Diagram illustrating the effect of the Feshbach-resonance cooling scheme on an s-wave distribution of atoms. Shown is the population in arbitrary units as a function of the relative-coordinate quantum number n. Population from the state $n = Q$ is increased in energy, and assumed to be removed from the trap. All population with $n > Q$ is decreased in energy by one relative-coordinate oscillator unit of energy.

The energy efficiency E_{eff}, defined as the amount of energy removed per atom removed, is then given by

$$E_{\text{eff}}(Q,\tau) = 2\hbar\omega Q + 4\tau. \tag{2.95}$$

Since Q determines the efficiency of the cooling process, it is referred to as the cooling parameter. Results from the numerical model indicate that Eq. (2.95) provides a good estimate of the efficiency.

The time scale for one cooling cycle is determined by the speed of the adiabatic field ramp. This speed in turn is determined by the strength of the coupling between the resonance state and the trap states. The smaller the coupling for an avoided crossing, the slower is the field ramp required to maintain adiabaticity. The coupling between the resonance state and the trap states is related to the resonance width parameter Γ_E, which can be used in a Landau-Zener estimate of the transition probability [36],

$$P_{\text{tr}} \cong \exp\left(-\frac{2}{|\mathrm{d}B/\mathrm{d}t|}\frac{\omega\Gamma_E}{|\mathrm{d}E/\mathrm{d}B|}\right). \tag{2.96}$$

Motivated by the possibility of experimentally trapping a small, deterministic number of atoms [38, 39], the experimental feasibility of this cooling scheme is now explored. A Feshbach-resonance cooling experiment involves a sequence of cooling cycles. As discussed above, a single experiment could result in a heated atom pair, which in turn would be lost from the trap. To see the effect of multiple field ramps, Eqs. (2.92) and (2.93) can be iterated. For a variety of cooling efficiency parameters Q, Fig. 2.8 shows the probability for an atom pair to remain trapped vs. the average total kinetic energy (the energy of both the relative and the center-of-mass degrees of freedom) of the two atoms in oscillator units. Included in this calculation is the probability that the atom pair is in an s-wave state to begin with, because the field ramp has no effect on other partial waves. It is assumed that rethermalization occurs between cooling cycles, which could be ensured by, for example, introducing a slight anharmonicity into the trapping potential. (In the absence of anharmonicity, the relative and center-of-mass

degrees of freedom would remain uncoupled.)

To be more specific, a crossed-beam optical dipole trap [40] can be considered, which offers a good blend of large trap frequency (for a large s-wave fraction), isotropy, and anharmonicity (for rethermalization between the relative and center-of-mass degrees of freedom). Assuming the dipole trap has an average frequency of $\nu = 10\,\mathrm{kHz}$ and contains two atoms taken from a source with temperature $T = 8\,\mu\mathrm{K}$ ($\langle E_{\mathrm{tot}}\rangle/\hbar\omega = 100$), it is seen from Fig. 2.8, solid line, that a temperature of $0.16\,\mu\mathrm{K}$ ($\langle E_{\mathrm{tot}}\rangle/\hbar\omega = 2$, both atoms in the ground state) could be reached 10% of the time by performing less than 2000 cooling cycles. For a range in magnetic field for the ramps of $\Delta B \approx 1\,\mathrm{G}$, and using Eq. (2.96) with $P_{\mathrm{tr}} = 0.1$, it can be seen that such a series of field ramps could take place in under 1 s. A pertubative calculation accounting for the trap anharmonicity indicates that rethermalization between the relative and center-of-mass degrees of freedom should occur on a time scale comparable to a single ramp time for a crossed-beam dipole trap. This will ensure that the relative s-wave distribution will rethermalize with each ramp and that the cooling of the relative coordinate will also cool the center-of-mass coordinate (both of which have been assumed up to this point).

Feshbach resonance cooling could also be applied to atom pairs in an optical lattice. In this case, field ramps could be performed on the lattice ensemble of atom pairs, with a certain percentage of sites resulting in cooled pairs, while other sites will have either zero atoms or one (uncooled) atom. It may also be possible to prepare the optical lattice by some other means to have a high probability of exactly double occupancy at each lattice cite (see for example Ref. [41]). From such an initial state, a Feshbach resonance cooling scheme could be used to efficiently cool atom pairs to low-lying trap states.

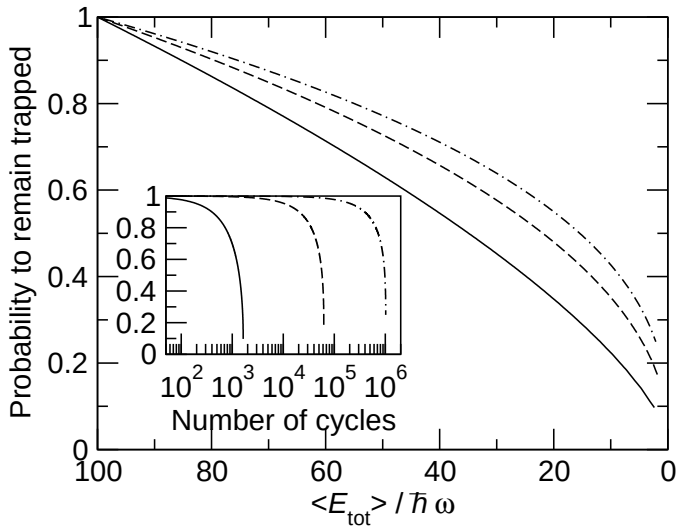

Figure 2.8: Probability that a pair of atoms remains trapped vs. the average total kinetic energy of the two atoms in oscillator units (note that $k_{\mathrm{B}}T = \langle E_{\mathrm{tot}} \rangle / 6$ for two harmonically trapped atoms). Three different cooling parameters are used: $2\hbar\omega Q = 5\tau$ (solid line), 9τ (dashed line), and 12τ (dot-dashed line). It is assumed that rethermalization occurs between cooling cycles (see text), although this scheme does not necessarily require it. Inset: probability to remain trapped vs. the number of cooling cycles for the same three cooling parameters. This figure is adapted from Ref. [1].

2.8 Conclusion

In summary, this chapter has developed a two-body theory that describes how the energy of an atom pair can be reduced. The resulting novel cooling scheme, which makes use of Feshbach resonances, offers a viable new means to manipulating small, deterministic numbers of trapped atoms [38, 39] with present-day technology. Since it is not clear at present how efficiently other cooling methods such as evaporation can be applied to small atom samples, this proposal may prove quite useful. Extension of this scheme to atom clouds is possible.

Chapter 3

Dynamics of Multilevel Atoms in Three-Dimensional Polarization-Gradient Fields

3.1 Introduction

This chapter continues the discussion of theoretical descriptions of cooling by focusing on the technique of using lasers to cool atoms. In particular the dynamics of atom-laser interactions is analyzed for atoms having multiple, closely spaced, excited-state hyperfine manifolds. The atom's motion is described in a polarization gradient field created by a three-dimensional laser configuration. .

The system is treated first in a semiclassical approximation, in which the center-of-mass of the atom is approximated to be a classical variable rather than a quantum-mechanical operator. This semiclassical problem allows much easier solutions than a fully quantum problem, and yields quantities with intuitive appeal because they are classical in nature. For example, the friction that an atom feels while moving in the optical field can be obtained, as well as the diffusion coefficient for the atom's motion. These two quantities work against each other to obtain a steady-state thermal distribution of a given temperature. In the end, such semiclassical approximations can be quite problematic and limited, as is the case when the atomic momentum approaches the recoil limit. Other problems can occur also: it is not unusual for semiclassical methods, when applied naively, to yield unphysical negative temperatures.

After this, the system is treated fully quantum mechanically, including the atom's

center-of-mass degree of freedom. The master equation describing this system is developed, and then specialized to the low-intensity limit by adiabatically eliminating the excited states. It is shown how this master equation can be simulated using the Monte Carlo wave function technique, and details are provided on the implementation of this procedure.

Monte Carlo calculations of steady state atomic momentum distributions for two fermionic alkaline earth isotopes, ^{25}Mg and ^{87}Sr, interacting with a three-dimensional lin-$\perp$-lin laser configuration are presented, providing estimates of experimentally achievable laser-cooling temperatures.

The complex behavior that occurs when a multilevel atom interacts with polarization-gradient fields has been of interest for some time now. Sub-Doppler cooling [42] occurs because of elaborate optical-pumping processes produced by laser light in atoms with sublevel structure, as seen, for example, in the lin-$\perp$-lin and the σ_+-σ_- laser configurations. The semiclassical understanding of these interactions [16, 17, 43, 44, 45, 46] in one or more dimensions has led to a reasonably good qualitative understanding of the underlying mechanisms. Semiclassical analysis has even in some cases provided quantitative predictions of sub-Doppler laser cooling temperatures measured in experiments [46].

However, the most direct route to a quantitative understanding of atom-laser interactions is via a fully quantized master equation for the atom, in which the center-of-mass motion of the atom is taken into account quantum mechanically. This allows behavior at low laser intensities and low atomic velocities, the regime laser cooling strives to reach, to be described correctly. The drawback of solving such a master equation, however, is the large number of basis states required for the calculation, due to the additional momentum states. This problem becomes especially pronounced when attempting to model three-dimensional systems, where the state space grows as the cube of the number of one-dimensional momentum states needed.

The Monte Carlo wave-function (MCWF) technique, introduced in the early

1990's has allowed significant progress to be made on the subject of atom-photon interactions in three dimensions as well as lower-dimensional calculations. The MCWF technique is a simulation procedure for the master equation that involves propagation of single stochastic wave functions, rather than density operators, with random processes occurring at random intervals due to interactions with the photon field that cause spontaneous emission. It has been shown that this method is equivalent to the master equation in the limit of a large number of independent stochastic wave functions [10]. The MCWF technique has been successfully utilized to calculate three-dimensional sub-Doppler laser cooling temperatures for atoms with Zeeman degeneracy in the ground and excited states [11].

The majority of the research done on laser cooling has involved essentially two-level systems, consisting of a ground state and an excited state, which may or may not contain degenerate sublevels. However, some investigations have explored atomic systems in which multiple distinct excited states come into play. In particular, the use of bichromatic laser fields [47, 48] to cool three-level Λ systems have been extensively studied (see Refs. [49, 50, 51] for example).

The focus in this chapter is primarily on monochromatic laser cooling for atoms with multiple closely spaced hyperfine excited-state manifolds. Figure 3.1 provides a graphical illustration of this type of atomic configuration. This situation is of importance, for example, in alkaline-earth atoms with nonzero nuclear magnetic moment. If the excited state manifolds are spaced in energy on the order or smaller than the excited state linewidth Γ, coherences between these manifolds become nonnegligible, and can have a significant effect on the optical pumping processes required for sub-Doppler cooling and on the dynamics of the atom-photon interaction. Sub-Doppler laser cooling was experimentally identified in fermionic ^{87}Sr [52], despite significant spectral overlap in the excited state. At the time, it was hypothesized that the large ground-state degeneracy in ^{87}Sr (due to the large nuclear spin $I = 9/2$) was somehow able to overcome the de-

crease in cooling due to the spectral overlap. Other systems with spectral overlap in the excited state are ^{39}K [53], ^{7}Li [54], and the fermionic isotopes of Yb [55]. In ^{87}Rb, the effects of excited-state spectral overlap on the effectiveness of velocity-selective coherent population trapping have been explored, both experimentally and theoretically [56]. The goal in this chapter is to provide a detailed discussion of the theoretical techniques required to model such systems realistically.

The structure of this chapter is as follows. Section 3.2 develops the master equation for a laser-driven atom with multiple excited-state manifolds. Within this section, the a general fully quantized master equation is first derived, pulling from the detailed derivation of the spontaneous-emission relaxation operator in Appendix B. Next, this master equation is specialized to the low-intensity limit, which reduces the number of internal atomic states necessary to describe the problem, and which is justified for the low-power laser configurations which result in optimum cooling of the gas. Section 3.3 then goes on to demonstrate the semiclassical method of solving this problem, with results provided which will aid in a qualitative understanding of the later, more quantitative results obtained from the Monte Carlo. Section 3.4 introduces the MCWF technique and applies it to the low-intensity master equation. Section 3.5, full Monte Carlo master-equation simulations are performed for ^{25}Mg and ^{87}Sr atoms in a three-dimensional lin-$\perp$-lin laser configuration as an example of using this technique determine expected temperatures for these atoms in a laser cooling experiment.

Parts of this chapter are developed from research by this author which has been published in Ref. [2], and some of the text and figures have been adapted from the work therein.

3.2 Master equation

In this section we develop the master equation describing a multilevel atom interacting with a coherent laser field and coupled to a vacuum photon field. It is this

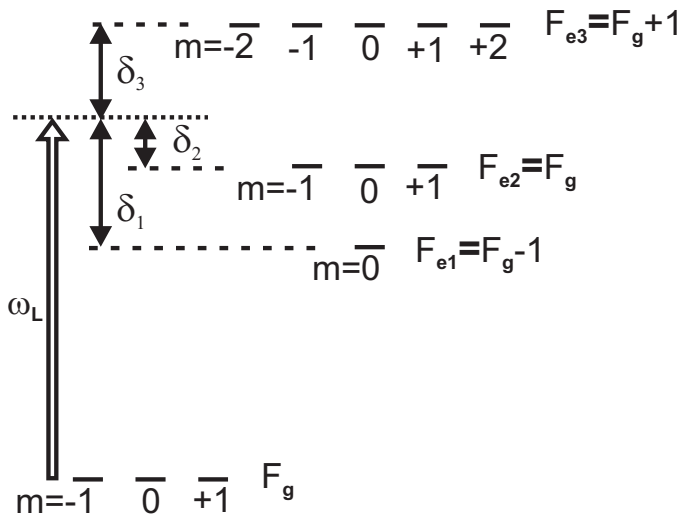

Figure 3.1: Energy level diagram of an atom with multiple hyperfine manifolds. If the energy spacing of the excited-state manifolds are of the order or smaller than the natural linewidth of the transition, the usual sub-Doppler cooling transition ($F_g \leftrightarrow F_e = F_g + 1$) is not isolated and the other manifolds must be taken into account. This figure is adapted from Ref. [2].

equation, with quantized atomic center-of-mass, that will provide an accurate description of atom-photon dynamics, and this master equation will provide the basis for the Monte Carlo simulations that will be discussed later.

3.2.1 General form of the master equation

The full Hamiltonian for the atom-laser system plus the radiation field is

$$H = H_A + H_R + V_{A-L} + V_{A-R}, \tag{3.1}$$

where $H_A = \sum_i \hbar\omega_i P_i + \frac{P^2}{2m}$ is the bare atomic Hamiltonian, H_R is the vacuum radiation field Hamiltonian, and V_{A-L} and V_{A-R} are the atom-laser and atom-radiation field coupling terms, respectively. In the atomic Hamiltonian, P_i is a projection operator onto the i-th internal excited-state manifold, $\hbar\omega_i$ is the energy of the i-th excited-state manifold relative to the ground-state manifold, P is the atomic center-of-mass momentum operator, m is the atomic mass, and the sum runs over all excited-state manifolds. Equation (3.1) assumes that the effects of atom-laser and atom-radiation-field coupling are independent [8].

Equation (3.1) can be viewed in terms of system-reservoir interactions. The system consists of the atom, the laser, and their interaction. The system Hamiltonian is

$$H_S = H_A + V_{A-L}. \tag{3.2}$$

The reservoir is the vacuum radiation field, having many more modes than the system. With the Markov approximation, along with a few other approximations, the master equation is then given by

$$\dot{\sigma} = \frac{i}{\hbar}\left[\sigma, H_S\right] + \mathcal{L}_{\rm sp}[\sigma]. \tag{3.3}$$

The operator σ is the system reduced density operator element, i.e., the reservoir degrees of freedom have been traced over, $\sigma = \mathrm{Tr}_R\rho$. The remaining term, $\mathcal{L}_{\rm sp}[\sigma]$, encompasses

the interaction between the atom and the vacuum photon field, and provides for the phenomenon of spontaneous emission.

The relaxation operator due to spontaneous emission, which is derived in detail in the Appendix B, is given by

$$\mathcal{L}_{\rm sp}[\sigma] = \frac{3\Gamma}{8\pi}\int d^2\Omega \sum_{\boldsymbol{\epsilon}\perp\mathbf{k}}\sum_{i,j} e^{-i\mathbf{k}\cdot\mathbf{R}}(\boldsymbol{\epsilon}^*\cdot\mathbf{A}^{(i)})\sigma(\boldsymbol{\epsilon}\cdot\mathbf{A}^{(j)\dagger})e^{i\mathbf{k}\cdot\mathbf{R}} - \frac{3\Gamma}{16\pi}\int d^2\Omega \sum_{\boldsymbol{\epsilon}\perp\mathbf{k}}\sum_{i,j}\Big[(\boldsymbol{\epsilon}\cdot\mathbf{A}^{(i)\dagger})e^{i\mathbf{k}\cdot\mathbf{R}}e^{-i\mathbf{k}\cdot\mathbf{R}}(\boldsymbol{\epsilon}^*\cdot\mathbf{A}^{(j)})\sigma + \sigma(\boldsymbol{\epsilon}\cdot\mathbf{A}^{(i)\dagger})e^{i\mathbf{k}\cdot\mathbf{R}}e^{-i\mathbf{k}\cdot\mathbf{R}}(\boldsymbol{\epsilon}^*\cdot\mathbf{A}^{(j)})\Big], \quad (3.4)$$

where $\mathbf{A}^{(i)\dagger}$ and $\mathbf{A}^{(i)}$ are vector raising and lowering operators, respectively, between the ground state and the ith excited state, $\mathbf{R}$ is the atomic center-of-mass position, $\mathbf{k}$ is the direction of the photon emitted in the relaxation process, and Γ is the decay rate of the exited states. The integral is performed over solid angle in the vector $\mathbf{k}$ and the sum over $\boldsymbol{\epsilon}\perp\mathbf{k}$ refers to the two polarization directions perpendicular to $\mathbf{k}$. Note that here and throughout this chapter, it is assumed that each of the excited-state hyperfine manifolds has the same lifetime $\tau=\Gamma^{-1}$. Expanding these vector operators in a basis of spherical unit vectors, $\hat{\epsilon}_{\pm1}=\mp(\hat{x}\pm i\hat{y})/\sqrt{2}$ and $\hat{\epsilon}_0=\hat{z}$, we have

$$\mathbf{A}^{(i)} = \sum_{q=0,\pm1}(-1)^q\hat{\epsilon}_{-q}A_q^{(i)}. \quad (3.5)$$

The spherical components of the vector operators are

$$A_q^{(i)} = \sum_{M_g,M_{e_i}} \alpha_{F_g,F_{e_i},M_g,M_{e_i},J_g,J_e,I}\,|J_gIF_gM_g\rangle\langle J_eIF_{e_i}M_{e_i}| \quad (3.6)$$

$$A_q^{(i)\dagger} = \sum_{M_g,M_{e_i}} \alpha_{F_g,F_{e_i},M_g,M_{e_i},J_g,J_e,I}\,|J_eIF_{e_i}M_{e_i}\rangle\langle J_gIF_gM_g|, \quad (3.7)$$

where

$$\alpha_{F_g,F_{e_i},M_g,M_{e_i},J_g,J_e,I} = (-1)^{F_g+F_{e_i}+M_g+J_e+I}\sqrt{(2F_g+1)(2F_{e_i}+1)(2J_e+1)} \times \begin{pmatrix} F_g & 1 & F_{e_i}\\ -M_g & M_g-M_{e_i} & M_{e_i}\end{pmatrix}\begin{Bmatrix} J_g & F_g & I\\ F_{e_i} & J_e & 1\end{Bmatrix}. \quad (3.8)$$

Eq. (3.4) is written in a way that makes explicit that it is in Lindblad form [57, 58, 59]. As will be shown later, it is important for the relaxation operator to be of this form in order to make use of the MCWF technique. Because the complex exponentials in the second line cancel each other, the remaining integral over solid angle can be evaluated, whereby Eq. (3.4) can be equivalently written as [10]

$$\mathcal{L}_{\rm sp}[\sigma] = \frac{3\Gamma}{8\pi}\int d^2\Omega \sum_{\boldsymbol{\epsilon}\perp\mathbf{k}}\sum_{i,j} e^{-i\mathbf{k}\cdot\mathbf{R}}(\boldsymbol{\epsilon}^*\cdot\mathbf{A}^{(i)})\sigma(\boldsymbol{\epsilon}\cdot\mathbf{A}^{(j)\dagger})e^{i\mathbf{k}\cdot\mathbf{R}} - \frac{\Gamma}{2}\sum_i \left[P_{e_i}\sigma + \sigma P_{e_i}\right]. \quad (3.9)$$

The atom-laser interaction term, which is given in the electric-dipole approximation by

$$V_{A-L}(\mathbf{R},t) = -\mathbf{D}\cdot\mathbf{E}_L(\mathbf{R},t), \quad (3.10)$$

where $\mathbf{E}_L(\mathbf{R},t)$ is the electric field of the laser and $\mathbf{D}$ is the electric dipole operator. As is typical, the laser is treated as a classical field, since it is a densely populated mode of the electric field. The laser electric field can be written in terms of its positive and negative frequency components, $\mathbf{E}_L(\mathbf{R},t) = \mathbf{E}_L^{(+)}(\mathbf{R})e^{-i\omega t} + \text{c.c.}$, and then expanded into spherical components,

$$\mathbf{E}_L^{(+)}(\mathbf{R}) = \frac{E_0}{2}\sum_{q=0,\pm1}(-1)^q a_q(\mathbf{R})\hat{\epsilon}_{-q}, \quad (3.11)$$

where E_0 is the electric-field amplitude and $a_q(\mathbf{R})$ are the expansion coefficients. Making the rotating-wave approximation, so that

$$V_{A-L}(\mathbf{R},t) = -\mathbf{D}^{(+)}\cdot\mathbf{E}_L^{(+)}(\mathbf{R})e^{-i\omega t} - \mathbf{D}^{(-)}\cdot\mathbf{E}_L^{(-)}(\mathbf{R})e^{i\omega t}, \quad (3.12)$$

where $\mathbf{D}^{(+)} = \sum_i P_{e_i}\mathbf{D}P_g$ and $\mathbf{D}^{(-)} = \sum_i P_g\mathbf{D}P_{e_i}$, we find

$$V_{A-L} = -\frac{\Omega}{2}\sum_i \mathcal{D}_i(\mathbf{R})e^{-i\omega t} + \text{H.c.}. \quad (3.13)$$

The previous equation introduced the atom-laser raising operator,

$$\mathcal{D}_i^\dagger(\mathbf{R}) = \sum_{q=0,\pm1} a_q(\mathbf{R})A_q^{(i)\dagger}, \quad (3.14)$$

and lowering operator,

$$\mathcal{D}_i(\mathbf{R}) = \sum_{q=0,\pm1} a_q^*(\mathbf{R}) A_q^{(i)}, \tag{3.15}$$

and also introduced the so-called "invariant" Rabi frequency,

$$\Omega = \frac{E_0 \langle J_e || D || J_g \rangle}{\sqrt{2J_e + 1}}, \tag{3.16}$$

where $\langle J_e || D || J_g \rangle$ is the reduced dipole matrix element between the ground and excited states. This form of a Rabi frequency, defined in terms of the reduced matrix element between the $J = J_g$ ground state and the $J = J_e$ excited state, is convenient because, in general, Rabi frequencies for transitions to different excited-state manifolds will not be the same.

Next, observe that the second term in Eq. (3.9) is comprised of excited-state projection operators both pre- and post-multiplying the system density operator. Thus, it is clear that this term can be absorbed into the free-evolution commutator term in Eq. (3.3), allowing the master equation to be equivalently described by Hamiltonian evolution determined by an effective Hamiltonian H_{eff}, plus a term which is commonly called a jump term, and which cannot be written in the form of a commutator with the system density operator. This results in

$$\dot{\sigma} = -\frac{i}{\hbar}\left(H_{\text{eff}}\sigma - \sigma H_{\text{eff}}^\dagger\right) + \frac{3\Gamma}{8\pi}\int d^2\Omega \sum_{\boldsymbol{\epsilon}\perp\mathbf{k}} \sum_{i,j} e^{-i\mathbf{k}\cdot\mathbf{R}} (\boldsymbol{\epsilon}^* \cdot \mathbf{A}^{(i)}) \sigma (\boldsymbol{\epsilon} \cdot \mathbf{A}^{(j)\dagger}) e^{i\mathbf{k}\cdot\mathbf{R}}, \tag{3.17}$$

where the effective Hamiltonian H_{eff} is given by

$$H_{\text{eff}} = \frac{P^2}{2m} - \sum_i \hbar\left(\delta_i + i\frac{\Gamma}{2}\right) P_{e_i} + V_{A-L}, \tag{3.18}$$

where V_{A-L} is as given in Eq. (3.13). In obtaining Eqs. (3.17) and (3.18), the usual rotating-frame transformation, which removes the free-evolution atomic Bohr frequencies from the problem, has been made. The more relevant frequencies are instead the laser detunings $\delta_i = \omega - \omega_i$ from the ith excited-state hyperfine manifold. The master equation given in Eq. (3.17) is fully general, but has been written in a form that will

facilitate setting up a stochastic wave function simulation using the MCWF technique described later.

3.2.2 Master equation in the low-intensity limit: adiabatic elimination of excited states

The master equation just discussed will now be specialized to the limit of low laser intensity. Specifically, this limit is valid when the saturation parameter for the atom in the ith excited-state hyperfine manifold,

$$s_i = \frac{\Omega^2/2}{\delta_i^2 + (\Gamma/2)^2}, \tag{3.19}$$

is small, which occurs when the laser intensity is small or the laser detuning from the atomic transition is large. In this limit, the excited states are said to adiabatically follow the ground states. The excited states can then be eliminated from the equations of motion, resulting in a master equation in terms of only the ground-state sub-density-matrix,

$$\sigma_{gg} = P_g \sigma P_g. \tag{3.20}$$

In this limit, the master equation becomes (see section 8.3.3 of Ref. [60])

$$\dot{\sigma}_{gg} = -\frac{i}{\hbar}\left(h_{\text{eff}}\sigma_{gg} - \sigma_{gg}h_{\text{eff}}^\dagger\right) + \int d^2\Omega \sum_{\boldsymbol{\epsilon}\perp\mathbf{k}} \sum_{i,j} (\boldsymbol{\epsilon}^* \cdot \mathbf{B}^{(i)}(\mathbf{R},\mathbf{k}))\sigma_{gg}(\boldsymbol{\epsilon}\cdot\mathbf{B}^{(i)^\dagger}(\mathbf{R},\mathbf{k})). \tag{3.21}$$

The new effective Hamiltonian is given by

$$h_{\text{eff}} = \frac{P^2}{2m} + \sum_i \frac{s_i}{2}\hbar\left(\delta_i - i\frac{\Gamma}{2}\right)\mathcal{D}^{(i)}(\mathbf{R})\mathcal{D}^{(i)^\dagger}(\mathbf{R}). \tag{3.22}$$

The new decay raising and lowering operators are given by

$$B_q^{(i)^\dagger}(\mathbf{R},\mathbf{k}) = \sqrt{\frac{3s_i\Gamma}{8\pi}} A_q^{(i)^\dagger} e^{i\mathbf{k}\cdot\mathbf{R}} \mathcal{D}^{(i)}(\mathbf{R}), \tag{3.23}$$

and

$$B_q^{(i)}(\mathbf{R},\mathbf{k}) = \sqrt{\frac{3s_i\Gamma}{8\pi}} A_q^{(i)} e^{-i\mathbf{k}\cdot\mathbf{R}} \mathcal{D}^{(i)^\dagger}(\mathbf{R}). \tag{3.24}$$

Note that this new lowering (raising) operator contains two components: a raising (lowering) operator $\mathcal{D}^{(i)\dagger}(\mathbf{R})$ ($\mathcal{D}^{(i)}(\mathbf{R})$) between the ground state and the ith excited-state manifold due to the atom-laser interaction, and a lowering (raising) operator $A_q^{(i)\dagger} e^{i\mathbf{k}\cdot\mathbf{R}}$ ($A_q^{(i)} e^{-i\mathbf{k}\cdot\mathbf{R}}$) of type q corresponding to coupling with the reservoir photon field via a photon with polarization q. Thus, the jump operator in the low-intensity equations describes a transition cycle of the atom involving coupling to both the laser and the reservoir photon field. Note also that this new operator and the effective-Hamiltonian term in the equation of motion are both proportional to the saturation parameter s_i, the perturbation parameter.

3.3 Direct solutions of the semiclassical master equation

In Appendix C, the semiclassical master equation is derived in detail. This section presents an overview of solution techniques of the resulting equations, called the optical Bloch equations because of their similarity to the Bloch equations that describe the precession of a nuclear magnetic moment in a magnetic field.

The optical Bloch equations for the multilevel atomic system considered here are,

$$\dot{\tilde{\rho}}\left(e_i^{(m)}, g_j\right) = i\left[\delta\omega^{(m)} - \Delta - k_L v(i-j)\right]\tilde{\rho}\left(e_j^{(m)}, g_i\right) - \frac{i}{\hbar}e^{i\omega_L t}\left[\tilde{V}, \tilde{\rho}\right]_{\left(e_i^{(m)}, g_j\right)} \tag{3.25}$$

$$\dot{\tilde{\rho}}\left(g_i, e_j^{(m)}\right) = i\left[\Delta - \delta\omega^{(m)} - k_L v(i-j)\right]\tilde{\rho}\left(g_i, e_j^{(m)}\right) - \frac{i}{\hbar}e^{-i\omega_L t}\left[\tilde{V}, \tilde{\rho}\right]_{\left(g_i, e_j^{(m)}\right)} \tag{3.26}$$

$$\dot{\tilde{\rho}}\left(g_i, g_j\right) = -ik_L v(i-j)\tilde{\rho}\left(g_i, g_j\right) - \frac{i}{\hbar}\left[\tilde{V}, \tilde{\rho}\right]_{(g_i, g_j)} \tag{3.27}$$

$$\dot{\tilde{\rho}}\left(e_i^{(m)}, e_j^{(n)}\right) = i\left[\delta\omega^{(m)} - \delta\omega^{(n)} - k_L v(i-j)\right]\tilde{\rho}\left(e_i^{(m)}, e_j^{(n)}\right) - \frac{i}{\hbar}\left[\tilde{V}, \tilde{\rho}\right]_{\left(e_i^{(m)}, e_j^{(n)}\right)}. \tag{3.28}$$

The above equations describe the evolution of the various matrix elements of the density matrix, with the shorthand notation $\rho(i,j) = \langle i|\rho|j\rangle$. The subscripts on the commutators likewise indicate a matrix element, $[,]_{i,j} = \langle i|[,]j\rangle$. The tildes over the density

matrix elements imply the following redefinition corresponding to optical coherences as

$$\tilde{\rho}\left(e_i^{(m)}, g_j\right) \rightarrow \tilde{\rho}\left(e_i^{(m)}, g_j\right) e^{i\omega_L t}, \tag{3.29}$$

$$\tilde{\rho}\left(g_i, e_j^{(m)}\right) \rightarrow \tilde{\rho}\left(g_i, e_j^{(m)}\right) e^{-i\omega_L t}. \tag{3.30}$$

For elements that are not optical coherences, the redefinition has no effect.

This system of equations can be solved by putting the various matrix elements of $\tilde{\rho}$ into a vector, corresponding to all of the possible combinations of N internal atomic states and yielding a N^2 elements. The optical Bloch equations given above then provide an $N^2 \times N^2$ matrix, labeled here as $\mathbf{M}_{sc}$, for the time evolution of the ρ vector,

$$\dot{\tilde{\rho}} = \mathbf{M}_{sc}\tilde{\rho}. \tag{3.31}$$

This equation can be solved by specifying an initial state for $\tilde{\rho}$ and numerically integrating the above differential matrix equation. For atomic systems with on the order of 10 to 100 internal states, this is usually numerically tractable.

If only the steady state of the system is desired, as is the case here in which final laser-cooling temperature is the goal, it is faster to simply set $\dot{\tilde{\rho}} = 0$ in the above equation and then solve for $\tilde{\rho}$. This involves a numerical inversion of the matrix $\mathbf{M}_{sc}$. However, this matrix is singular and cannot be inverted. It turns out that the system is overspecified, and this can be remedied by supplying the additional condition that the sum of the populations is always equal to unity, a fundamental requirement for the density matrix of a system with conserved norm. This condition can be enforced by modifying one of the rows of $\mathbf{M}_{sc}$ corresponding to a population element to have zeros in all locations except population elements. Then, the steady state solution to the matrix equation is given by

$$\tilde{\rho}_{ss} = \mathbf{M}_{sc}^{-1}\mathbf{v}, \tag{3.32}$$

where $\mathbf{v}$ is a vector with all zeros except for a 1 in the position corresponding to the modified row of $\mathbf{M}_{sc}$.

Once the steady-state density matrix of the system is obtained, any steady-state properties of the system can be determined by performing traces over this density matrix multiplied by the appropriate quantum mechanical operator $\hat{O}$

$$O = \langle \hat{O} \rangle = \mathrm{Tr}\left[\hat{O}\tilde{\rho}_{ss}\right]. \tag{3.33}$$

3.4 Stochastic wave-function solutions of the fully quantum master equation

The MCWF [9, 10, 11, 12, 13, 14, 15] technique is a means of interpreting a system-reservoir master equation — which describes the evolution of a density operator for a system interacting with a large external reservoir — as the evolution of an ensemble of individual wave functions, each undergoing random quantum jumps. The free evolution of the stochastic wave functions is determined by the effective Hamiltonian that was derived in section 3.2. The nature of the quantum jumps is determined by the leftover term in the master equation, which cannot be absorbed into the free-evolution commutator. The components of this leftover term are often called quantum-jump operators.

The following discussion will deal primarily with the master equation in the low-intensity limit, as developed in the previous section, although the methods could just as easily be applied to the arbitrary-intensity master equation. The low-intensity limit, however, provides a reduction in the number of internal atomic states required in the calculation, and this will be beneficial for performing calculations later. Furthermore, since the lowest temperatures are achieved for low laser intensities, such a specialization does not hinder the ability to calculate lower bounds of temperature.

Having already expressed the master equation in a form involving an effective Hamiltonian and a jump term, the application of the MCWF technique is rather straightforward along the lines developed in the literature (see, in particular, Ref. [10]). For a single stochastic wave function, the procedure is as follows. First, set the wave function

to an initial value. Then, numerically propagate the wave function for a time step δt according to the effective Hamiltonian H_{eff} only, from an initial value $|\psi(t)\rangle$ to a final value $|\psi^{(1)}(t+\delta t)\rangle$,

$$|\psi^{(1)}(t+\delta t)\rangle = \left(1 - \frac{iH_{\text{eff}}\delta t}{\hbar}\right)|\psi(t)\rangle\,. \tag{3.34}$$

Restrictions on the size of δt are given such that the first-order truncation of the time-evolution operator in Eq. (3.34) is approximately valid. We note that H_{eff} is non-Hermitian by construction, as a result of absorbing parts of the relaxation operator into the original (Hermitian) bare system Hamiltonian. Because of this, propagation with H_{eff} will not conserve the norm of the wave function when propagated to $|\psi^{(1)}(t+\delta t)\rangle$. The time step δt of the propagation must be chosen so that $\delta p \ll 1$ in the inner product,

$$\left\langle \psi^{(1)}(t+\delta t) \,\middle|\, \psi^{(1)}(t+\delta t) \right\rangle = 1 - \delta p. \tag{3.35}$$

The quantity δp is the loss of norm resulting from propagating with H_{eff} for a time step δt, and is found to be

$$\begin{aligned}
\delta p &= \delta t \,\langle\psi(t)| \sum_i \mathbf{B}^{(i)\dagger}(\mathbf{R},\mathbf{k}) \cdot \mathbf{B}^{(i)}(\mathbf{R},\mathbf{k})|\psi(t)\rangle \\
&= \delta t \,\langle\psi(t)| \sum_i \sum_{q=0,\pm1} B_q^{(i)\dagger}(\mathbf{R},\mathbf{k}) B_q^{(i)}(\mathbf{R},\mathbf{k})|\psi(t)\rangle \\
&= \sum_i \sum_{q=0,\pm1} \delta p_{i,q}.
\end{aligned} \tag{3.36}$$

The total loss of norm has been decomposed into individual elements each corresponding to a particular type of interaction with the reservoir (i.e., the q-value of the interaction, or the excited state i involved). These individual contributions are given by

$$\delta p_{i,q} = \delta t \,\langle\psi(t)| B_q^{(i)\dagger}(\mathbf{R},\mathbf{k}) B_q^{(i)}(\mathbf{R},\mathbf{k})|\psi(t)\rangle\,. \tag{3.37}$$

It is seen that the loss of norm due to a given type of interaction with the reservoir is determined by the quantum-mechanical expectation value of the product of jump operators of this type of interaction. The loss of norm δp can also be interpreted as the probability for a quantum jump to occur.

After the wave function has been propagated as described above, and the values of $\delta p_{i,q}$ calculated, it must then be determined whether or not a quantum jump occurred. This is achieved by generating a pseudo-random number on a computer and comparing it to the value of the total jump probability δp. If the random number is less than δp, a quantum jump occurred, and if it is greater, no quantum jump occurred. If a quantum jump does occur, the type of quantum jump must also be calculated by comparing the random number with the individual sub-probabilities $\delta p_{i,q}$ in the same manner.

If a quantum jump of type q, i occurs, the quantum jump lowering operator $B_q^{(i)}(\mathbf{R}, \mathbf{k})$ must be applied to the wave function from the beginning of the time step,

$$|\psi(t+\delta t)\rangle = \sqrt{\frac{\delta t}{\delta p_{i,q}}} B_q^{(i)}(\mathbf{R}, \mathbf{k}) \, |\psi(t)\rangle \, . \tag{3.38}$$

The square-root factor in front of the lowering operator is necessary for renormalization. If no quantum jump occurs, then the stochastic wave function is simply renormalized.

The resulting wave function is then used as the starting point for propagation over the next time step, and the procedure is repeated.

A good approximation of the true system density matrix is achieved by combining the trajectories of a number of independently propagated stochastic wave functions, each trajectory having a unique sequence of pseudo-random numbers. (A thorough discussion of the statistical issues involved with the MCWF technique can be found in Ref. [10].) Once a suitable ensemble of stochastic wave function trajectories has been obtained, an estimate of the true expectation value of an operator is found by taking the ensemble average of the expectation value of that operator with respect to the stochastic wave functions. For example, an estimate of the average kinetic energy at a time t for a system for which N independent stochastic wave functions have been calculated is given by

$$\langle E \rangle (t) = \frac{1}{N} \sum_{i=1}^{N} \left\langle \psi_i(t) \left| \frac{P^2}{2m} \right| \psi_i(t) \right\rangle , \tag{3.39}$$

where $\psi_i(t)$ is the ith stochastic wave function, given at time t.

Figure 3.2 demonstrates a simple example of the application of the MCWF technique, wherein the average kinetic energy is calculated for a two-level atom interacting with a one-dimensional standing-wave field. For this calculation, we have used a Rabi frequency of $\Omega = \Gamma/2$ and a detuning of $\delta = -\Gamma/2$, where Γ is the decay rate of the upper to the lower atomic state, and we have set $\Gamma = 400E_{\rm rec}$, where $E_{\rm rec} = \hbar^2k^2/2m$ is the recoil energy. The atomic kinetic energy, averaged over 500 stochastic wave functions each initialized to zero momentum, is plotted as a function of time, with error bars indicating the error in the ensemble average for a given time. The separation of the transient relaxation period from the steady-state is clear, the steady state regime being characterized by fluctuations in the average energy about a mean. This noise is due to the finite number of stochastic wave functions being used, and if a greater number of wave functions were used, the amplitude of the fluctuations would be decreased. In the limit of an infinite number of wave functions, the true density-matrix solution of the master equation would be obtained. An estimate of the steady-state kinetic energy is found by time-averaging the calculated data over the entire steady-state regime. Since this is a larger ensemble than the set of wave functions for a single time, the error of such an average will be smaller than the error bars shown in the figure.

As a test of the model, it is useful to perform a calculation for which the analytical solution is known. For a two-level atom moving in a one-dimensional field of two opposing, linearly polarized lasers, it is expected that the steady-state temperature will coincide with the Doppler limit when the detuning is set to it's optimal value of $\delta = -\Gamma/2$, and when the intensity of the laser is vanishing, $\Omega \to 0$. This limiting temperature is achieved because there is no internal structure to the atom which would allow sub-Doppler dynamics. Generally, in the literature, the Doppler limit will be quoted as $T_D = \hbar\Gamma/2k_B$. This value of the Doppler temperature is useful as a rough estimate, and, indeed, most experiments are unable to sufficiently eliminate heating factors — such as background-gas collisions and imperfections in the laser — to warrant such precision in

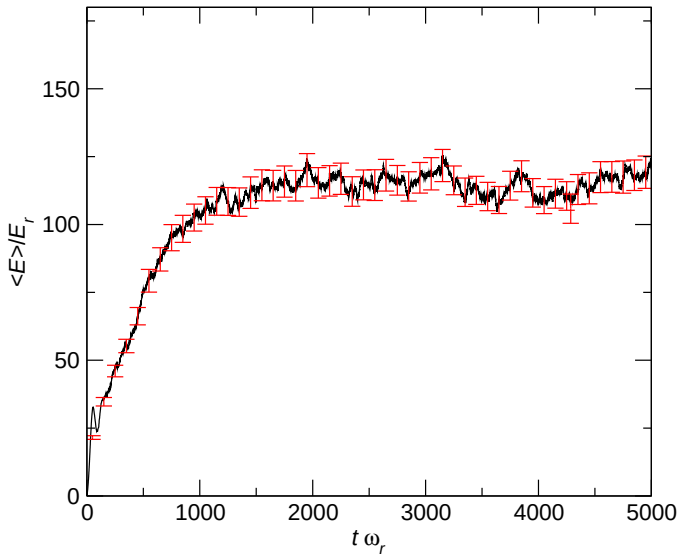

Figure 3.2: An example of a characteristic MCWF stochastic trajectory. Shown is the average of the atomic center-of-mass energy over 500 independent stochastic wave functions, as a function of time, for a two-level atom in a 1D standing-wave laser field. The energy is given in units of the recoil energy $E_{\rm rec} = \hbar^2 k^2/2m$, and time is given in units of the inverse recoil frequency $\omega_r^{-1} = \hbar/E_{\rm rec}$. All wave functions are initialized in the ground state of the atom and localized in momentum space with zero momentum. The steady state, wherein the system fluctuates around an average value, is seen to be achieved after a transient relaxation period. Error bars indicate the variance in the data at each given time for the ensemble of 500 stochastic wave functions. An estimate of the steady-state atomic center-of-mass energy is obtained by performing a time-average over all wave functions for all times after the relaxation regime. The error bar of such an average will be smaller than the error bars in the figure, which apply only to the data for a given time. This figure is adapted from Ref. [2].

the first place. However, to check the Monte Carlo calculations, a more accurate value will be needed, as is obtained in the 1989 paper by Castin, Wallis, and Dalibard [61], in which they survey the analytical understanding of Doppler atom-laser dynamics. Using an innovative technique called the *Family Method*, they find that the one-dimensional Doppler limit is in fact $T_D = 7\hbar\Gamma/40k_B$. Employing a Monte Carlo wave-function calculation for this rather trivial system with $\delta = -\Gamma/2$ and $\Gamma = 400\,\omega_{\rm rec}$, and performing the calculation for a variety of laser intensities, the limiting behavior shown in Fig. 3.3 is found, with the dots indicating the numerical results of the Monte Carlo calculation, and a quadratic fit to the data denoted by a solid line. In the low-intensity limit, the temperature goes to $T_D = \frac{7}{40}\,\hbar\Gamma/k_B = 70\,\hbar\omega_{\rm rec}/k_B$, in agreement with the result of Castin *et al.* [61].

3.5 Calculations for ^{25}Mg and ^{87}Sr

The purpose of this section is to illustrate the application of the theory developed up to this point to a complicated system. We wish to quantitatively study the dynamics of particular atoms interacting with three-dimensional polarization-gradient laser fields. The balance of the frictional cooling forces along with the diffusion experienced by the atom due to spontaneous emission and its interaction with the laser leads to a steady-state momentum distribution that determines the temperature of a gas of such atoms. In particular, we will study here the cooling of the fermionic isotopes of two alkaline-earth atoms, ^{25}Mg (nuclear spin $I = 5/2$, $^1S_0$-$^1P_1$ width $\Gamma/2\pi = 81\,$MHz, hyperfine splittings $\Delta\omega_{13}/2\pi = 46\,$MHz and $\Delta\omega_{23}/2\pi = 27\,$MHz, where we have assumed a hyperfine quadrupole parameter $B = 0$ [62]) and ^{87}Sr ($I = 9/2$, $^1S_0$-$^1P_1$ width $\Gamma/2\pi = 32\,$MHz, hyperfine splittings $\Delta\omega_{13}/2\pi = 43\,$MHz and $\Delta\omega_{23}/2\pi =$ -17 MHz). These atoms, having nonzero nuclear magnetic moment, have degenerate (assuming zero magnetic field) Zeeman sublevels. These sublevels allow for the mechanism of sub-Doppler cooling in an appropriate laser configuration. Both ^{25}Mg and ^{87}Sr exhibit significant excited-state

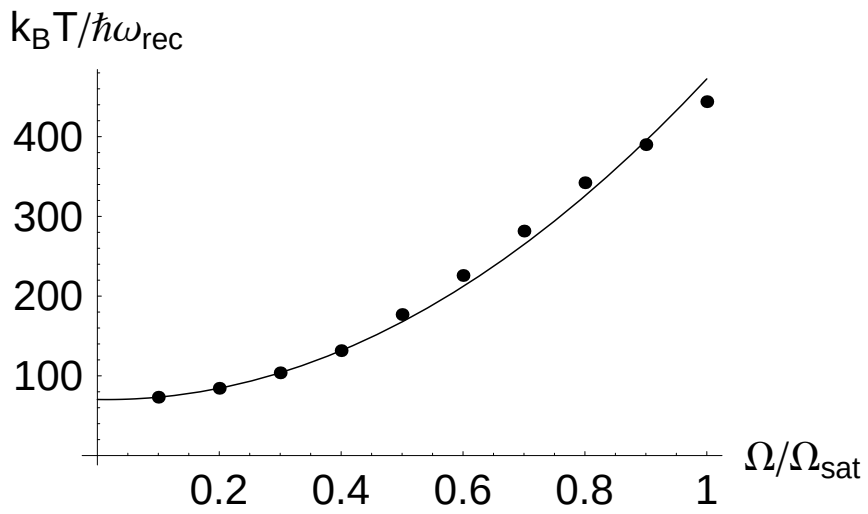

Figure 3.3: Simulation of a two-level atom with $\delta = -\Gamma/2$ and $\Gamma = 400\,\omega_{\rm rec}$ interacting with a one-dimensional laser field, as a test of the Monte Carlo wave-function technique. Plotted is k_B multiplied by the steady-state temperature, in units of the recoil energy $\hbar\omega_{\rm rec}$. The dots are the numerical results of the Monte Carlo simulation, and the line indicates a quadratic least-squares fit the data. The calculation yields a low-intensity limit for the one-dimensional Doppler temperature in agreement with the known value $T_D = \frac{7}{40}\,\hbar\Gamma/k_B = 70\,\hbar\omega_{\rm rec}/k_B$.

spectral overlap, with $\Delta\omega_{13}/\Gamma = 0.57$, $\Delta\omega_{23}/\Gamma = 0.33$, and $\Delta\omega_{13}/\Gamma = 1.3$, $\Delta\omega_{23}/\Gamma =$ -0.53, respectively. We consider the three-dimensional lin-$\perp$-lin laser configuration, consisting of a pair of opposing beams along each cartesian axis, in which each beam is linearly polarized orthogonal to its opposing beam. Furthermore, for this calculation, we set to zero the relative phases of the three sets of laser pairs.

Having a nuclear spin of $I = 5/2$, the $^1S_0$ state of ^{25}Mg results in a hyperfine ground state with 6 sublevels. Use of the low-intensity master equation given in Eq. (3.17) allows us to consider only these 6 internal states of the atom, since the excited states have been adiabatically eliminated in this regime. However, as noted in Ref. [11], a momentum grid extending to $20\hbar k$ in each direction with a spacing of $\hbar k$ would yield a density matrix with $(6 \times 41^3)^2 \approx 2 \times 10^{11}$ elements. A direct solution of this master equation is not numerically feasible, even without considering the further increases in matrix size necessary to describe the master equation relaxation operator in Liouville space [63]. On the other hand, the MCWF method only requires numerical propagation of individual wave functions, which would be represented by vectors with $6 \times 41^3 \approx 4 \times 10^5$ elements. If the number of independent stochastic wave functions required to achieve satisfactory convergence for the calculation of a particular property of the system is not unreasonably large, the MCWF method provides a distinct advantage over a direct master-equation solution.

We follow the procedure outlined in Section 3.4, working in the low-intensity limit in order to reduce the number of internal atomic states in the calculation, which increases the efficiency of calculation. Since laser cooling is most effective at low laser intensities, this turns out to be a useful regime in which to work, with the additional benefit that lower temperatures require a smaller number of atomic center-of-mass momentum states in the calculation. We must determine the effective Hamiltonian as given in Eq. (3.22) and the jump operators as given in Eqs. (3.23) and (3.24) for each atom, and for the particular laser field being considered.

We consider here the lin-⊥-lin laser configuration in three dimensions, with the relative phases of the beams set to zero. The positive-frequency component of the electric field is

$$\begin{aligned}\mathbf{E}_L(\mathbf{R},t) &= \frac{E_0}{2}\left[\hat{y}e^{ikX} + \hat{z}e^{-ikX} + \hat{z}e^{ikY} + \hat{x}e^{-ikY} + \hat{x}e^{ikZ} + \hat{y}e^{-ikZ}\right] \\ &= \frac{E_0}{2}\sum_{q=0,\pm1}(-1)^q a_q(\mathbf{R})\hat{\epsilon}_{-q},\end{aligned} \tag{3.40}$$

with spherical coefficients

$$a_{+1}(\mathbf{R}) = -\frac{1}{\sqrt{2}}\left(e^{-ikY} + e^{ikZ} + ie^{ikX} + ie^{-ikZ}\right), \tag{3.41}$$

$$a_{-1}(\mathbf{R}) = +\frac{1}{\sqrt{2}}\left(e^{-ikY} + e^{ikZ} - ie^{ikX} - ie^{-ikZ}\right), \tag{3.42}$$

$$a_0(\mathbf{R}) = e^{-ikX} + e^{ikY}. \tag{3.43}$$

With these coefficients, along with parameters appropriate to the particular atom under consideration, the atom-laser raising and lowering operators given in Eqs. (3.14) and (3.15) can be constructed. With knowledge of the effective Hamiltonian and the raising and lowering operators, we can then proceed with the MCWF procedure as outlined.

Our example entails propagating 20 stochastic wave functions each for three different values of the light-shift parameter, $\hbar|\delta_3|s_3/(2E_{\rm rec})$ =10, 20, and 30, for both ^{25}Mg ($I = 5/2$) and ^{87}Sr ($I = 9/2$). We consider only $\delta_3 = -5\Gamma$. As in Figure 3.2, we calculate the stochastic trajectories of the ensemble average (i.e., averaged over the 20 wave functions) kinetic energy for each atom as a function of time. We continue this propagation until the transient regime has been passed for some time, and use the time average over the steady-state ensemble-average kinetic energy to provide an estimate of the total average kinetic energy and the final error. The results are shown in Fig. 3.4, along with the energies for atoms with an isolated cooling transition for comparison, $J_e = J_g + 1$ with J_g =1, 2, 3, and 4, with detuning $\delta = -5\Gamma$, as first calculated by Castin and Mølmer in Ref. [11]. From this cursory analysis, we can see that ^{25}Mg

should exhibit a sharp rise in temperature with increasing laser intensity, while ^{87}Sr will cool to sub-Doppler temperatures even for higher intensities, as has been noted experimentally [52].

Detailed calculations of this sort, for realistic atoms, are quite computationally expensive. For example, a single data point for the Mg and Sr calculations presented here required on the order of 200 hours wall time for a 20 processor parallel code, running on a cluster of 2.4 GHz Intel Zeon processors.

It is insightful to make a qualitative illustration of the effects of increasing the atomic degeneracy for an isolated transition as would be the case for a system having no hyperfine overlap. Using the semiclassical calculation method discussed in Section 3.3, the force on such an atom can be determined as a function of the atom's velocity. Figure 3.5 shows plots of this force, in arbitrary units, as a function of the atom's velocity in units of the recoil velocity, in for increasing internal atomic degeneracy. The top-left plot is for a system with a ground hyperfine quantum number of $F_g = 0$ to an excited state of $F_e = 1$. For these parameters, no sub-Doppler cooling is expected, and the force curve displayed is simply that of normal Doppler cooling. In the top-right plot, with $F_g = 1$ and $F_e = 2$, the appearance of a small sub-Doppler force occurs. This force usually appears in a small range of velocities around zero. Nevertheless, the force curve is steepened dramatically, and even over this small range can have a significant impact on the effectiveness of cooling. The bottom-left plot, with $F_g = 2$ and $F_e = 3$ shows an even more dramatic sub-Doppler force, and the bottom-right curve, with $F_g = 3$ and $F_e = 4$ even more so. This qualitative observation supports the more quantitative results shown in Fig. 3.4 for isolated transitions.

As a final note, one of the advantages of performing detailed quantum calculations is the ability to create illustrative pictures. Figure 3.6 provides one such example, using the three-dimensional data obtained from the above Monte Carlo simulations in the ray-tracing rendering program Pov-Ray, and illustrating the reduction in three-momentum

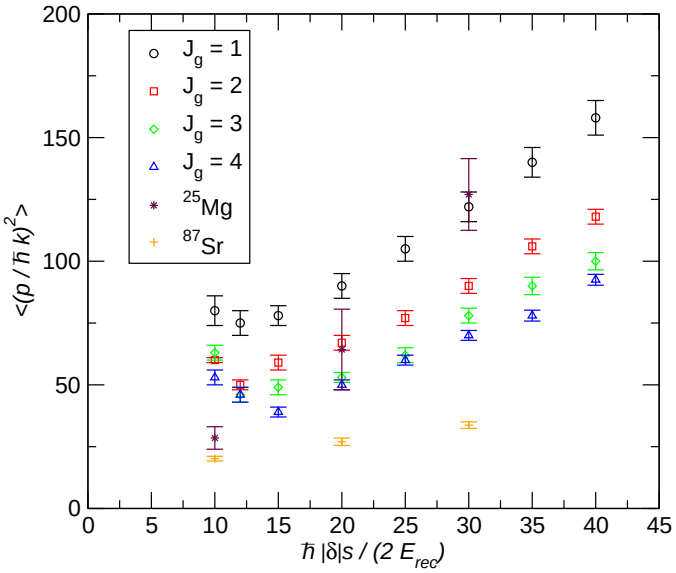

Figure 3.4: Results for calculated ensemble-average energies (rms momentum squared) for ^{25}Mg and ^{87}Sr, as a function of the light-shift parameter $\hbar|\delta_3|s_3/(2E_{\rm rec})$. For comparison, also shown are the calculated energies for atoms with isolated transitions, $J_e = J_g + 1$, with J_g =1, 2, 3, and 4, with detuning $\delta = -5\Gamma$. This figure is adapted from Ref. [2].

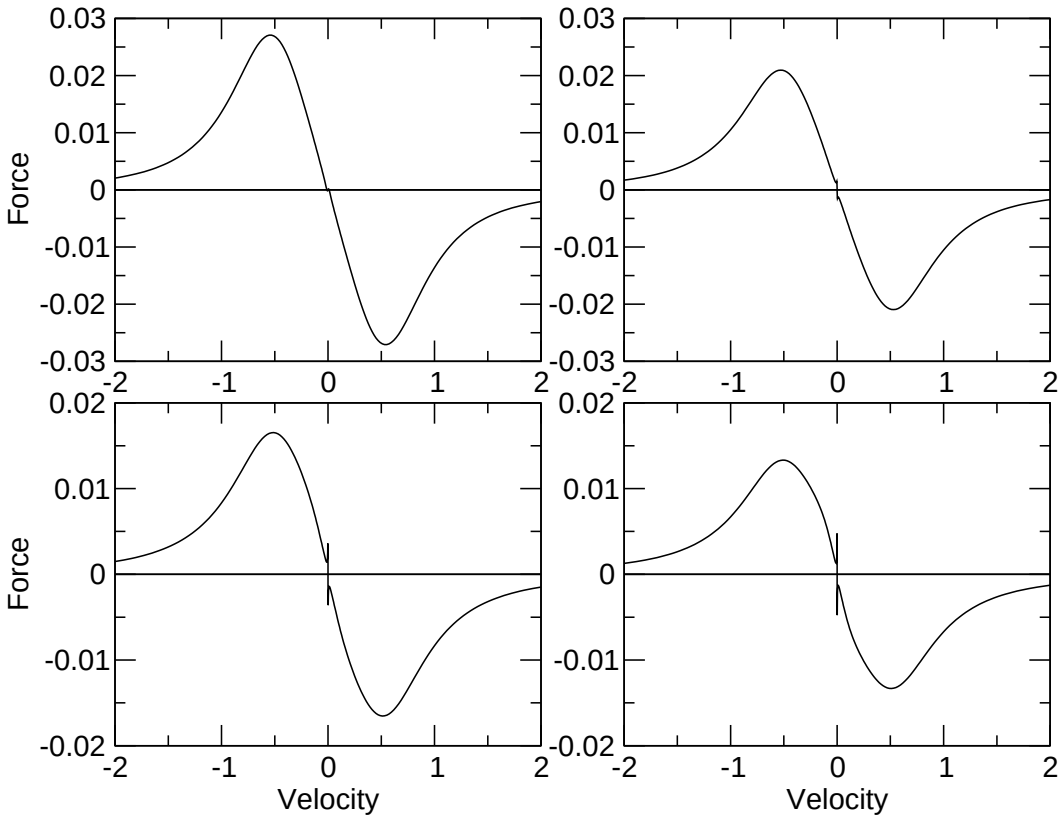

Figure 3.5: Semiclassical force curves illustrating the effect of increasing degeneracy on the laser cooling of idealized atoms with isolated cooling transition and no overlap of hyperfine manifold. As the internal atomic degeneracy is increased and all other parameters held fixed, the appearance of a sub-Doppler force grows. See text for details.

space of a cloud of ^{87}Sr atoms undergoing sub-Doppler polarization-gradient cooling.

3.6 Conclusion

In conclusion, this chapter has provided a detailed description of the fully quantum-mechanical master equation that describes an atom with multiple internal internal structure interacting with a three-dimensional polarization-gradient laser field. It has been shown how the spontaneous-emission relaxation operator is generalized for atoms of this type. The MCWF technique has been applied to these equations of motion, providing a more efficient means of performing calculations for these systems compared to a full solution of the master equation. A few example calculations have been presented to illustrate the application of this theory to atomic systems interacting with laser configurations commonly used in experiments.

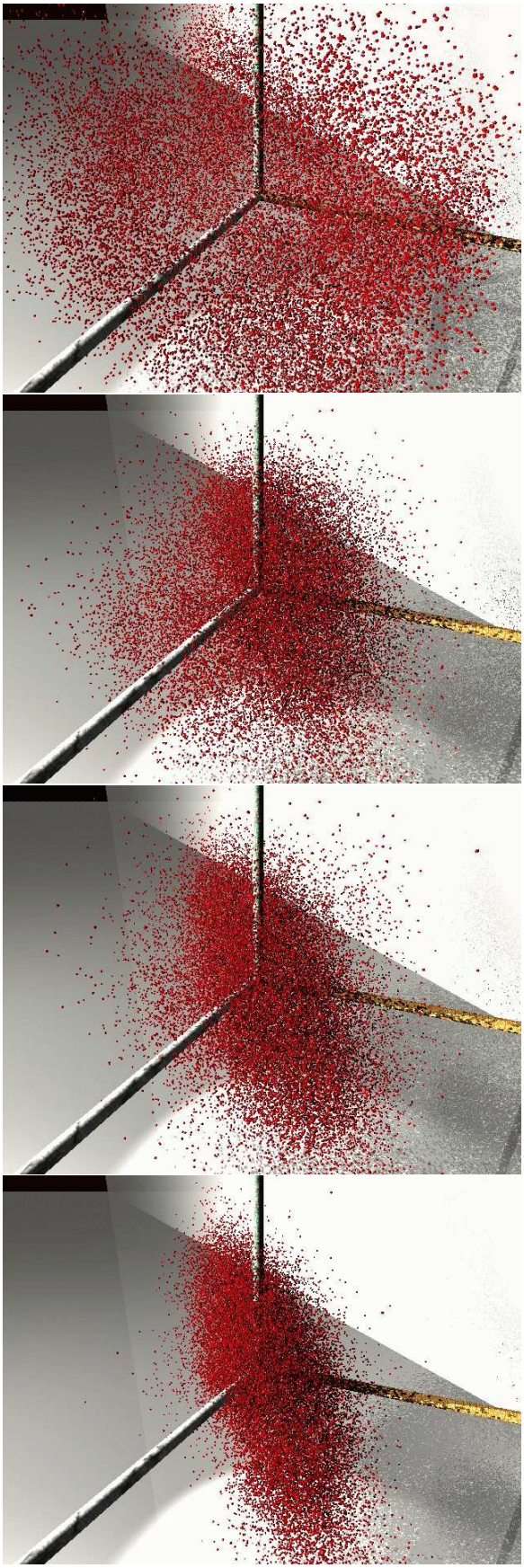

Figure 3.6: Three-dimensional renderings illustrating the time evolution of an atomic cloud in momentum space, based on the numerical simulations of cooling ^{87}Sr.

Chapter 4

Bichromatic Cooling of Three-Level Atoms

4.1 Introduction

In this chapter, the subject of laser-cooling dynamics is further explored, this time applied to a three-level atomic system. This type of atomic configuration is much simpler than the elaborate multi-manifold systems discussed in Chapter 3. Moreover, instead of applying complicated polarization-gradient electromagnetic fields in three dimensions, only two standing-wave laser beams in one dimension will be utilized here. Nonetheless, this basic configuration yields a rich variety of novel phenomena with some unexpected conclusions.

As in Chapter 3, the types of atoms that will be focused on will be group-II atoms, the alkaline earths. Alkaline-earth atoms are difficult to laser cool to the μK or nK regime, but this technique exhibits encouraging potential to circumvent current roadblocks.

The work here also introduces a sparse-matrix technique that permits efficient solution of the master equation for the stationary density matrix, including the quantized atomic momentum. This overcomes longstanding inefficiencies of exact solution methods, and it sidesteps inaccuracies of frequently-implemented semiclassical approximations. The realistic theoretical limiting temperatures are optimized over the full parameter space of detunings and intensities. A qualitative interpretation based on the phenomenon of electromagnetically-induced transparency reveals dynamical effects due

to photon-atom dressing interactions that generate non-Lorentzian lineshapes. Through coherent engineering of an asymmetric Fano-type profile, the temperature can be lowered down to the recoil limit range.

The inability to cool alkaline-earth atoms down to the 100 nK range has proven to be a formidable bottleneck in the study of ultracold dilute gases. Novel cooling techniques have limited applicability and so far quantum degeneracy has been obtained only for ytterbium, a lanthanide atom with similar level structure, despite extensive efforts by numerous groups [64, 65, 52, 2]. The theoretical description of laser cooling took strides in the 1990s, primarily utilizing the semiclassical approximation which resulted in complicated calculations [45]. Few realistic calculations have treated the atomic motion quantum mechanically and predict realistic cooling temperatures. Here, a direct method is introduced, based on sparse-matrix techniques, which efficiently yields the fully quantized stationary density matrix. In contrast to Monte Carlo approaches [10, 12, 2], the temperature and other observables emerge without statistical monitoring; the efficiency enables a complete mapping of the large parameter space of laser intensities and detunings. Here, this mapping is computed for a three-level cooling scheme and develop a qualitative interpretation based on the physics of electromagnetically induced transparency (EIT). The calculations predict that promising regimes exist that should produce record-low temperatures and overcome the difficulty of alkaline-earth atom cooling. This is orders of magnitude cooler than could be obtained using the main resonance line alone. Moreover, the cooling can be controlled and adjusted in real time, which should make this method competitive with or superior to other proposed ways of cooling alkaline-earth atoms.

Although leading to many advances [19, 66, 67], internal atomic structure greatly restricts the species for which laser cooling can be applied successfully, and determines whether ultracold temperatures — on the order of a few μK — can be achieved. Basic Doppler cooling [18, 68] has a minimum temperature proportional to the width of the

atomic transition. Lower temperatures can be achieved by exploiting the multilevel hyperfine structure [16, 17, 69, 70], by modifying the atomic scattering [71], or by using narrow optical transitions as a second-stage for pre-cooled atoms [64, 65]. Here, sub-Doppler cooling with three-level systems under two-color excitation is explored. The published literature discusses some similar schemes, for both atoms [72, 73, 74] and trapped ions [75, 76, 77]. In particular, the work of Tan *et al.* [73] appears initially to be the most exciting, since it claims to permit cooling to below the recoil temperature, believed to be a rigorous quantum lower bound for this type of laser cooling. However, this is an artifact of the errors associated with a semiclassical treatment of atomic momentum in Ref. [73], since that approximation is known to produce incorrect, arbitrarily low (and even negative) temperatures. In order to realistically evaluate the promise of three-level cooling based on dressed-state ideas, it is thus critical to carry out fully quantum solutions with great efficiency, as in the sparse solution technique introduced here.

Parts of this chapter are developed from research by this author which has been submitted for publication, and some of the text and figures have been adapted from the work therein. A preprint form of this submitted publication can be found in Ref. [3].

4.2 Three-level atomic systems

There are three basic types of three-level systems — the Λ, V, and Ξ systems — each classified according to the ordering of the bare quantum states in energy, and the possible decay pathways. The Λ-configuration is commonly used for studying EIT [78] and related phenomena. The focus here is on a Ξ system, shown in Fig. 4.1, because of its relevance to current experimental work [79, 80]. Note, however, that the general conclusions can be applied to any type of three-level system, and can be extended to systems with more than three levels. The level structure and internal parameters for the Ξ system are depicted in the left-hand side of the figure. This cooling technique seems

well suited to alkaline-earth atoms, which are good candidates for the next generation of optical atomic clocks, studies of ultracold collisions, optical Feshbach resonances [81], and quantum degeneracy [82].

The linewidths, $\Gamma_i = \gamma_i/2\pi$ for i =1, 2, of both the upper and lower transitions for some of the most relevant alkaline-earth (^{24}Mg, ^{40}Ca, and ^{88}Sr) and alkaline-earth-like (^{174}Yb)systems are given in Table. 4.1. From an initial analysis, it might seem that mixing of the bare atomic states could allow cooling to a temperature set by the narrowest of the two transitions. This seems reasonable because traditional Doppler cooling with a single laser and two-level system predicts temperatures proportional to the transition linewidth. Since the upper transition in all cases considered in Table. 4.1 is narrower than the lower transition, this simplistic analysis predicts that sub-Doppler cooling should occur by a factor of Γ_1/Γ_2 below the Doppler limit. This ratio is also given in Table. 4.1, and it can be seen that, for example, magnesium offers the possibility of beating the Doppler limit by the rather large factor of 36. Later in this chapter, the detailed workings of this type of cooling will be explained, and it will be shown that this limit is in fact an underestimate of effectiveness of the cooling, and the Doppler limit can be beat by significantly more than a factor of 36.

Table 4.1: Transition linewidths, $\Gamma_i = \gamma_i/2\pi$ for i =1, 2, of the $^1S_0$-$^1P_1$-$^1S_0$ three-level Ξ systems for common alkaline-earth atoms ^{24}Mg, ^{40}Ca, and ^{88}Sr, as well as the alkaline-earth-like atom ^{174}Yb. The ratio of Γ_1/Γ_2 is also shown, indicating the factor below the lower-transition Doppler limit which might be expected using a three-level bichromatic scheme, neglecting the more detailed lineshape analysis provided in this chapter.

	^{24}Mg	^{40}Ca	^{88}Sr	^{174}Yb
Γ_1 (MHz)	79	34.63	32	28.01
Γ_2 (MHz)	2.2	4.77	2.96	4.81
Γ_1/Γ_2	36	7.3	11	5.8

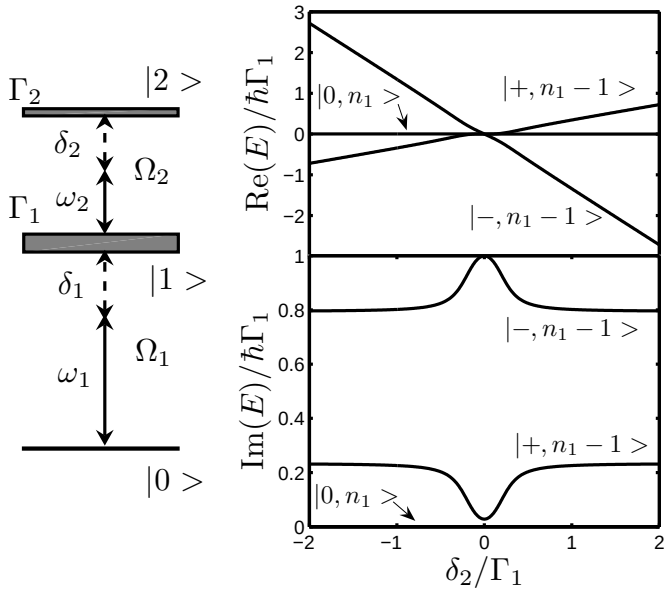

Figure 4.1: Left side: Atomic configuration for generic three-level Ξ system. Right side: The dressed eigenenergies for the $^1S_0$-$^1P_1$-$^1S_0$ Ξ system in ^{24}Mg with $s_1(\delta_1) = 0.001$ and $s_2(\delta_2) = 1$. Real (top) and imaginary (bottom) parts of the eigenvalues of Eq. (4.3), with dressed atomic states labeled. The real parts are the energies and the imaginary parts are the effective linewidths of the dressed atomic system. Both are plotted as functions of δ_2, with fixed $\delta_1 = 0$. This figure is adapted from Ref. [3].

4.3 Fully quantum model and its advantages

Fig. 4.1 shows the internal atomic states in order of increasing energy as $|0\rangle$, $|1\rangle$, and $|2\rangle$. The transition energy of the lower transition, $|0\rangle \rightarrow |1\rangle$, and of the upper transition, $|1\rangle \rightarrow |2\rangle$, are $\hbar\omega_0^{(1)}$ and $\hbar\omega_0^{(2)}$, respectively. Two lasers are included, of frequency ω_1 and ω_2, and their detunings are defined from the appropriate atomic transitions as $\delta_i = \omega_i - \omega_0^{(i)}$, for $i = 1,2$. The intensities of lasers 1 and 2 are characterized by their Rabi frequencies $\Omega_1 = -\langle 0|\mathbf{d}|1\rangle \cdot \mathbf{E}_1(\mathbf{x})$ and $\Omega_2 = -\langle 1|\mathbf{d}|2\rangle \cdot \mathbf{E}_2(\mathbf{x})$, respectively, where $\mathbf{d}$ is the electric-dipole operator of the atom and $\mathbf{E}_i$ is the electric-field amplitude for the ith laser. The spontaneous-emission linewidths of states $|1\rangle$ and $|2\rangle$ are $\Gamma_1/2\pi$ and $\Gamma_2/2\pi$, (79 MHz and 2.2 MHz, respectively, for ^{24}Mg). The time evolution for the atom in the laser field, with mass m and center-of-mass momentum operator $\mathbf{p}$, is given by the master equation,

$$\dot{\rho}(t) = \frac{i}{\hbar}[\rho, H] + \mathcal{L}[\rho], \tag{4.1}$$

where ρ is the reduced density matrix of the atom system, the vacuum photon field degrees of freedom having been traced over, $H = \mathbf{p}^2/2m + \hbar\omega_0^{(1)}|1\rangle\langle 1| + \hbar\omega_0^{(2)}|2\rangle\langle 2| + V_{\text{laser}}^{(1)}(\mathbf{x}) + V_{\text{laser}}^{(2)}(\mathbf{x})$ is the Hamiltonian of the atom-laser system, and the superoperator Liouvillian $\mathcal{L}$ describes effects due to coupling of the atom to the vacuum photon field, resulting in spontaneous emission [8].

4.4 Numerical solution

Eq. (4.1) treats all the atomic degrees of freedom quantum mechanically, so its solutions generally provide an accurate description of the atom's dynamics. Thus, much of the difficulty associated with semiclassical approximations of the system is avoided. For reasonable temperatures, however, the number of numerical basis states required to directly solve the problem, even in one dimension, is impractical for most computers. Here, this problem is resolved without resorting to Monte Carlo methods by noting

that the matrix for the linear system equivalent to Eq. (4.1) is very sparse: only a small fraction of its elements are nonzero. For a typical calculation, the Hilbert space involves 3 internal degrees of freedom for the atom, and 150 momentum states in one dimension. The resulting number of complex density matrix elements is thus $450\times451/2$ independent elements for this case owing to symmetry, and $\mathcal{L}$ would take over 160GB to store if it was a full matrix. But the particular structure shared by Liouvillian operators $\mathcal{L}$ that describe relaxation processes simplifies the numerics, and requires less than 2 GB to solve the sparse system; specifically, the microscopic properties of atomic operators in $\mathcal{L}$ permit construction of the matrix $\mathcal{L}$ with the zero elements eliminated. The steady-state solution of Eq. (4.1) is then found using a standard sparse-matrix inversion, giving an exact direct solution of a fully-quantized master equation in just 1-2 minutes of CPU time on a current workstation.

The steady-state density matrix has been calculated this way in one dimension. The average kinetic energy is $\langle p^2/2m\rangle = \mathrm{Tr}(\rho\, p^2/2m)$, which in thermodynamic equilibrium can be equated with $\frac{1}{2}k_BT$, where T is the temperature. The large parameter space of the problem has been explored, e.g., varying the detunings, δ_1 and δ_2, as well as the strengths Ω_1 and Ω_2 of the two lasers. However, the lasers are better characterized by how strongly they dress the atom. The saturation parameters s_1 and s_2 for the respective transitions are

$$s_i = \frac{1}{2}\frac{\Omega_i^2}{\delta_i^2 + (\Gamma_i/2)^2}. \tag{4.2}$$

4.5 Results

The parameter space has three distinct regimes. In the first, with $s_1 \gtrsim 1$ and s_2 arbitrary, only heating occurs, as expected from Doppler-cooling theory since the lower transition is driven strongly. Numerical results for the second regime, with $s_1 \ll 1$ and $s_2 \ll 1$, are shown in Fig. 4.2, with the temperature normalized to the lower-level Doppler limit $T_D^{(1D)}$, $T_D^{(1D)} = 7\hbar\Gamma_1/40k_B$ [16], which is the optimum temperature

expected for cooling with just one laser. In this plot, the location of the bare two-photon resonance ($\delta_1 + \delta_2 = 0$) is denoted by the dashed line. It is clear from this plot (note the normalization of the temperature axis) that cooling occurs only to the Doppler limit for the lower transition $T_D^{(1D)} = \hbar\Gamma_1/2k_B$, and only in the range near $\delta_1 = -\Gamma_1/2$. In this case, laser 2 has no effect, as this amounts to simple two-level Doppler cooling on the lower transition with laser 1.

In the final regime, when $s_1 \ll 1$ and $s_2 \gtrsim 1$, cooling occurs down to substantially below $T_D^{(1D)}$. Figure 4.3 illustrates cooling in this regime, also for ^{24}Mg, with the temperature again normalized to the lower-level Doppler limit and the bare two-photon resonance indicated. The steady-state temperature is plotted as a function of δ_1 and δ_2 for $s_1(\delta_1) = 0.001$ in both the upper and lower plots, and with $s_2(\delta_2) = 1$ in the upper plot and $s_2(\delta_2) = 5$ in the lower plot. Note that the saturation parameters are being held fixed as the detunings are varied, so that the Rabi frequencies are being continuously adjusted. The lowest temperatures, on the order of $10^{-2}\, T_D^{(1D)}$, are found in the quadrant with $\delta_1 > 0$ and $\delta_2 < 0$, as well as less extreme cooling in other regions. Observe that the lowest temperatures are obtained for frequencies detuned to the blue of the two-photon resonance. This seems counterintuitive, since a red detuning is usually required in order to have a net decrease of atomic kinetic energy in a photon-scattering event.

4.6 EIT explanation

Qualitative understanding of the cooling mechanism emerges from analysis of the simpler Hamiltonian,

$$H = \frac{\hbar}{2}\begin{pmatrix} 0 & \Omega_1 & 0 \\ \Omega_1^* & -2\delta_1 - i\Gamma_1 & \Omega_2 \\ 0 & \Omega_2^* & -2(\delta_1+\delta_2)i\Gamma_2 \end{pmatrix}. \tag{4.3}$$

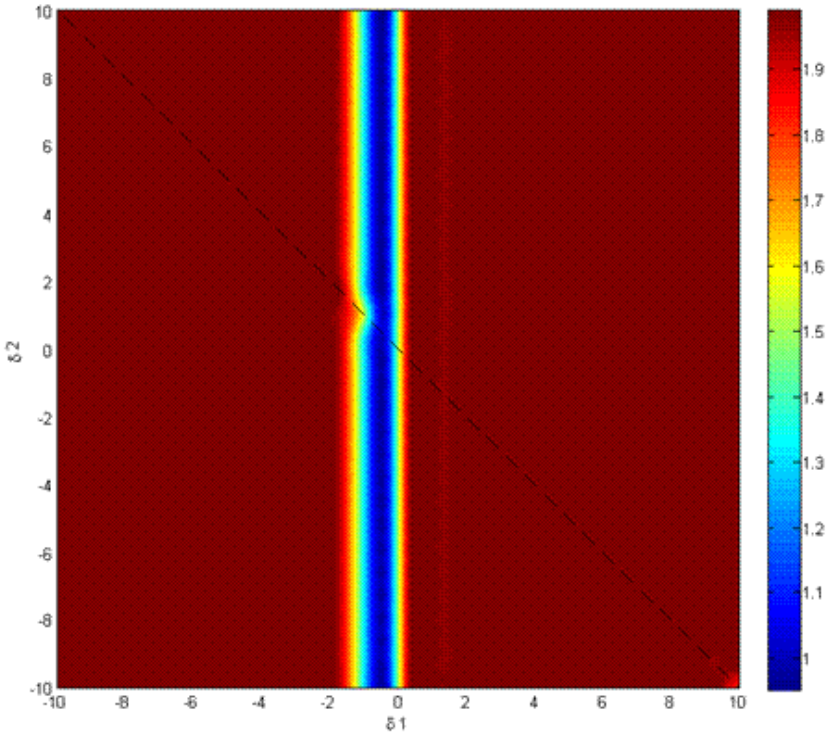

Figure 4.2: Steady-state temperatures for bichromatic three-level laser cooling, as a function of both detunings δ_1 and δ_2, with both atomic transitions perturbatively probed, $s_1 \ll 1$ and $s_2 \ll 1$. The bare two-photon resonance is indicated with a dashed line.

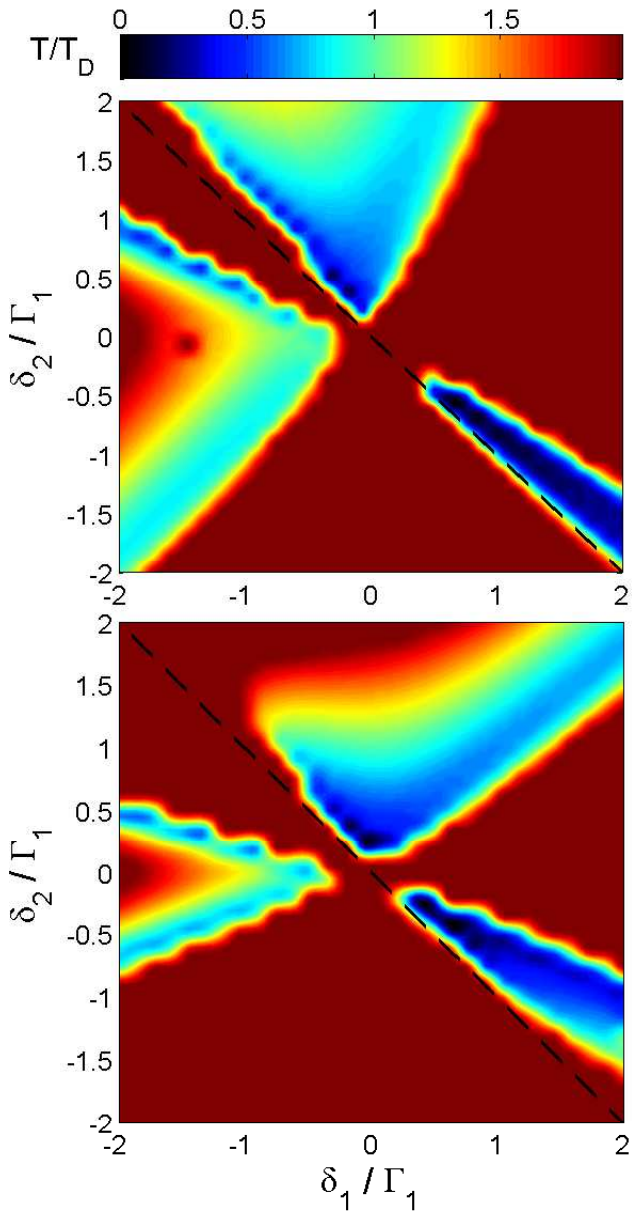

Figure 4.3: Steady-state temperatures for bichromatic three-level laser cooling, as a function of both detunings δ_1 and δ_2, with the lower atomic transition perturbatively probed, $s_1 \ll 1$, for both plots, and the upper atomic transition dressed to varying degrees in the two plots, with $s_2 = 1$ in the upper plot and $s_2 = 5$ in the lower plot. The bare two-photon resonance is indicated with a dashed line. This figure is adapted from Ref. [3].

Its complex eigenvalues have real dressed energies, and imaginary parts giving dressed-state linewidths. These dressed energies and widths are plotted on the right side of Fig. 4.1 as functions of δ_2, for the same parameters used in Fig. 4.3. The cancelation of one of the widths can be viewed as an EIT effect: since laser 1 is perturbative while laser 2 strongly dresses the upper transition, the new eigenstates of the system, denoted $|+\rangle$ and $|-\rangle$, are well approximated as linear combinations of the bare states $|1\rangle$ and $|2\rangle$. These states have the modified energies and widths shown in Fig. 4.1. The linewidth modifications can be viewed as a Fano interference [34], in which the dressing-laser transitions caused by the probe laser enable multiple coherent pathways among the bare states. Constructive or destructive interference respectively increases or decreases the atomic linewidth.

The cooling mechanism is thus qualitatively explained as ordinary two-level Doppler cooling. But instead of using a transition between two bare states of an atom, the transition occurs between a (mostly) unmodified ground state, and a dressed excited state, with a shifted energy and a new linewidth that can be narrower than the bare linewidth of the lower transition. As the probe laser is scanned, the detuning relative to the dressed energy levels is varied, but since these levels are shifted from their bare energies, resonance occurs for different detunings than are encountered in the bare system. In fact, the shifts of the eigen-energies in Fig. 4.1 from the bare energies explain the apparent observation of blue two-photon cooling in Fig. 4.3. In the dressed system, the bare two-photon resonance is no longer meaningful, and the cooling region is in fact *to the red* of a dressed resonance.

4.7 Atom-photon dynamics for asymmetric lineshapes

When mapping this system onto Doppler cooling theory, note that the lineshapes are not Lorentzian, but are asymmetric Fano lineshapes for the dressed system, as illustrated by the solid line in the upper part of Fig. 4.4 as a function of δ_1 for a fixed

of $\delta_2 = -\Gamma_1/2$ [74, 3]. This changes the optimum-detuning condition to be that the maximum cooling for a given transition occurs when the probe laser is detuned from the dressed excited state *precisely to the inflection point of the absorption spectrum.* This can be understood by noting that the applied force f due to the laser beam is proportional to the absorption rate, for a given δ_1. As in semiclassical cooling theories, the friction coefficient α for the atom in the laser field is

$$\alpha = -\frac{d}{dv} f(v), \tag{4.4}$$

where v is the atomic velocity. Since the detuning of the laser and the resonant atomic velocity are linearly related, the derivative of the absorption spectrum with respect to δ_1 also yields a maximum in the cooling force. This is evident in normal Doppler cooling because the optimum detuning occurs when $\delta = -\Gamma/2$, the inflection point of the Lorentzian. In general then, for asymmetric lineshapes, the optimum detuning does not obey such a simple relation, but depends on the degree of asymmetry.

This point is illustrated in the upper portion of Fig. 4.4, which compares the actual asymmetric absorption spectrum (solid line) of the dressed system as a function of δ_1 and for fixed $\delta_2 = -\Gamma_1$, with the more simplistic predictions for the absorption spectrum using symmetric Lorentzian lineshapes (dotted line). The peak of each lineshape is located at a dressed eigenenergy, and lineshapes at the same energies and widths. As an example, optimum-cooling detunings relative to the leftmost resonance are illustrated with a black arrow for the true asymmetric lineshape and with a gray arrow for the hypothetical symmetric-lineshape case. The value of the optimum detuning, as well as the slope of the lineshape is seen to be different for these two cases.

From this complete picture of the cooling mechanism, the minimum temperatures can now be determined, allowing for the detuning modification due to asymmetric lineshapes. The lower part of Fig. 4.4 shows the ratio of the maximum slope of a Lorentzian lineshape with width Γ_1 to the slope of the asymmetric lineshape, as a function of δ_1

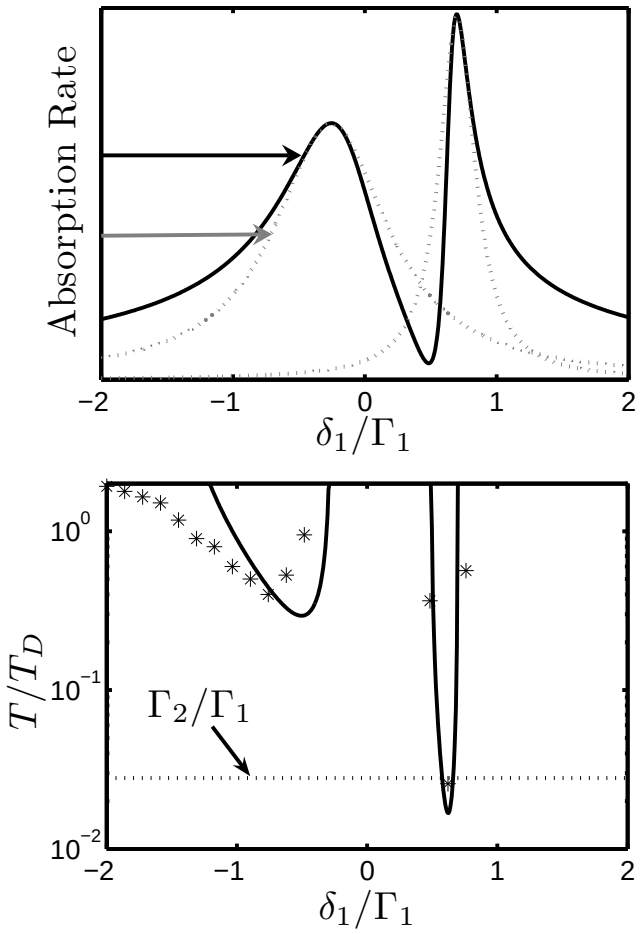

Figure 4.4: Upper plot: Comparison of the true absorption spectrum of the dressed three-level Ξ system (solid line) with a simplistic absorption spectrum with Lorentzian lineshapes (dotted line). Optimum laser-cooling detuning is indicated with arrows for each type of spectrum. Lower plot: Comparison of the numerical three-level-cooling temperature results (data points) with the ratio of the maximum slope of a Lorentzian lineshape with width Γ_1 to the slope of the asymmetric lineshape, as a function of δ_1 with $\delta_2 = -\Gamma_1/2$ (solid line). This ratio provides an indication of the expected cooling for the dressed system relative to the Doppler limit for the lower transition. This figure is adapted from Ref. [3].

with $\delta_2 = -\Gamma_1/2$. This ratio provides an indication of the expected cooling for the dressed system relative to the Doppler limit for the lower transition. For comparison, fully quantum numerical results are indicated by data points. Note that the expected temperature, due to the asymmetric lineshape, is predicted to be lower than the upper-transition Doppler limit, indicated by the dotted line in the lower plot of Fig. 4.4, a prediction supported by the numerical data.

4.8 Conclusion

In conclusion, coherent engineering of a three-level system can optimize the effectiveness of two-level Doppler cooling. Dressed states are created with modified linewidths in the range between the smallest and the largest of the two bare linewidths, and the additional effect of asymmetric lineshapes can lead to temperatures below the Doppler limit of either bare transition. The ability to tailor the degree of cooling lends this technique additional utility, and may be particularly useful when applied the notoriously difficult-to-cool alkaline-earth atoms. A dressing scheme can be suited to the characteristics of a particular atom, and real-time adjustment of the cooling properties can allow narrowing of the velocity-capture range as an atomic gas is cooled. Utilizing such coherent effects should lead to simple schemes for cooling far below the typical Doppler limit.

Chapter 5

Cavity Cooling of Atoms and Molecules

5.1 Introduction

In this chapter, a cooling scheme is explored which, in addition to an atom (or molecule) and a laser, utilizes an optical cavity. The idea of using a cavity to help cool atoms was first proposed in the early 1990's [83], and early experimental explorations [84] confirmed the feasibility of the method. Further investigation [71, 85] found situations in which the cooling was much more effective than expected, reaching temperatures far below the predictions of the basic theory. Further theoretical investigations [86, 87] were able to attribute the excess cooling to the presence of so-called collective effects: basically, phenomena occurring due to the presence of multiple atoms, all interacting with the cavity at the same time. This was not really a many-body effect, as the collective enhancement could be modeled without including any atomic interaction physics.

The previous work in this field has led to a good understanding of cavity cooling applied to atoms. However, the cooling scheme, which stipulates driving an atom with a laser having a frequency very far detuned from the atomic transition, holds the possibility of being effective also for molecules, which are traditionally not amenable to laser-cooling schemes. Almost all types of typical laser cooling require a closed internal transition in the object being cooled — the excited state must decay back to the original ground state in order for the process to be repeated — and molecules with their dense forest of energy levels usually do not provide this. Cavity cooling, being far detuned so

that coherent-scattering processes are dominant, offers a means of avoiding this problem. Additionally, the collective effects that were found to enhance cavity cooling of atoms may also bolster the cavity cooling of molecules, leading to even more effective cooling than might be expected.

The study of the cavity cooling of molecules offers another opportunity to apply the quantum-optics master-equation techniques developed throughout this thesis, and, as it turns out, another application of the stochastic wave-function techniques developed in Chapter 3. In this chapter, the fundamental picture of the mechanism for cavity cooling is presented, as well as the particular details, such as Raman transitions, that must be considered when considering the cooling of molecules instead of atoms. Following this is the development of a fully quantum-mechanical theory of a particle, driven by a laser, and coupled to a high-finesse optical cavity, with both the atom and the cavity coupled to the vacuum photon field. The methods of system-reservoir theory are clearly useful again here, but with some generalization to accommodate the more complex situation at hand. Certain approximations are introduced to make the problem more amenable to numerical solution, and their validity is discussed. Next, it is shown how the resulting master equation can be simulated using the same stochastic wave-function framework developed in Chapter 3 to describe the dynamics of multilevel atoms. Finally, some results are shown.

In the end, the technique of solving a fully quantized master equation proves mostly unfeasible for describing collective effects. Despite the greatly enhanced calculation possibilities provided by the stochastic wave-function methods, the large number of particles required to model the desired collective effects is simply too large, with the existing semiclassical calculations [86, 87, 88] having a distinct advantage in this respect. The fully quantum methods presented here, however, allow for a more detailed description of the cooling process, as well as easily describing the time-evolution of the cooling. This turns out to be important in aiding the design of experiments.

5.2 Physical picture of the cooling mechanism

This section discusses the basic physical mechanism by which cavity laser cooling occurs. Atoms and molecules will be considered, both treated as two-level systems, but with the difference that the two-level molecule can decay from its excited state either back to the ground state or to one or more other internal states. The latter process is called a Raman transition, and it is assumed here that a molecule undergoing such a transition becomes no longer trapped by the experiment, and the molecule is lost. These other internal atomic states are not included in the model explicitly, but the possibility of a Raman transition occurring and the molecule being lost will be built in. The branching ratio for either going back to the ground state or undergoing a Raman transition is determined by the various internal oscillator strengths for the molecule, and it can be adjusted in the model to suit the molecule being considered.

When an atom interacts with a laser, photons are absorbed and scattered. In general, two different processes can occur, incoherent and coherent scattering. Incoherent scattering dominates at higher laser intensities which saturate the atom. The absorbing photons arrive often enough that, by the energy-time uncertainty principle, the scattered photons do not necessarily have the same energy as the incoming photons. If, say, two photons are absorbed and scattered in a short enough time, only the sum of the frequencies of the outgoing photons must equal the sum of the two absorbed photons. Coherent scattering on the other hand, dominates at low laser intensities for which the atom is only weakly perturbed. Photons arrive spaced apart far enough in time that the scattered photons must have the same frequency of the incoming photons.

By detuning far from the atomic transition, and using an appropriately small Rabi frequency, that is, the intensity of the probe laser, the incoherent scattering peaks are suppressed, and coherent scattering becomes the dominant process. However, coherent Raman transitions to untrapped states remain. In free space, the ratio of the

rate of Rayleigh (good) scattering events to the rate of Raman (bad) scattering events is independent of the detuning, and depends only on the various molecular oscillator strengths. Introducing a cavity can, however, enhance one process over the other, for the right parameter values. Momentum and energy conservation will be imposed for the scattering process, and the possibility of Raman transitions will be included.

A molecule is in a cavity oriented along the z-axis and interacts with a transverse probe laser aligned along the x-axis. The laser frequency is $\omega_L = ck_L$ and the cavity frequency is $\omega_c = ck_c$. The molecule scatters a photon with wave vector $\mathbf{k}_s$. Conservation of momentum requires

$$\mathbf{p}' = \mathbf{p} + \hbar\mathbf{k}_L - \hbar\mathbf{k}_s, \tag{5.1}$$

where $\mathbf{p} = m\mathbf{v}$, and $\mathbf{v}$ is the velocity of the molecule, the prime referring to the state after scattering. Energy conservation requires

$$\omega_s = \omega_L + \Delta + \delta_r, \tag{5.2}$$

where

$$\Delta = -(\mathbf{k}_L - \mathbf{k}_s)\cdot\mathbf{v} - \frac{\hbar}{2m}(\mathbf{k}_L - \mathbf{k}_s)^2, \tag{5.3}$$

and $\delta_r = \omega_r - \omega_a$, is the internal energy difference for the Raman transition. The first term is the so-called two-photon Doppler effect, and the second term describes recoil heating due to laser and cavity photons. Rayleigh-scattering processes are described by the above equations with $\delta_r = 0$.

Equation (5.2) indicates that the scattered photon has a frequency determined by the probe-laser frequency, the angle of the scattered photon relative to the initial velocity of the molecule, and the Raman energy difference. Since the motion along the x-axis is not of importance here, it will be convenient to set $v_x = 0$. Defining $\omega_{\mathrm{rec},L} = \frac{\hbar k_L^2}{2m}$ as the recoil frequency associated a laser photon and $\omega_{\mathrm{rec},s} = \frac{\hbar k_s^2}{2m}$ as the recoil frequency associated with a cavity photon, Eq. (5.3) then becomes

$$\Delta = \mathbf{k}_s\cdot\mathbf{v} - \omega_{\mathrm{rec},L} - \omega_{\mathrm{rec},s}. \tag{5.4}$$

If the scattered photon has a frequency greater than the frequency of the laser photons, $\omega_s > \omega_L$, then Eq. (5.4) implies that Δ must be positive for a Rayleigh scattering event ($\delta_r = 0$), which implies that $\mathbf{k}_s \cdot \mathbf{v} > \omega_{\mathrm{rec},L} + \omega_{\mathrm{rec},s}$. This in turn implies that $\mathbf{k}_s \cdot \mathbf{v}$ is positive, so that the vectors $\mathbf{k}_s$ and $\mathbf{v}$ must point in the same direction along the z-axis. With this information, it is clear from Eq. (5.1) that the final molecular momentum along the z-axis p'_z must be less than the initial molecular momentum along the z-axis p_z. Thus, for a scattering event in which $\omega_s > \omega_L$ and in which the scattered photon is emitted in the z-direction, the molecule's momentum is decreased.

Up to this point, none of this is terribly useful for cooling since scattered photons can of course be emitted in directions other than along the z-axis and with frequencies that are not greater than the laser frequency. However, if an optical cavity with frequency ω_c is introduced along the z-axis, it will greatly enhance photon emission into the cavity mode from an atom or molecule in the cavity. If the cavity frequency is set such that $\omega_c > \omega_L$, then from the discussion in the preceding paragraph, scattering processes which decrease the particle's momentum along the z-axis will occur preferentially, more often than processes that increase its momentum. The effect of this on a gas of atoms or molecules over repeated scattering events is to cool the gas.

In a cooling experiment, Raman transitions are undesirable since they lead to a loss of molecules. The process of cavity cooling acts to suppress Raman processes. The enhancement by the cavity of emissions along the z-axis with frequency ω_c implies in Eq. (5.2) that if Rayleigh processes ($\delta_r = 0$) are resonant with the cavity, then Raman processes ($\delta_r \neq 0$) will not be, and will not be enhanced.

5.3 Theoretical models

For the purposes of developing the basic physical model, only atoms and not molecules will be considered for the time being. As before, the atom will be approximated as a simple two-level system. Later, once the underlying theory has been de-

veloped, the behavior of molecules will be integrated into the equations. The model is intended to describe a situation in which one or more two-level atoms in a cavity, interacting with a single cavity mode along the z-axis, and driven by a transverse pump laser along the x-axis. The equations of motion will first be developed for a single atom in a cavity. After that, they will be extended to treat the case of multiple atoms, each interacting with the cavity but neglecting interactions between atoms. Master-equation techniques will be used to describe the fully quantum system. The cavity mode will then be approximated as a classical field, a valid approximation in the limit of large numbers of cavity photons. This will keep the number of quantum states needed for a numerical calculation to a minimum when the cavity is well populated. If the cavity population is very small and the semiclassical approximation is not valid, the fully quantum equations will remain numerically tractable since only a few modes of the cavity will need to be included in a calculation. Stochastic wave function simulations similar to those employed in Chapter 3 will be applied to perform calculations.

5.3.1 Single atom

The master equation describing an atom, coupled to the photon vacuum, in a cavity, also coupled to the photon vacuum, with the atom driven transversely by a laser, is

$$\dot{\rho} = \frac{i}{\hbar}\left[\rho, H_s\right] + \mathcal{L}\rho + \mathcal{K}\rho, \tag{5.5}$$

where ρ is the reduced density matrix of the atom-cavity-mode system, $\mathcal{L}$ is a superoperator describing spontaneous emission (characterized by the parameter Γ), $\mathcal{K}$ is a superoperator describing damping of the cavity mode (characterized by the parameter κ), and the system Hamiltonian is given by

$$H_s = -\hbar\delta_c a^\dagger a - \hbar\delta_a \sigma^\dagger\sigma + \hbar\left[\sigma^\dagger(g(x)a + \Omega) + \text{H.c.}\right], \tag{5.6}$$

where a ($a^\dagger$) is the annihilation (creation) operator for a cavity photon, σ ($\sigma^\dagger$) is the annihilation (creation) operator for an internal atomic excitation, $\delta_c = \omega_l - \omega_c$ is the laser-cavity detuning, and $\delta_a = \omega_l - \omega_0$ is the laser-atom detuning.

The equation of motion for the cavity mode can be determined by first writing down the Heisenberg equation of motion for the cavity-mode operator. This will yield a hybrid set of equations, with the atom-laser system being described by a density-operator equation of motion (master equation) and the cavity mode described by an operator equation of motion with fluctuation terms (Langevin equation), in which form it can be more easily be approximated as a classical field. The process of transitioning from a master equation to a Langevin equation is discussed in the literature [58, 15, 89]. Skipping these details, the resulting equation of motion for the cavity mode is

$$\begin{aligned} \dot{a} &= \frac{i}{\hbar}\left[H_s, a\right] - \frac{\kappa}{2}a + F_1 \\ &= \left(i\delta_c - \frac{\kappa}{2}\right)a - ig(x)\sigma + F_1. \end{aligned} \tag{5.7}$$

To treat the cavity mode classically, it is necessary to find the equation of motion for the average value of the mode operator a, which is denoted here by $\alpha = \langle a \rangle$. Utilizing the characteristic of noise operators that they average to zero, $\langle F_1 \rangle = 0$, a set of two coupled equations is obtained, the first of which is

$$\dot{\alpha} = \left(i\delta_c - \frac{\kappa}{2}\right)\alpha - ig(x)\sigma, \tag{5.8}$$

and the second of which is

$$\dot{\rho} = \frac{i}{\hbar}\left[\rho, H_s\right] + \mathcal{L}\rho, \tag{5.9}$$

with the density matrix now only consisting of internal and external atomic states (the cavity states having been traced over), and with the system Hamiltonian given now by

$$H_s = -\hbar\delta_c\alpha^2 - \hbar\delta_a\sigma^\dagger\sigma + \hbar\left[\sigma^\dagger(g(x)\alpha + \Omega) + \text{H.c.}\right]. \tag{5.10}$$

Note that in obtaining Eq. (5.9), the fact that $\text{Tr}_{\text{cav}}\mathcal{K}\rho = 0$ has been used, which is a general property of superoperators of Lindblad form when the states to which they

correspond are traced over. The number of photons n in the cavity mode is given by $n = \alpha^2$. The solution of this system of equations should agree with the solution of the fully quantum density matrix equation in the limit that the cavity mode is well populated.

Given that only situations in which the pump laser will drive the atom weakly are being considered here, it is possible to make the further approximation that the excited state of the atom can adiabatically eliminated. This will decrease the state space required for the calculation by a factor of two, thus improving the efficiency. This will be especially necessary when considering more than one atom at a time, which is expected to be computationally intensive.

The adiabatic-elimination procedure is easiest to implement using projection-operator techniques. The goal is to break Eq. (5.9) into four separate equations, one each for the sub-density-matrices $\rho_{ij} = P_i \rho P_j$, for i,$j = g$,e, and where P_i is the projection operator into the i subspace. These sub-equations are

$$\dot{\rho}_{ee} = -\Gamma \rho_{ee} + i\left[g(x)\alpha + \Omega\right]\left(\rho_{eg}\sigma - \sigma^\dagger \rho_{ge}\right) \tag{5.11}$$

$$\dot{\rho}_{eg} = -\left(\frac{\Gamma}{2} - i\delta_a\right)\rho_{eg} + i\left[g(x)\alpha + \Omega\right]\left(\rho_{ee}\sigma^\dagger - \sigma^\dagger \rho_{gg}\right) \tag{5.12}$$

$$\dot{\rho}_{ge} = -\left(\frac{\Gamma}{2} + i\delta_a\right)\rho_{ge} - i\left[g(x)\alpha + \Omega\right]\left(\sigma\rho_{ee} - \rho_{gg}\sigma\right) \tag{5.13}$$

$$\dot{\rho}_{gg} = \Gamma \rho_{ee} + i\left[g(x)\alpha + \Omega\right]\left(\rho_{ge}\sigma^\dagger - \sigma\rho_{eg}\right). \tag{5.14}$$

The next step is to set $\dot{\rho}_{ee} = \dot{\rho}_{eg} = \dot{\rho}_{ge} = 0$ (detailed explanations of this procedure can be found, for example, in Refs [8] and [60]). The term ρ_{ee} in the two optical coherence equations can also be neglected (again, see [60]) to obtain

$$\rho_{eg} = \frac{g(x)\alpha + \Omega}{\delta_a + i\frac{\Gamma}{2}}\sigma^\dagger \rho_{gg} \tag{5.15}$$

$$\rho_{ge} = \frac{g(x)\alpha + \Omega}{\delta_a - i\frac{\Gamma}{2}}\rho_{gg}\sigma. \tag{5.16}$$

The condition $\dot{\rho}_{ee} = 0$ can now be imposed on the ρ_{ee} equation, and, substituting in the

values of the optical coherences just obtained,

$$\begin{aligned}\rho_{ee} &= \frac{i}{\Gamma}\left[g(x)\alpha+\Omega\right]^2\left[\frac{1}{\delta_a+i\frac{\Gamma}{2}}-\frac{1}{\delta_a-i\frac{\Gamma}{2}}\right]\sigma^\dagger\rho_{gg}\sigma \\ &= \frac{\left[g(x)\alpha+\Omega\right]^2}{\delta_a^2+\left(\frac{\Gamma}{2}\right)^2}\sigma^\dagger\rho_{gg}\sigma \\ &= s\sigma^\dagger\rho_{gg}\sigma,\end{aligned} \tag{5.17}$$

where the saturation parameter of the atom due to interaction with both the laser and the cavity field has been defined,

$$s = \frac{\left[g(x)\alpha+\Omega\right]^2}{\delta_a^2+\left(\frac{\Gamma}{2}\right)^2}. \tag{5.18}$$

Inserting the expression for ρ_{ee} along with the previously obtained optical-coherence expressions into the ground-state equation of motion,

$$\begin{aligned}\dot{\rho}_{gg} &= \Gamma s\sigma^\dagger\rho_{gg}\sigma + i\left[g(x)\alpha+\Omega\right]^2\left[\frac{\rho_{gg}\sigma\sigma^\dagger}{\delta_a-i\frac{\Gamma}{2}}-\frac{\sigma\sigma^\dagger\rho_{gg}}{\delta_a+i\frac{\Gamma}{2}}\right] \\ &= \Gamma s\sigma^\dagger\rho_{gg}\sigma + i\left[g(x)\alpha+\Omega\right]^2\left[\frac{\delta_a+i\frac{\Gamma}{2}}{\delta_a^2+\left(\frac{\Gamma}{2}\right)^2}\rho_{gg}\sigma\sigma^\dagger-\frac{\delta_a-i\frac{\Gamma}{2}}{\delta_a^2+\left(\frac{\Gamma}{2}\right)^2}\sigma\sigma^\dagger\rho_{gg}\right] \\ &= i\delta_a s\left[\rho_{gg},\sigma\sigma^\dagger\right]-\frac{\Gamma}{2}s\left\{\rho_{gg},\sigma\sigma^\dagger\right\}+\Gamma s\sigma^\dagger\rho_{gg}\sigma,\end{aligned} \tag{5.19}$$

where the square brackets denote a commutator while the curly brackets denote an anticommutator. Note that the last two terms comprise a decay operator of Lindblad form. This is encouraging, since the adiabatic elimination applied to Lindblad-type system should yield another Lindblad-type system. Note also that all terms are of first order in the perturbation parameter s. This makes sense because the above adiabatic-elimination procedure is equivalent to expanding the equations of motion in powers of the intensity of the laser driving transitions within the atom, then truncating this expansion and keeping only terms up to first order.

The ground-state equation of motion that has been obtained can now be solved using the same wave-function Monte Carlo technique described in Chapter 3, where at each time step the other coupled equation of the cavity mode amplitude α found

above must be consistently solved. Note that, as opposed to the atom-laser system studied in Chapter 3, the equations here consist of two separate entities coupled to the photon reservoir. These must each be treated separately, with appropriate quantum jump operators. In any given time step, it is possible for either or both the atom and the cavity to undergo a quantum jump. The jump operator for the atom is identical to the operator used in Chapter 3, except that it is much simpler since the atom here is only a two-level system. The jump operator for the cavity causes the cavity mode, which is a quantum harmonic oscillator, to decay down the ladder by one step. The properties of this operator are easily obtained from the atomic case, with the lowering operator a playing the role of the internal atomic lowering operator (i.e., Pauli spin matrix) σ.

5.3.2 Multiple atoms

For N atoms, with each atom interacting individually with the cavity, and neglecting interactions between different atoms, the system Hamiltonian becomes

$$H_s = -\hbar\delta_c a^\dagger a + \sum_{i=1}^{N} H_i, \tag{5.20}$$

where H_i is the Hamiltonian describing a single atom and its interaction with the pump laser,

$$H_i = -\hbar\delta_a \sigma_i^\dagger \sigma_i + \hbar\left[\sigma_i^\dagger (ga + \Omega) + \text{H.c.}\right]. \tag{5.21}$$

5.3.3 Accounting for Raman losses and other experimental effects

In order to extend the model just developed to describe Raman transitions that occur in molecules, the following procedure can be employed during the Monte Carlo wave-function procedure. At the end of each time step, the saturation of the atom given in Eq. (5.18), due to the atom's interaction with both the laser and the cavity mode, can be calculated. Then, using a random number generated in the simulation, along

with the knowledge of the branching ratio for Rayleigh to Raman scattering processes obtained from details of the internal structure of the molecule, it can be determined whether or not a Raman transition has occurred. The probability of this occurrence is proportional to the value of the saturation parameter. If a Raman transition does occur, the molecule can be removed from the simulation.

The detailed time-dependent calculations that the method presented here yields also allow for the ability to include realistic experimental effects that simpler calculations must ignore. This can be useful when the success of an experiment depends on factors such as the loading of a pulse of molecules into the cavity region, or the escape of fast-moving molecules out of the cavity region. In principle, it is possible to include all of these features in the Monte Carlo procedure. For example, using the many-atom model, the simulation could begin with a certain number of atoms of a given temperature. These atoms then begin cooling, while new atoms can be introduced as time evolves.

5.4 Comparison of fully quantum to semiclassical model

The validity of the classical-cavity-mode approximation made earlier can be tested by performing Monte Carlo simulations using both the fully quantum equations of motion and the semiclassical equations of motion. A simulation is set up in which an ensemble of atoms is cooled using cavity laser cooling. The possibility of Raman transitions is neglected for the present case. The parameters for the simulation are $\Omega = 5\omega_r$, $g = \omega_r$, $\eta = 20\omega_r$, $\delta_a = -10\omega_r$, $\delta_c = -20\omega_r$, $\Gamma = 2\omega_r$, $\kappa = 5\omega_r$, and an initial temperature of around $T = 50\hbar\omega_r/k_B$. The calculation utilizes the single-atom model developed above, and propagates 25 stochastic wave functions. The cavity-laser detuning δ_c is held fixed.

The ensemble-average population distribution for a series of times during the propagation is shown in Fig. 5.1. From these plots, it can be seen how the cooling affects only the population with velocities (both positive and negative) that satisfy the

resonance condition in Eq. (5.2), and also including velocities in a range of $\pm\kappa/2k_L$ around that point. Population around $p = \pm 8\hbar k_L$ is shifted into lower momentum states as the scattering proceeds, leading to a buildup of population in the middle of the distribution. The cavity-laser detuning could then be tuned slowly as the population shifted down, squeezing the ensemble towards the center of the graph. Thus, it would be expected that the limiting temperature should be on the order of κ, which is in accordance with other cooling theories. This limit has been verified by the simulations.

The average kinetic energy over time for the same calculation is shown in Fig. 5.2. The black line represents the calculation performed using the fully quantum model, while the red line represents the calculation performed using the model with the classical-cavity-mode approximation. The results are in good agreement within the error bars of the calculation, which used only 25 stochastic wave functions. This indicates that the numerically faster semiclassical model provides a good alternative to the slower fully quantum model.

Figure 5.3 illustrates the evolution of the population of the cavity mode over time for the same calculation. The black line is again obtained using the fully quantum model, and the quantity calculated is the quantum-mechanical average of the cavity photon number operator $n = a^\dagger a$. And again, the red line is obtained using the semiclassical model, with the quantity calculated being the average of the square of the cavity-mode amplitude α^2. The fully quantum calculation was performed including only the first 5 cavity states ($n = 0$ - 4) in the numerical basis. It can be observed in the figure that the results do not agree well in the short term, with the semiclassical calculation oscillating with much greater amplitude than the fully quantum calculation, before the two settle down in agreement at a value of 1. This is not surprising, though, since a cavity population of unity is hardly in the high-population limit for which the classical-mode approximation is valid. Despite this discrepancy, the evolution of the atomic momentum distribution in Fig. 5.2 agrees quite well. This is encouraging, as the important quantity

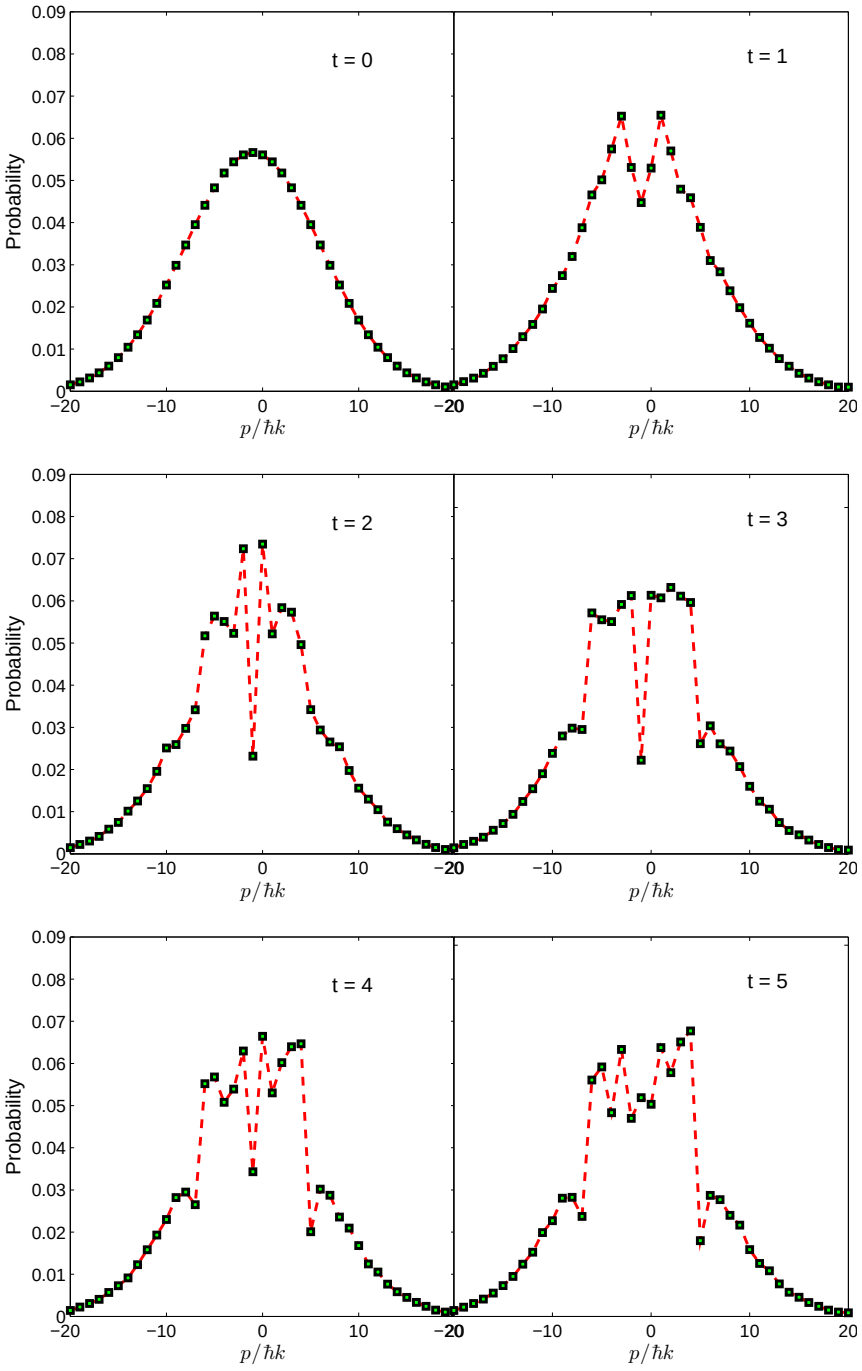

Figure 5.1: Time evolution of the momentum probability distribution for an ensemble of particles undergoing cavity laser cooling. Time is indicated, measured in units of the inverse recoil frequency ω_r^{-1}.

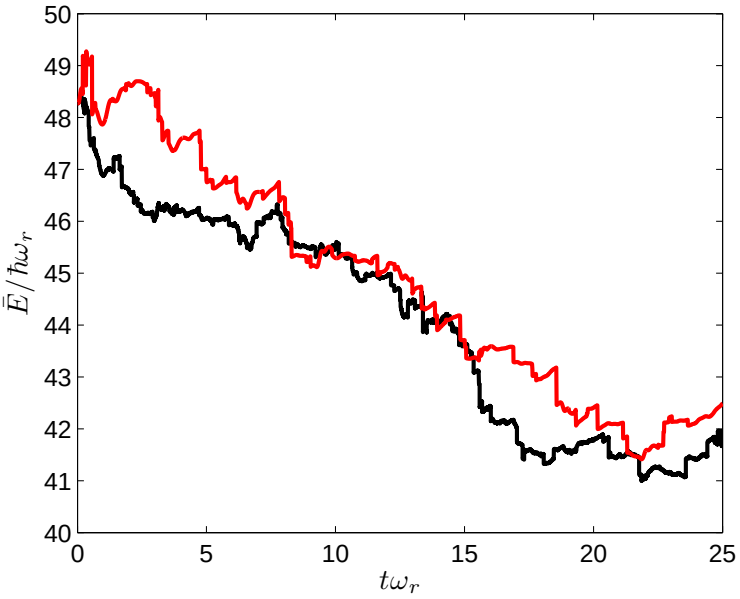

Figure 5.2: Time evolution of the average kinetic energy of an ensemble of particles undergoing cavity laser cooling. Energy is given in units of the recoil energy $\hbar\omega_r$ and time is measured in units of the inverse recoil frequency ω_r^{-1}. The black line was obtained using the fully quantum model while the red line was obtained using the semiclassical model.

for studying cooling processes is the momentum distribution, and not the cavity-mode properties.

5.5 Conclusion

This section has explored an interesting application of the master equation techniques built up elsewhere in this thesis. The generalization of the equations of motion for an atom and a laser, to include a cavity, adds a great deal of richness to the phenomena that can be explored. Extending the stochastic wave-function methods first applied to an atom to a cavity interacting with the photon vacuum provided another example of the utility of such techniques. In the end, however, the number of atoms required to explore the collective effects as originally intended proved to be out of reach of these methods, given the computing speeds of the present. More efficient models that treat the center of mass of the atom classically have had more success in observing collective-cooling phenomena. The main practical use of the calculation methods presented here has been in providing realistic modeling of experimental details.

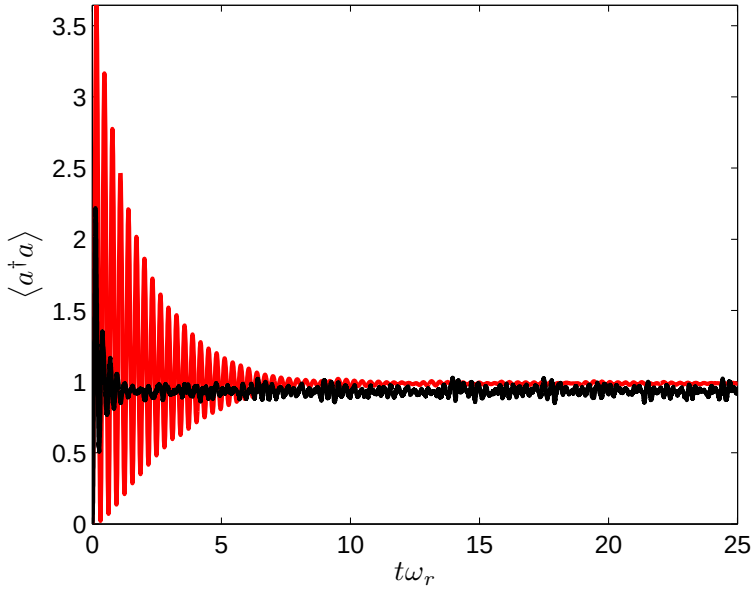

Figure 5.3: Time evolution of the cavity-mode population. The black line was obtained using the fully quantum model, calculating the quantum-mechanical average of the cavity photon number operator $n = a^\dagger a$. The red line was obtained using the semiclassical model, calculating the average of the square of the cavity-mode amplitude α^2. Time is measured in units of the inverse recoil frequency ω_r^{-1}.

Chapter 6

Nonlinear Optical Spectroscopy

6.1 Introduction

The goal of this chapter is to bring together some of the ideas developed in this thesis and apply them to the subject of nonlinear optical spectroscopy. The problem is formulated in a rather general manner, while the eventual aim is to provide a theoretical analysis of the physics of collisional effects on atomic lineshapes. An important application of this theory is the investigation of the experimental technique of transient four-wave mixing, in which a series of short, temporally spaced laser pulses are applied to an atomic or molecular gas or to a condensed-matter system. This setup can provide a great deal of information about the interaction properties of the system. Importantly, details of collisions within the system can be probed on a time scale for which the Markov approximation, which has been utilized in Chapter 3 and Appendices B and C of this thesis, is no longer valid. The physics of these short time scales, for which the interaction properties are affected by the system's memory of previous events, is referred to as non-Markovian dynamics.

The current state of ultrafast laser technology has made possible the production of laser pulses short enough to effectively probe the non-Markovian regime. Recent experiments at JILA have made use of these advances in order to observe non-Markovian dynamics in the collisions between atoms in a dense gas of potassium [90]. A common signature of physics beyond the Markov approximation is revealed by lineshapes that

do not conform to a Lorentzian profile.

The field of nonlinear optical spectroscopy is well established and contains a refined set of concepts, formalism, and techniques [91]. The development in this chapter aims to marry these established methods to a detailed microscopic theory of atomic collisions. Beginning in the 1950's, physicists have approached the problem of a theoretical treatment of the phenomenon called pressure broadening, in which collisions within a gas of atoms have the effect of broadening the spectral lines obtained by probing the gas with light. An atom, by itself in free space, will exhibit a finite-width lineshape when probed. This lineshape is a result of the atom's constant interaction with the surrounding photon vacuum, and it is this coupling that produces the phenomenon known as spontaneous emission, a subject explored in detail elsewhere in this thesis. Introducing the interaction with surrounding particles, which can be thought of as another reservoir in addition to the photon vacuum, causes the lineshapes to be further broadened.

Some of the earliest work on the theory of pressure broadening was done by Baranger [92, 93, 94], who developed an extensive theory utilizing relaxation theory, in which a single atom was modeled as interacting with a reservoir of other atoms, as well as the photon reservoir. This provided the basis for further work by others such as Fano [95, 96, 97] and Ben-Reuven [98, 99, 100, 101]. Fano's biggest contribution to this field was to rework Baranger's theory into a much more elegant formalism of relaxation theory, as presented initially in Ref. [96] and in a more pedagogical format in Ref. [97]. Ben-Reuven, whose early work was with Fano, continued along these lines to extend and apply the theory to pressure-broadening experiments.

The theory up to this point was mostly within what is called the impact approximation, in which it is assumed that particles interact with each other instantaneously before moving on, and which is equivalent to the Markov approximation. Later work by Cooper and Burnett [102, 103, 104], Silbey and Harris [105], Szudy and Balis [106, 107], Allard and Keilkopf [108], and Mukamel [109] built on previous work, applying the

theory to newer experiments as well as considering physics outside the impact approximation.

In the theory presented in the chapter, the modern methods of nonlinear optical spectroscopy will be used, with the physics of the interparticle interactions described by extending the relaxation-theory techniques cited above. The nonlinear spectroscopy techniques offer the advantage of being well suited to describing time-dependent phenomena and experimental techniques such as transient multiwave mixing. The established relaxation-theory techniques offer the advantage of a detailed description of particle scattering using realistic potentials and one or more collision channels. The main goal of this chapter is to present the basic ideas of this theory, with the hope that they can be used in the future to better understand the physics of the experiments currently being conducted.

6.2 Basics of nonlinear optical spectroscopy

Many sources describe the formalism of nonlinear optics, and the basics will be summarized in this section before attempting to incorporate scattering relaxation theory. In particular, Ref. [91] by Mukamel provides an elegant and detailed development of the methods of nonlinear optics, and this section will employ the same notation and terminology. Beginning with the the Hamiltonian of the total system,

$$H = H_0^{(S)} + H_0^{(B)} + H_{SB} + H_{SL}(t), \tag{6.1}$$

where $H_0^{(S)}$ is the Hamiltonian of the atom or molecule (system), $H_0^{(B)}$ is the Hamiltonian of the bath, which could be the photon vacuum and/or other perturbing particles, H_{SB} is the interaction of the system with the bath, and H_{SL} is the interaction of the system with all of the probe lasers. The density matrix obeys the Liouville equation,

$$\frac{d\rho}{dt} = -\frac{i}{\hbar}\mathcal{L}\rho - \frac{i}{\hbar}\mathcal{L}_{\text{int}}(t)\rho. \tag{6.2}$$

Here, the following Liouville-space operators have been defined (see Appendix A for a brief review of Liouville space),

$$\mathcal{L}A = \left[H_0^{(S)} + H_0^{(B)} + V_{SB}, A\right], \tag{6.3}$$

$$\mathcal{L}_{\text{int}}A = \left[H_{SL}(t), A\right], \tag{6.4}$$

$$\mathcal{V}A = \left[V, A\right], \tag{6.5}$$

where V is the dipole operator such that $H_{SL}(t) = -E(\mathbf{r},t)\cdot V$. Expanding the density matrix in powers of the electric field yields

$$\rho(t) = \rho^{(0)}(t) + \rho^{(1)}(t) + \rho^{(2)}(t) + \ldots \tag{6.6}$$

The polarization,

$$P(\mathbf{r},t) = \text{Tr}\left[V\rho(t)\right] = \langle\langle V|\rho(t)\rangle\rangle, \tag{6.7}$$

is expanded similarly, and the nth order contribution, $P^{(n)}(\mathbf{r},t) = \langle\langle V|\rho^{(n)}(t)\rangle\rangle$, can be shown to be

$$\begin{aligned} P^{(n)}(\mathbf{r},t) = \int_0^\infty dt_n \int_0^\infty dt_{n-1} \ldots \int_0^\infty dt_n S^{(n)}(t_n, t_{n-1}, \ldots, t_1) \\ \times E(\mathbf{r}, t-t_n)E(\mathbf{r}, t-t_n-t_{n-1})\ldots E(\mathbf{r}, t-t_n-t_{n-1}\ldots-t_1), \end{aligned} \tag{6.8}$$

with

$$S^{(n)}(t_n, t_{n-1}, \ldots, t_1) = \left(\frac{i}{\hbar}\right)^n \langle\langle V|\mathcal{G}(t_n)\mathcal{V}\mathcal{G}(t_{n-1})\mathcal{V}\ldots\mathcal{G}(t_1)\mathcal{V}|\rho(-\infty)\rangle\rangle\,, \tag{6.9}$$

the nth-order nonlinear response function. The retarded Liouville-space Green function for evolution of the system and bath without interaction with the probe laser is given by

$$\mathcal{G}(t) = \theta(t)\exp\left(-\frac{i}{\hbar}\mathcal{L}t\right). \tag{6.10}$$

The first order response function gives the usual linear response of a system. The present work will be primarily concerned with the first important nonlinear contribution.

Since the second-order contribution vanishes for homogeneous systems [91], this will be the third-order nonlinear response function,

$$S^{(3)}(t_3, t_2, t_1) = \langle\langle V|\mathcal{G}(t_3)\mathcal{V}\mathcal{G}(t_2)\mathcal{V}\mathcal{G}(t_1)\mathcal{V}|\rho(-\infty)\rangle\rangle\,. \tag{6.11}$$

This equation separates the physics due to interactions with the probe-laser field $\mathcal{V}$, from the physics of the atom interacting with the other atoms and with the vacuum photon reservoir, described by the Green function $\mathcal{G}(t)$. This is convenient, and the theory developed later derives an expression for this Green function utilizing a detailed scattering theory framed in a relaxation-theory format. With a method of calculating $\mathcal{G}(t)$ in hand, Eq. (6.11) can be used to determine a variety of features relevant to transient four-wave mixing experiments.

6.3 Phenomenological damping model

Some important concepts are now introduced, in the context of a simple model damping. The effects of collisions on an atomic lineshape can be divided into two categories, homogeneous and inhomogeneous. Homogeneous broadening is a dynamical effect that is caused by the repeated collisions an atom undergoes, leading to a fluctuation in the atom's transition energy. This fluctuation, over time, results in a net broadening. Inhomogeneous broadening, on the other hand, is a static effect due to the fact that atoms see different interaction-induced frequency shifts depending on their location, and becomes more prominent at low temperatures and in solids. In experiments, the basic CW photon-echo technique allows for the cancelation of the effects of inhomogeneous broadening. Each atom's transition frequency, having a static shift, causes the phase to evolve at a different rate when the system is probed. When the second pulse is applied and the evolution reversed, the disparate atoms all catch up with each other at the same time, and an echo pulse is emitted. Homogeneous broadening, however, is unaffected by this technique, and remains in the observed signal.

The JILA experiment mentioned above [90] uses transient four-wave mixing techniques to probe collision physics on very short time scales. Over such short probe times, the collision physics that usually produces homogeneous broadening is now approximately static (the so-called quasi-static approximation), with each atom's relative distance changing very little over the probe time. Thus, although the scattering is still a fundamentally dynamical process, the physics being probed is of the inhomogeneous type. This means that a photon echo technique can be applied to cancel out this new type of inhomogeneous broadening, and details about the interatomic potentials can by probed. As a result, this type of technique is generally not considered to be a true photon echo, since there is no fundamentally static interaction shifts in the problem, as there is in the traditional sense of photon echoes. Nevertheless, the basic idea is the same.

A basic understanding of collisional damping can be obtained by following the phenomenological approach presented in many introductory quantum-optics textbooks, a good example of which is Meystre and Sargent [57]. To begin with, take a simple density-matrix model of a two level atom, ground state $|g\rangle$ and excited state $|e\rangle$, including spontaneous emission with a rate Γ, i.e., the optical Bloch equations. Since homogeneous collisional broadening is caused by a fluctuation of the atomic transition frequency over time as the atom interacts with other atoms, it affects the off-diagonal density-matrix element. Representing the fluctuation as $\delta\omega(t)$ results in an equation of motion for the coherence density-matrix term of

$$\dot{\rho}_{ge} = -\left(i\omega_0 + i\delta\omega(t) + \Gamma\right)\rho_{ge}, \tag{6.12}$$

which has the formal solution

$$\rho_{ge}(t) = \rho_{ge}(0)\exp\left(-(i\omega_0+\Gamma)t - \int_0^t dt' i\delta\omega(t')\right). \tag{6.13}$$

If, as is often the case, the time scale considered is long enough that the fluctuating term oscillates many times over that period, the integral will evaluate to zero. (Actually,

the integral might yield a nonzero constant, but this could just be absorbed into the bare transition frequency ω_0. This is the case for an atom interacting with the photon vacuum: the resulting Lamb shift is considered to be a part of the bare atomic energy splittings.) This will yield an equation describing exponential decay of the coherence matrix element, and is the case for most descriptions of spontaneous emission.

6.4 Transient multiwave mixing using relaxation theory

6.4.1 Relaxation theory of static pressure broadening

It is now necessary to summarize the essential results of the relaxation theory of pressure broadening. The work by Fano [96] formalizes and generalizes earlier work [92, 93, 94], and the notation and techniques used by Fano will be employed here.

Consider a system, consisting of one, or possibly more atoms or molecules, and a bath, consisting of a large number of perturbing atoms. The two can interact with each other. Note that, for simplicity, spontaneous emission (another form of relaxation) has been left out for now. However, this does not affect the equations in any nontrivial way, and it can be easily inserted later. The total Hamiltonian is

$$H = H_0^{(S)} + H_0^{(B)} + V_{SB}, \tag{6.14}$$

where $H_0^{(S)}$ is the Hamiltonian of the system, $H_0^{(S)}$ is the Hamiltonian of the particle bath, and V_{SB} is the interaction between the two.

An important part of the development in Ref. [96] is to show that the resolvent operator for the total evolution can be disentangled into a contribution of the bare system and bath, and a contribution of the interaction of the two by using a known operator identity,

$$\frac{1}{\omega - \mathcal{L}_0 - \mathcal{L}_1} = \frac{1}{\omega - \mathcal{L}_0}\left[1 + M(\omega)\frac{1}{\omega - \mathcal{L}_0}\right]. \tag{6.15}$$

The operator $M(\omega)$ contains all of the physics of the interaction, with everything else

simply free evolution, and it can be expressed in various forms,

$$\begin{aligned} M(\omega) &= \frac{1}{1-\mathcal{L}_1(\omega-\mathcal{L}_0)^{-1}}\mathcal{L}_1 \\ &= \mathcal{L}_1\frac{1}{1-(\omega-\mathcal{L}_0)^{-1}\mathcal{L}_1} \\ &= \mathcal{L}_1+\mathcal{L}_1\frac{1}{\omega-\mathcal{L}_0-\mathcal{L}_1}\mathcal{L}_1 \\ &= \mathcal{L}_1\sum_{n=0}^{\infty}\left[\frac{1}{\omega-\mathcal{L}_0}\mathcal{L}_1\right]^n. \end{aligned} \tag{6.16}$$

The interaction operator M is then expanded in terms of density,

$$M=\sum_{i}^{n}M_i^{(1)}+\sum_{i=2}^{n}\sum_{j}^{i-1}M_{ij}^{(2)}+\sum_{i}^{n}\sum_{j}^{i-1}\sum_{k}^{j-1}M_{ijk}^{(3)}\ldots, \tag{6.17}$$

where n is the number of atoms or molecules. Reference [96] restricts its analysis to include only the first term in the above expansion, describing only binary collisions, and defining $m=M_i^{(1)}$. The present work will make the same assumption.

Also assumed in Ref. [96], and common to most of the early work on pressure broadening, is that the total density matrix can be factorized into a product of a system density matrix and a bath density matrix,

$$\rho=\rho^{(S)}\rho^{(B)}. \tag{6.18}$$

The validity of this assumption is explored in later papers [100, 102] by other authors. For present purposes, this factorization is assumed to be valid.

Having made the binary-collision approximation, the operator m, which it is useful to think of as a Liouville-space version of the t-matrix, obeys the equation

$$m(\omega)=\mathcal{L}+\mathcal{L}\frac{1}{\omega-\mathcal{L}_0}t(\omega), \tag{6.19}$$

which is a Liouville-space version of the Lippman-Schwinger equation. Ref. [96] shows that this equation is solved by

$$\begin{aligned} m(\omega)=\frac{\omega-\mathcal{L}_0}{2\pi i}\int_{-\infty+i\eta}^{\infty+i\eta}d\psi\Bigg\{&\frac{1}{\psi-H_0}t(\psi)+\frac{1}{\psi-\omega-H_0^*}t^*(\psi-\omega) \\ &+\frac{1}{\psi-H_0}\frac{1}{\psi-\omega-H_0^*}t(\psi)t^*(\psi-\omega)\Bigg\}\frac{\omega-\mathcal{L}_0}{(\psi-H_0)\,(\psi-\omega-H_0^*)}, \end{aligned} \tag{6.20}$$

with

$$\epsilon = \mathrm{Im}\omega > \eta > 0. \tag{6.21}$$

This ensures that $\mathrm{Im}(\psi - \omega) < 0$.

6.4.2 Extension to transient nonlinear-optics problems

Reference [96] manipulates the expression for the Liouville-space interaction operator given in Eq. (6.20), expanding it in a series of terms involving the two-particle t-matrix. Although this series of terms is rather complicated, it provides a starting point for making approximations.

Now, a method will be developed that utilizes m, obtained in some manner, and applies it to the nonlinear optics formalism earlier in this chapter. This means obtaining a Green function that can be used in determining the third-order nonlinear response function in Eq. (6.11). Using Eq. (6.15) and taking the Fourier transform to go to the time domain, the time-domain Green function for evolution of the system interacting with the perturber bath is given by

$$\mathcal{G}(t) = \mathcal{G}_0(t) - \frac{1}{2\pi i}\int_{-\infty}^{\infty} d\omega \mathcal{G}_0(\omega) m(\omega) \mathcal{G}_0(\omega) e^{-i\omega t}. \tag{6.22}$$

Expanding the frequency-space Green function in a basis of bare-system Liouville-space eigenstates,

$$\begin{aligned} \mathcal{G}_0(\omega) &= \frac{1}{\omega - \mathcal{L}_0 + i\epsilon} \\ &= \sum_{n,m} \frac{|nm\rangle\rangle\langle\langle nm|}{\omega - \omega_{nm} + i\epsilon}, \end{aligned} \tag{6.23}$$

which yields

$$\begin{aligned}\mathcal{G}(t) &= \mathcal{G}_0(t) - \sum_{n,m,n',m'} |nm\rangle\rangle\langle\langle n'm'| \frac{1}{2\pi i}\int_{-\infty}^{\infty} d\omega \frac{\langle\langle nm|m(\omega)|n'm'\rangle\rangle e^{-i\omega t}}{(\omega-\omega_{nm}+i\epsilon)(\omega-\omega_{n'm'}+i\epsilon)} \\ &= \mathcal{G}_0(t) + \sum_{n,m,n',m',\omega_{nm}\neq\omega_{n'm'}} |nm\rangle\rangle\langle\langle n'm'|\,\theta(t) \\ &\qquad \times\left(\frac{m_{nm,n'm'}(\omega_{nm})}{\omega_{nm}-\omega_{n'm'}}e^{-i\omega_{nm}t} + \frac{m_{nm,n'm'}(\omega_{n'm'})}{\omega_{n'm'}-\omega_{nm}}e^{-i\omega_{n'm'}t}\right)\end{aligned} \tag{6.24}$$

In obtaining the above expression, integration has been performed along the real line, skirting the poles and obtaining residues.

If the methods in Ref. [96] are used to calculate m, then it can be applied to Eq. (6.24) to determine a time-dependent Green function for use in Eq. (6.11). In turn, this quantity will provide a powerful means of understanding the physics of non-Markovian dynamics in experiments.

6.5 Conclusion

The theory in this chapter represents a preliminary idea for merging the elegant techniques of relaxation theory — applied successfully to static pressure broadening in the past — to the time-dependent nonlinear optics experiments being conducted today. In it's current form, it is an interesting exercise in the methods of Liouville space, system-reservoir interactions, and relaxation theory that have been discussed extensively in this thesis. Additionally, the ideas here show promise for obtaining a better understanding of non-Markovian dynamics.

Bibliography

[1] J. W. Dunn, D. Blume, B. Borca, B. E. Granger, and C. H. Greene. Feshbach resonance cooling of trapped atom pairs. Phys. Rev. A, 71(3):033402, 2005.

[2] J. W. Dunn and C. H. Greene. Predictions of laser-cooling temperatures for multilevel atoms in three-dimensional polarization-gradient fields. Phys. Rev. A, 73(3):033421, 2006.

[3] J. W. Dunn, J. W. Thomsen, C. H. Greene, and F. C. Cruz. Coherent Quantum Engineering of Free-Space Laser Cooling. submitted to Phys. Rev. Lett., Arxiv preprint physics/0610272, 2006.

[4] A. Einstein. Uber die von der molekularkinetischen Theorie der Warme geforderte Bewegung von in ruhenden Flussigkeiten suspendierten Teilchen. Ann. Phys. (Leipzig), 17:549.

[5] M. Smoluchowski. Zur kinetischen Theorie der Brownschen Molekularbewegung und der Suspensionen. Ann. Phys. (Leipzig), 21(756), 1906.

[6] C. W. Gardiner. Handbook of Stochastic Methods. Springer, New York, 1985.

[7] P. Langevin. Sur la theorie du mouvement brownien. C. R. Acad. Sci., 46:530, 1908.

[8] C. Cohen-Tannoudji, J. Dupont-Roc, and G. Grynberg. Atom-Photon Interactions. Wiley, New York, 1998.

[9] K. Berg-Sorenson, Y. Castin, E. Bonderup, and K. Molmer. Momentum diffusion of atoms moving in laser fields. J. Phys. B, 25(20):4195, 1992.

[10] K. Mølmer, Y. Castin, and J. Dalibard. Monte Carlo wave-function method in quantum optics. J. Opt. Soc. Am. B, 10(3):524, 1993.

[11] Y. Castin and K. Mølmer. Monte Carlo Wave-Function Analysis of 3D Optical Molasses. Phys. Rev. Lett., 74(19):3772, 1995.

[12] R. Dum, P. Zoller, and H. Ritsch. Monte Carlo simulation of the atomic master equation for spontaneous emission. Phys. Rev. A, 45(7):4879, 1992.

[13] N. Gisin and I. C. Percival. Wave-function approach to dissipative processes: are there quantum jumps? Phys. Lett. A, 167(4):315, 1992.

[14] N. Gisin and I. C. Percival. The quantum-state diffusion model applied to open systems. J. Phys. A, 25(21):5677, 1992.

[15] H. J. Carmichael. An Open-Systems Approach to Quantum Optics. Springer-Verlag, Berlin, 1993.

[16] J. Dalibard and C. Cohen-Tannoudji. Laser cooling below the Doppler limit by polarization gradients: simple theoretical models. J. Opt. Soc. Am. B, 6(11):2023, 1989.

[17] P. J. Ungar, D. S. Weiss, E. Riis, and S. Chu. Optical molasses and multilevel atoms: theory. J. Opt. Soc. Am. B, 6(11):2058, 1989.

[18] P. D. Lett, W. D. Phillips, S. L. Rolston, C. E. Tanner, R. N. Watts, and C. I. Westbrook. Optical molasses. J. Opt. Soc. Am. B, 6(11):2084, 1989.

[19] M. H. Anderson, J. R. Ensher, M. R. Matthews, C. E. Wieman, and E. A. Cornell. Observation of Bose-Einstein Condensation in a Dilute Atomic Vapor. Science, 269(5221):198, 1995.

[20] K. B. Davis, M. O. Mewes, and W. Ketterle. An analytical model for evaporative cooling of atoms. Appl. Phys. B, 60(2):155, 1995.

[21] J. Herbig, T. Kraemer, M. Mark, T. Weber, C. Chin, H. C. Nägerl, and R. Grimm. Preparation of a Pure Molecular Quantum Gas. Science, 301(5639):1510, 2003.

[22] S. Dürr, T. Volz, A. Marte, and G. Rempe. Observation of Molecules Produced from a Bose-Einstein Condensate. Phys. Rev. Lett., 92(2):020406, 2004.

[23] K. E. Strecker, G. B. Partridge, and R. G. Hulet. Conversion of an Atomic Fermi Gas to a Long-Lived Molecular Bose Gas. Phys. Rev. Lett., 91(8):080406, 2003.

[24] K. Xu, T. Mukaiyama, J. R. Abo-Shaeer, J. K. Chin, D. E. Miller, and W. Ketterle. Formation of Quantum-Degenerate Sodium Molecules. Phys. Rev. Lett., 91(21):210402, 2003.

[25] H. Feshbach. Theoretical Nuclear Physics. Wiley, New York, NY, 1992.

[26] W. C. Stwalley. Stability of Spin-Aligned Hydrogen at Low Temperatures and High Magnetic Fields: New Field-Dependent Scattering Resonances and Predissociations. Phys. Rev. Lett., 37(24):1628, 1976.

[27] E. Tiesinga, B. J. Verhaar, and H. T. C. Stoof. Threshold and resonance phenomena in ultracold ground-state collisions. Phys. Rev. A, 47(5):4114, 1993.

[28] B. Borca, D. Blume, and C. H. Greene. A two-atom picture of coherent atom-molecule quantum beats. New J. Phys., 5(1):111, 2003.

[29] T. Busch, B. G. Englert, K. Rzażewski, and M. Wilkens. Two Cold Atoms in a Harmonic Trap. Found. Phys., 28(4):549, 1998.

[30] D. Blume and C. H. Greene. Fermi pseudopotential approximation: Two particles under external confinement. Phys. Rev. A, 65(4):043613, 2002.

[31] B. Borca. Two-Channel Zero-Range-Potential Model for the Feshbach Resonance. Private communication, 2003.

[32] C. H. Greene. Two-body Ultracold Feshbach Resonance Behavior versus Energy and Magnetic Field. Private communication, 2004.

[33] M. Greiner, C. A Regal, and D. S. Jin. Probing the Excitation Spectrum of a Fermi Gas in the BCS-BEC Crossover Regime. Phys. Rev. Lett., 94(7):070403, 2005.

[34] U. Fano. Effects of Configuration Interaction on Intensities and Phase Shifts. Phys. Rev., 124(6):1866, 1961.

[35] E. L. Bolda, E. Tiesinga, and P. S. Julienne. Effective-scattering-length model of ultracold atomic collisions and Feshbach resonances in tight harmonic traps. Phys. Rev. A, 66(1):013403, 2002.

[36] F. H. Mies, E. Tiesinga, and P. S. Julienne. Manipulation of Feshbach resonances in ultracold atomic collisions using time-dependent magnetic fields. Phys. Rev. A, 61(2):022721, 2000.

[37] W. Ketterle and D. E. Pritchard. Atom cooling by time-dependent potentials. Phys. Rev. A, 46(7):4051, 1992.

[38] D. Frese, B. Ueberholz, S. Kuhr, W. Alt, D. Schrader, V. Gomer, and D. Meschede. Single Atoms in an Optical Dipole Trap: Towards a Deterministic Source of Cold Atoms. Phys. Rev. Lett., 85(18):3777, 2000.

[39] N. Schlosser, G. Reymond, I. Protsenko, and P. Grangier. Sub-poissonian loading of single atoms in a microscopic dipole trap. Nature (London), 411(6841):1024, 2001.

[40] M. D. Barrett, J. A. Sauer, and M. S. Chapman. All-Optical Formation of an Atomic Bose-Einstein Condensate. Phys. Rev. Lett., 87(1):010404, 2001.

[41] P. Rabl, A. J. Daley, P. O. Fedichev, J. I. Cirac, and P. Zoller. Defect-Suppressed Atomic Crystals in an Optical Lattice. Phys. Rev. Lett., 91(11):110403, 2003.

[42] P. D. Lett, R. N. Watts, C. I. Westbrook, W. D. Phillips, P. L. Gould, and H. J. Metcalf. Observation of Atoms Laser Cooled below the Doppler Limit. Phys. Rev. Lett., 61(2):169, 1988.

[43] A. Bambini and A. Agresti. Radiative cooling force in atoms with multiplet structure. Phys. Rev. A, 56(4):3040, 1997.

[44] K. Mølmer. Friction and diffusion coefficients for cooling of atoms in laser fields with multidimensional periodicity. Phys. Rev. A, 44(9):5820, 1991.

[45] J. Javanainen. Numerical experiments in semiclassical laser-cooling theory of multistate atoms. Phys. Rev. A, 46(9):5819, 1992.

[46] J. Javanainen. Polarization gradient cooling in three dimensions: comparison of theory and experiment. J. Phys. B, 27(3):L41, 1994.

[47] A. P. Kazantsev and I. V. Krasnov. Rectification of the gradient force of resonant radiation pressure. JETP Lett., 46:332, 1987.

[48] R. Grimm, Y. B. Ovchinnikov, A. I. Sidorov, and V. S. Letokhov. Observation of a strong rectified dipole force in a bichromatic standing light wave. Phys. Rev. Lett., 65(12):1415, 1990.

[49] P. R. Hemmer, M. S. Shahriar, M. Prentiss, D. P. Katz, K. Berggren, J. Mervis, and N. P. Bigelow. First Observation of Forces on Three-Level Atoms in Raman Resonant Standing-Wave Optical Fields. Phys. Rev. Lett., 68(21):3148, 1992.

[50] R. Gupta, C. Xie, S. Padua, H. Batelaan, and H. Metcalf. Bichromatic Laser Cooling in a Three-Level System. Phys. Rev. Lett., 71(19):3087, 1993.

[51] M. Drewsen. Effective stimulated laser cooling of atoms with a three-level λ configuration by two negatively detuned standing light waves. Phys. Rev. A, 51(2):1407, 1995.

[52] X. Xu, T. H. Loftus, J. W. Dunn, C. H. Greene, J. L. Hall, A. Gallagher, and J. Ye. Single-Stage Sub-Doppler Cooling of Alkaline Earth Atoms. Phys. Rev. Lett., 90(19):193002, 2003.

[53] C. Fort, A. Bambini, L. Cacciapuoti, FS Cataliotti, M. Prevedelli, GM Tino, and M. Inguscio. Cooling mechanisms in potassium magneto-optical traps. Euro. Phys. J. D, 3(2):113, 1998.

[54] U. Schünemann, H. Engler, M. Zielonkowski, M. Weidemüller, and R. Grimm. Magneto-optic trapping of lithium using semiconductor lasers. Optics Communications, 158(1):263, 1998.

[55] R. Maruyama, R. H. Wynar, M. V. Romalis, A. Andalkar, M. D. Swallows, C. E. Pearson, and E. N. Fortson. Investigation of sub-Doppler cooling in an ytterbium magneto-optical trap. Phys. Rev. A, 68(1):011403, 2003.

[56] D. Lucas, P. Horak, and G. Grynberg. Sisyphus cooling of rubidium atoms on the D_2 ($F = 1 - F' = 1$) line: The role of the neighbouring transitions. Euro. Phys. J. D, 7(3), 1999.

[57] P. Meystre and M. Sargent III. Elements of Quantum Optics. Springer-Verlag, Berlin, 1998.

[58] C. W. Gardiner and P. Zoller. Quantum Noise. Springer-Verlag, Berlin, 2004.

[59] H. Spohn. Kinetic equations from Hamiltonian dynamics: Markovian limits. Rev. Mod. Phys., 52(3):569, 1980.

[60] C. Cohen-Tannoudji. In J. Dalibard, J.-M. Raimond, and J. Zinn-Justin, editors, Fundamental Systems in Quantum Optics, pages 1–164, Amsterdam, 1992. North-Holland.

[61] Y. Castin, H. Wallis, and J. Dalibard. Limit of Doppler cooling. J. Opt. Soc. Am. B, 6(2046):128, 1989.

[62] H. J. Kluge and H. Sauter. Levelcrossing experiments in the first excited $^1P_1$ states of the alkaline earths. Z. Phys., 270(4):295, 1974.

[63] K. Blum. Density Matrix Theory and Applications. Plenum, New York, NY, 1981.

[64] H. Katori, T. Ido, Y. Isoya, and M. Kuwata-Gonokami. Magneto-Optical Trapping and Cooling of Strontium Atoms down to the Photon Recoil Temperature. Phys. Rev. Lett., 82(6):1116, 1999.

[65] T. Kuwamoto, K. Honda, Y. Takahashi, and T. Yabuzaki. Magneto-optical trapping of Yb atoms using an intercombination transition. Phys. Rev. A, 60(2):R745, 1999.

[66] P. Gill, editor. Proceedings of the 6th Symposium on Frequency Standards and Metrology, St. Andrews, Scotland. World Scientific, 2001.

[67] M. Takamoto, F. L. Hong, R. Higashi, and H. Katori. An optical lattice clock. Nature (London), 435(7040):321, 2005.

[68] H. J. Metcalf and P. van der Straten. Laser Cooling and Trapping. Springer-Verlag, New York, 1999.

[69] M. Kasevich and S. Chu. Laser Cooling Below a Photon Recoil with Three-Level Atoms. Phys. Rev. Lett., 69(12):1741, 1992.

[70] A. Aspect, E. Arimondo, R. Kaiser, N. Vansteenkiste, and C. Cohen-Tannoudji. Laser cooling below the one-photon recoil energy by velocity-selective coherent population trapping: theoretical analysis. J. Opt. Soc. Am. B, 6(11):2112, 1989.

[71] H. W. Chan, A. T. Black, and V. Vuletić. Observation of Collective-Emission-Induced Cooling of Atoms in an Optical Cavity. Phys. Rev. Lett., 90(6):063003, 2003.

[72] C. A. Sackett, J. Chen, J. J. Tollett, and R. G. Hulet. Dipole-Force Laser Cooling in Multilevel Atoms. Laser Physics, 4:861, 1994.

[73] L. Tan, C. K. Zhong, C. L. Zhang, and Q. Zhang. Two-Photon Doppler Cooling of Rubidium Atoms to the Recoil Limit Using Cascade Transitions. Chin. J. Phys., 44(3), 2006.

[74] G. Morigi and E. Arimondo. Two-photon and EIT-assisted Doppler cooling in a three-level cascade system. Arxiv preprint quant-ph/0610223, 2006.

[75] G. Morigi, J. Eschner, and C. H. Keitel. Ground State Laser Cooling Using Electromagnetically Induced Transparency. Phys. Rev. Lett., 85(21):4458, 2000.

[76] C. F. Roos, D. Leibfried, A. Mundt, F. Schmidt-Kaler, J. Eschner, and R. Blatt. Experimental Demonstration of Ground State Laser Cooling with Electromagnetically Induced Transparency. Phys. Rev. Lett., 85(26):5547, 2000.

[77] I. Marzoli, J. I. Cirac, R. Blatt, and P. Zoller. Laser cooling of trapped three-level ions: Designing two-level systems for sideband cooling. Phys. Rev. A, 49(4):2771, 1994.

[78] M. Fleischhauer, A. Imamoglu, and J. P. Marangos. Electromagnetically induced transparency: Optics in coherent media. Rev. Mod. Phys., 77(2):633, 2005.

[79] W. C. Magno, R. L. Cavasso Filho, and F. C. Cruz. Two-photon Doppler cooling of alkaline-earth-metal and ytterbium atoms. Phys. Rev. A, 67(4):043407, 2003.

[80] N. Malossi, S. Damkjær, P. L. Hansen, L. B. Jacobsen, L. Kindt, S. Sauge, J. W. Thomsen, F. C. Cruz, M. Allegrini, and E. Arimondo. Two-photon cooling of magnesium atoms. Phys. Rev. A, 72(5):051403, 2005.

[81] R. Ciuryło, E. Tiesinga, and P. S. Julienne. Optical tuning of the scattering length of cold alkaline-earth-metal atoms. Phys. Rev. A, 71(3):030701, 2005.

[82] Y. Takasu, K. Maki, K. Komori, T. Takano, K. Honda, M. Kumakura, T. Yabuzaki, and Y. Takahashi. Spin-Singlet Bose-Einstein Condensation of Two-Electron Atoms. Phys. Rev. Lett., 91(4):040404, 2003.

[83] V. Vuletić and S. Chu. Laser Cooling of Atoms, Ions, or Molecules by Coherent Scattering. Phys. Rev. Lett., 84(17):3787, 2000.

[84] V. Vuletić, H. W. Chan, and A. T. Black. Three-dimensional cavity Doppler cooling and cavity sideband cooling by coherent scattering. Phys. Rev. A, 64(3):033405, 2001.

[85] A.T. Black, H.W. Chan, and V. Vuletić. Observation of Collective Friction Forces due to Spatial Self-Organization of Atoms: From Rayleigh to Bragg Scattering. Phys. Rev. Lett., 91(20):203001, 2003.

[86] P. Domokos and H. Ritsch. Collective Cooling and Self-Organization of Atoms in a Cavity. Phys. Rev. Lett., 89(25):253003, 2002.

[87] S. Zippilli, G. Morigi, and H. Ritsch. Suppression of Bragg Scattering by Collective Interference of Spatially Ordered Atoms with a High-Q Cavity Mode. Phys. Rev. Lett., 93(12):123002, 2004.

[88] P. Domokos and H. Ritsch. Mechanical effects of light in optical resonators. J. Opt. Soc. of Am. B, 20(5):1098, 2003.

[89] H. J. Carmichael. Statistical Methods in Quantum Optics: Master Equations and Fokker-Planck Equations. Springer, 1999.

[90] V. O. Lorenz and S. T. Cundiff. Non-markovian dynamics in a dense potassium vapor. Phys. Rev. Lett., 95(16):163601, 2005.

[91] S. Mukamel. Principles of Nonlinear Optical Spectroscopy. Oxford University Press, USA.

[92] M. Baranger. Simplified Quantum-Mechanical Theory of Pressure Broadening. Phys. Rev., 111(2):481, 1958.

[93] M. Baranger. Problem of Overlapping Lines in the Theory of Pressure Broadening. Phys. Rev., 111(2):494, 1958.

[94] M. Baranger. General Impact Theory of Pressure Broadening. Phys. Rev., 112(3):855, 1958.

[95] U. Fano. Description of States in Quantum Mechanics by Density Matrix and Operator Techniques. Rev. Mod. Phys., 29(1):74, 1957.

[96] U. Fano. Pressure Broadening as a Prototype of Relaxation. Phys. Rev., 131(1):259, 1963.

[97] U. Fano. Lectures on the many-body problem, vol. 2, 1964.

[98] A. Ben-Reuven. Impact Broadening of Microwave Spectra. Phys. Rev., 145(1):7, 1966.

[99] A. Ben-Reuven. Symmetry Considerations in Pressure-Broadening Theory. Phys. Rev., 141(1):34, 1966.

[100] A. Ben-Reuven. Resonance broadening of spectral lines. Phys. Rev. A, 4(6):2115, 1971.

[101] Y. Prior and A. Ben-Reuven. Nonimpact theory of four-wave mixing and intracollisional dynamics. Phys. Rev. A, 33(4):2362, 1986.

[102] K. Burnett, J. Cooper, R. J. Ballagh, and E. W. Smith. Collisional redistribution of radiation. I. The density matrix. Phys. Rev. A, 22(5):2005, 1980.

[103] K. Burnett and J. Cooper. Collisional redistribution of radiation. II. The effects of degeneracy on the equations of motion for the density matrix. Phys. Rev. A, 22(5):2027, 1980.

[104] K. Burnett and J. Cooper. Collisional redistribution of radiation. III. The equation of motion for the correlation function and the scattered spectrum. Phys. Rev. A, 22(5):2044, 1980.

[105] R. Sibley and R. A. Harris. Tunneling of Molecules in Low-Temperature Media: An Elementary Description. J. Phys. Chem., 93:7062, 1989.

[106] J. Szudy and W. E. Baylis. Unified Franck-Condon Treatment of Pressure Broadening of Spectral Lines. J. Quant. Spectrosc. Radiat. Transfer, 15:641, 1975.

[107] J. Szudy and W. E. Baylis. Profiles of Line Wings and Rainbow Satellites Associated with Optical and Radiative Collision. Phys. Rep., 266(3-4):127, 1996.

[108] N. Allard and J. Kielkopf. The effect of neutral nonresonant collisions on atomic spectral lines. Rev. Mod. Phys., 54(4):1103, 1982.

[109] S. Mukamel. Nonimpact unified theory of four-wave mixing and two-photon processes. Phys. Rev. A, 28(6):3480, 1983.

[110] C. R. Vidal, J. Cooper, and E. W. Smith. Hydrogen Stark Broadening Calculations with the Unified Classical Path Theory, volume 116. National Bureau of Standards, Boulder, CO, 1970.

[111] C. Cohen-Tannoudji. In R. Balian, S. Haroche, and S. Liberman, editors, Frontiers in Laser Spectroscopy, volume 1, pages 3–104, Amsterdam, 1977. North-Holland.

[112] I. I. Sobelman. Atomic Spectra and Radiative Transitions. Springer-Verlag, Berlin, 1992.

Appendix A

Liouville Space

The primary purpose of the Liouville-space formalism is to provide a convenient notation for expressing operations of the type often encountered in relaxation problems and using density matrices. According to Ref. [91], the term "Liouville space" was first used by Fano in his 1963 publication on pressure broadening [96], and his work through the years made extensive use of these techniques. Fano's paper, in fact, is a very good illustration of the utility of the Liouville-space formalism. In it, equations are developed to describe the interaction of a single particle with a surrounding gas of particles, which is represented as a reservoir, and thus requires the use of a density matrix for the atom. By using the Liouville-space formalism, Fano is able to derive an equation for the operator m, given in Eq. (6.19) from Chapter 6 of this thesis, which contains all of the physics of the system-reservoir interaction. This equation has the form of the Lippman-Schwinger equation obtained in two-particle scattering theory, and, indeed, just as m is the Liouville-space version of the t-matrix, Eq. (6.19) is the Liouville-space version of the Lippman-Schwinger equation. Analogous equations such as this illustrate the power that using such a notation can offer.

The Liouville space formalism is described in a variety of places in the literature [91, 63, 96, 97, 102, 110], and the intention of this appendix is to provide a basic motivation for the formalism, and summarize its main tenants, for reference throughout the thesis. For a more detailed account, the reader is referred to any one of the

aforementioned references.

Ordinary quantum mechanics, using wave functions, is formulated in Hilbert space. The density matrix, a generalization of the wave function to account for non-pure states, can also be used in Hilbert space. This is, in fact, how the Liouville equation as it is usually written,

$$\dot{\rho}(t) = -\frac{i}{\hbar}\left[H, \rho(t)\right], \tag{A.1}$$

for the density operator ρ and the Hamiltonian H. This equation cannot be expressed as a linear system, since the commutator produces terms in which ρ appears left multiplying the Hamiltonian. In Liouville-space notation, an operator called a Liouvillian or a superoperator is introduced. This operator $\mathcal{L}$, when acting upon the density operator, provides the required commutator, and thus the Liouville equation written in Liouville-space notation is

$$\dot{\rho}(t) = -\frac{i}{\hbar}\mathcal{L}\rho. \tag{A.2}$$

The Liouville equation is now written in a form that is equivalent to the Schrödinger equation. This equivalence turns out to be very useful because many operations performed in Liouville space will appear to be formally identical to familiar operations performed in Hilbert space. Equation (A.2), when expanded in a basis, denotes the $N \times N$ density matrix now as a vector of length N^2, and the superoperator $\mathcal{L}$ appears as a $N^2 \times N^2$ matrix. This is now a linear system that can, for example, by plugged in to a linear solver on a computer. However, this advantage has come at a cost, since the size of the matrices involved are much larger than the Hamiltonian matrix represented in Hilbert space.

Superoperators have four indices when referring back to the original Hilbert-space operations, two that denote left multiplication of the density operator, and two that denote right multiplication of the density operator. Explicitly, the operator $\mathcal{L}$ given

above is expressed in terms of the Hamiltonian as

$$\mathcal{L}_{ij,kl} = H_{ik}\delta_{jl} - H^*_{jl}\delta_{ik}. \tag{A.3}$$

This four-index notation is often referred to as tetradic notation [91, 110].

Abstract quantum-state vectors in Liouville-space notation are often, especially in the more modern literature, written with two angle brackets as $|a\rangle\rangle$. The completeness relation in Liouville space is

$$\sum_{i,j} |ij\rangle\rangle\langle\langle ij| = 1, \tag{A.4}$$

and vectors can be expanded in basis in a manner analogous to Hilbert space,

$$|a\rangle\rangle = \sum_{i,j} |ij\rangle\rangle\langle\langle ij|\, |a\rangle\rangle. \tag{A.5}$$

The formalism of Liouville space is used extensively in Chapter 6 of this thesis. There, the formalism allows a great deal of simplification of the resulting equations, and makes clear the analogy to similar but less general equations in Hilbert space. The methods of Green functions is utilized in Liouville-space form. Liouville space concepts are also very useful when performing numerical calculations, and have been used in every calculation involving density matrices in this thesis. The author has constructed a suite of Fortran subroutines that allow conversion back and forth between Hilbert space and Liouville space.

Appendix B

Spontaneous-Emission Relaxation Operator for Atoms with Complex Internal Structure

This appendix is concerned with the derivation of the spontaneous-emission relaxation operator for an atom with hyperfine degeneracy, taking into account multiple hyperfine excited-state manifolds. This type of operator is important for atoms having multiple excited-state manifolds which are spaced in energy on the order of or smaller than the natural linewidth, the topic addressed in Chapter 3. When these atoms are driven with a laser near the transition frequency — as in, for example, laser cooling — coupling occurs for each of the excited-state manifolds and their effects must be considered. To understand the dynamics of such an atom in a polarization-gradient laser field, it is thus important to accurately describe the coherent effects of each substate in each hyperfine manifold, interacting with the vacuum photon field.

In addition to providing a detailed derivation of a quantity relevant to our numerical calculations, this appendix is meant to illustrate in a general manner the development of a relaxation operator. Through this rather elaborate example, it is shown how the description of a small system, interacting with a large reservoir approximated (or exactly described) as made up of a large number of harmonic oscillators, can be reduced to a simple, intuitive, parameterized description, as long as certain criteria (such as the Markov approximation) are met. In this manner, spontaneous emission, a phenomenon experimentally observed to behave according to a single parameter Γ, is

built up from a microscopic description of the atom interacting with the vacuum photon field. From this description, the phenomenologically determined Γ can be given a fundamental expression in terms of a series of microscopic interactions.

To begin, this problem is mapped onto the general class of system-reservoir interactions. In the present case, the atom is the system and the vacuum photon field is the reservoir. The full Hamiltonian for the system plus the reservoir is

$$H = H_A + H_R + V_{A-R}, \tag{B.1}$$

where H_A is the bare atomic Hamiltonian, which includes the internal states of the atom as well as its center of mass, H_R is the Hamiltonian of the radiation field, and V_{A-R} is the interaction between the two. The interaction is described within the electric-dipole approximation as

$$\begin{aligned} V_{A-R} &= -\mathbf{D}\cdot\mathbf{E}(\mathbf{R}) \\ &= -\sum_{q=0,\pm1}(-1)^q D_q E_{-q}(\mathbf{R}) \\ &= -i\sum_{q=0,\pm1}(-1)^q D_q \sum_i \sum_{\epsilon^{(i)}\perp\mathbf{k}_i} \sqrt{\frac{\hbar\omega_i}{2\epsilon_0 L^3}}\left[\epsilon_q^{(i)} a_i e^{i\mathbf{k}_i\cdot\mathbf{R}} - \epsilon_q^{(i)} a_i^\dagger e^{-i\mathbf{k}_i\cdot\mathbf{R}}\right], \end{aligned} \tag{B.2}$$

where $\mathbf{D}$ is the electric dipole operator for the atom, and $\mathbf{E}$ is the electric-field operator for the photon field. On the second line, the interaction has been expanded into its spherical components and on the third line the radiation field has been written in an explicit quantum-mechanical form, quantized in a box of length L, in terms of raising and lowering operators, $a^\dagger$ and a, respectively. The sum over i indicates a sum over field modes, and for each $\mathbf{k}_i$ there are two mutually perpendicular polarization vectors $\hat{\epsilon}^{(i)}$. To simplify the formalism, the atomic center of mass will initially be ignored, setting the position coordinate to be the origin, $\mathbf{R} = 0$. This will not affect the derivation fundamentally, and in the end the equations will be easily generalized to include the center-of-mass degrees of freedom.

The full system-plus-reservoir density matrix ρ evolves in time according to the

Liouville equation,

$$\dot{\rho}(t) = \frac{i}{\hbar}\left[\rho(t), H\right]. \tag{B.3}$$

This equation describes the evolution of all degrees of freedom of the problem, including the vacuum photon field. This is unnecessarily detailed and will be impractical to solve in most situations. The goal is to find an equation of motion for the reduced system density matrix, defined by taking the trace over all reservoir degrees of freedom of the full density matrix,

$$\sigma = \mathrm{Tr}_R \rho. \tag{B.4}$$

To this end, it is useful to utilize some of the the well-established methods of quantum system-reservoir theory. It is impractical to present a detailed discussion of this methodology here, but these techniques can be easily found in quantum-optics literature, and a particularly thorough presentation is given by Cohen-Tannoudji in Refs. [8] and [111]. Summarizing, it is assumed that the reservoir is unaffected by the interactions with the system and that the reservoir has a short memory (the Markov approximation). With these assumptions, an equation of motion is obtained for the system reduced density operator σ with temporal coarse graining on a time scale much larger than the time scale of reservoir fluctuations but shorter than the time scale of evolution of the system,

$$\begin{aligned}\dot{\sigma}(t) = &\frac{i}{\hbar}\left[\sigma(t), H_A\right] - \frac{1}{\hbar^2}\int_0^\infty d\tau \sum_q (-1)^q \\ &\times \left\{ g_q(\tau)\left[D_q\, e^{-iH_A\tau/\hbar}\, D_{-q}\, e^{iH_A\tau/\hbar}\, \sigma(t) - e^{-iH_A\tau/\hbar}\, D_q\, e^{iH_A\tau/\hbar}\, \sigma(t)\, D_{-q}\right] + \mathrm{H.c.}\right\}.\end{aligned} \tag{B.5}$$

In the previous equation, $g_q(\tau)$ is the two-time correlation function for vacuum fluctuations of the photon reservoir and is given by

$$\begin{aligned} g_q(\tau) &= \frac{\hbar c}{3\epsilon_0 (2\pi)^3}\int d\omega \frac{\omega^3}{c^4} e^{-i\omega\tau} \\ &= \mathrm{Tr}_R\left[\sigma_R \tilde{E}_q(\tau)\tilde{E}_q(0)\right]. \end{aligned} \tag{B.6}$$

where c is the speed of light and ϵ_0 is the permittivity of free space, and where the variables with tildes are operators in the interaction representation,

$$\tilde{E}_q(t) = e^{iH_R t/\hbar} E_q e^{-iH_R t/\hbar}. \tag{B.7}$$

It is assumed that the reservoir is initially the vacuum state, so that $\sigma_R = |0\rangle\langle 0|$. From this it can be seen that

$$g_q(\tau) = \sum_\nu |\langle \nu \,|\, E_q \,|\, 0\rangle|^2 \, e^{-i\omega_\nu t}, \tag{B.8}$$

where the kets and bras refer to reservoir states. Note that $g(\tau)^* = g(-\tau)$. The correlation time of the reservoir τ_C is defined such that $g(\tau) \to 0$ for $\tau \gg \tau_C$.

In addition to the above approximations, the secular approximation will also be made, which requires that the equation of motion for each density-matrix element $\dot{\sigma}_{ij}$ have only terms involving density-matrix elements σ_{kl} on the right-hand side such that $|\omega_{ij} - \omega_{kl}| \ll \gamma$, where γ is the order of magnitude of the system-reservoir coupling. The following discussion focuses on a system with a ground state coupled to multiple excited states that are separated in energy of the order or smaller than γ. Thus, the ground-excited energy splitting $|\omega_{ge}| \gg \gamma$ will be a non-secular frequency, while $\omega_{e_i e_j} \sim \gamma$ will be a secular frequency.

The particular atomic system under consideration consists of an ground state with electronic angular momentum $J = J_g = 0$ and an excited state with $J = J_e = 1$. The electronic angular momentum is coupled to the nuclear spin quantum number I, resulting in a ground state with total angular momentum $F_g = I$, and three excited states with $\{F_{e_i}\} = \{I-1, I, I+1\}$. Note, however, that this derivation can be easily extended to arbitrary angular momentum schemes. It is useful to decompose the system density operator as illustrated in Fig B.1,

$$\dot{\sigma}(t) = \dot{\sigma}_{gg}(t) + \sum_{i,j} \dot{\sigma}_{e_i e_j}(t) + \sum_i \left[\dot{\sigma}_{e_i g}(t) + \dot{\sigma}_{g e_i}(t)\right], \tag{B.9}$$

where $\sigma_{ij}(t) = P_i \sigma(t) P_j$; P_i is a projection operator onto the i-th hyperfine manifold, $P_i = \sum_{M_i} |JIFM_i\rangle\langle JIFM_i|$; and M_i is the substate label for the i-th manifold.

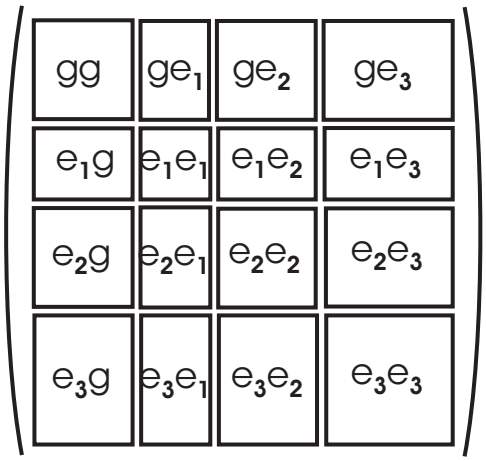

Figure B.1: The partitioning of the density operator for an atom with multiple coupled excited-state manifolds, each potentially having multiple substates.

It will be useful to first work out some relations involving sums over electric-dipole matrix elements related to reduced matrix elements and raising and lowering operators:

$$\begin{aligned}
&\sum_{M_g,M_{e_i}} \langle M_g|D_q|M_{e_i}\rangle \, |M_g\rangle \, \langle M_{e_i}| \\
&\quad = \sum_{M_g,M_{e_i}} \langle J_g I F_g M_g|D_q|J_e I F_{e_i} M_{e_i}\rangle \, |J_g I F_g M_g\rangle \, \langle J_e I F_{e_i} M_{e_i}| \\
&\quad = \sum_{M_g,M_{e_i}} (-1)^{F_g+M_g+J_g+I+F_{e_i}+1}\sqrt{(2F_g+1)(2F_{e_i}+1)} \\
&\qquad \times \begin{pmatrix} F_g & 1 & F_{e_i} \\ -M_g & q & M_{e_i} \end{pmatrix} \begin{Bmatrix} J_g & F_g & I \\ F_{e_i} & J_e & 1 \end{Bmatrix} \langle J_g||D||J_e\rangle \, |J_g I F_g M_g\rangle \, \langle J_e I F_{e_i} M_{e_i}| \\
&\quad = A_q^{(i)} \frac{\langle J_g||D||J_e\rangle}{\sqrt{2J_e+1}},
\end{aligned} \tag{B.10}$$

and

$$\begin{aligned}
&\sum_{M_g,M_{e_i}} (-1)^q \, \langle M_{e_i}|D_{-q}|M_g\rangle \, |M_{e_i}\rangle \, \langle M_g| \\
&\qquad = \sum_{M_g,M_{e_i}} (-1)^q \, \langle J_e I F_{e_i} M_{e_i}|D_{-q}|J_g I F_g M_g\rangle \, |J_e I F_{e_i} M_{e_i}\rangle \, \langle J_g I F_g M_g| \\
&\qquad = \sum_{M_g,M_{e_i}} (-1)^{F_{e_i}+M_{e_i}+J_e+I+F_g+1+q}\sqrt{(2F_g+1)(2F_{e_i}+1)} \\
&\qquad\quad \times \begin{pmatrix} F_{e_i} & 1 & F_g \\ -M_{e_i} & -q & M_g \end{pmatrix} \begin{Bmatrix} J_e & F_{e_i} & I \\ F_g & J_g & 1 \end{Bmatrix} \langle J_e||D||J_g\rangle \, |J_e I F_{e_i} M_{e_i}\rangle \, \langle J_g I F_g M_g| \\
&\qquad = - A_q^{(i)\dagger} \frac{\langle J_e||D||J_g\rangle}{\sqrt{2J_e+1}},
\end{aligned} \tag{B.11}$$

where $A_q^{(i)\dagger}$ and $A_q^{(i)}$ are the atomic raising and lowering operators defined in Eq. (3.6) and the symmetry properties of the three-J and six-J symbols have been exploited (see Ref. [112]).

The equation of motion for each type of sub-density-matrix in Eq. (B.9) will now be examined. Consider first the equation for the ground-state sub-density-matrix $\sigma_{gg}(t)$,

which evolves according to

$$\dot{\sigma}_{gg}(t) = -\frac{1}{\hbar^2}\int_0^\infty d\tau \sum_q (-1)^q \times \left\{ g(\tau)\left[\sum_i P_g D_q P_{e_i} D_{-q} P_g \sigma(t) P_g e^{-i\omega_0^{(i)}\tau} - \sum_{i,j} P_g D_q P_{e_i}\sigma(t) P_{e_j} D_{-q} P_g e^{i\omega_0^{(i)}\tau}\right] + g(-\tau)\left[\sum_i P_g\sigma(t) P_g D_q P_{e_i} D_{-q} P_g e^{i\omega_0^{(i)}\tau} - \sum_{i,j} P_g D_q P_{e_i}\sigma(t) P_{e_j} D_{-q} P_g e^{-i\omega_0^{(j)}\tau}\right]\right\}, \tag{B.12}$$

where $\omega_0^{(i)} = \omega_{e_i} - \omega_g$. It will first be shown that the first and third terms combine to give zero. This first term can be rearranged as

$$-\frac{1}{\hbar^2}\int_0^\infty d\tau \sum_q (-1)^q g(\tau) \sum_i P_g D_q P_{e_i} D_{-q} P_g \sigma(t) P_g e^{-i\omega_0^{(i)}\tau} = -\frac{1}{\hbar^2}\sum_q \sum_i (-1)^q P_g D_q P_{e_i} D_{-q} P_g \sigma(t) P_g \int_0^\infty d\tau g(\tau) e^{-i\omega_0^{(i)}\tau}, \tag{B.13}$$

and the third term can be rearranged as

$$-\frac{1}{\hbar^2}\int_0^\infty d\tau \sum_q (-1)^q g(-\tau) \sum_i P_g\sigma(t) P_g D_q P_{e_i} D_{-q} P_g e^{i\omega_0^{(i)}\tau} = -\frac{1}{\hbar^2}\sum_q \sum_i (-1)^q P_g\sigma(t) P_g D_q P_{e_i} D_{-q} P_g \int_0^\infty d\tau g(-\tau) e^{i\omega_0^{(i)}\tau}. \tag{B.14}$$

The portion involving atomic projection operators will now be considered. It is shown that the projection-operator factors in front of the first and third terms are identical, and can thus be factored out. Expanding out the projection-operator portion of the

first term,

$$
\begin{aligned}
(-1)^q P_g D_q P_{e_i} D_{-q} P_g \sigma(t) P_g = & \sum_{M_g, M_g', M_{e_i}} |J_g I F_g M_g\rangle \langle J_g I F_g M_g| D_q |J_e I F_{e_i} M_{e_i}\rangle \\
& \times (-1)^q \langle J_e I F_{e_i} M_{e_i}| D_{-q} |J_g I F_g M_g'\rangle \langle J_g I F_g M_g'| \sigma(t) P_g \\
= & \frac{|\langle J_g||D||J_e\rangle|^2}{2J_e+1} A_q^{(i)} A_q^{(i)\dagger} P_g \sigma(t) P_g \\
= & \frac{|\langle J_g||D||J_e\rangle|^2}{2J_e+1} P_g \sigma(t) P_g A_q^{(i)} A_q^{(i)\dagger} \\
= & \sum_{M_g, M_g', M_{e_i}} P_g \sigma(t) |J_g I F_g M_g\rangle \langle J_g I F_g M_g| D_q |J_e I F_{e_i} M_{e_i}\rangle \\
& \times (-1)^q \langle J_e I F_{e_i} M_{e_i}| D_{-q} |J_g I F_g M_g'\rangle \langle J_g I F_g M_g'| \\
= & (-1)^q P_g \sigma(t) P_g D_q P_{e_i} D_{-q} P_g,
\end{aligned}
\tag{B.15}
$$

where the final line is the projection-operator portion of the third equation. In obtaining the previous result, the fact that the product of raising and lowering operators $A_q^{(i)} A_q^{(i)\dagger}$ is proportional to the ground-state internal atomic projection operator P_g, and thus commutes with the ground-state sub-density-matrix σ_{gg} has been utilized. Combining the first and third terms of Eq. (B.12), the projection-operator terms can be factored out,

$$
\begin{aligned}
& -\frac{1}{\hbar^2} \sum_q \sum_i \frac{|\langle J_g||D||J_e\rangle|^2}{2J_e+1} A_q^{(i)} A_q^{(i)\dagger} P_g \sigma(t) P_g \int_0^\infty d\tau \left(g(\tau) e^{-i\omega_0^{(i)}\tau} + g(-\tau) e^{i\omega_0^{(i)}\tau} \right) \\
& \quad = -\frac{1}{\hbar^2} \sum_q \sum_i \frac{|\langle J_g||D||J_e\rangle|^2}{2J_e+1} A_q^{(i)} A_q^{(i)\dagger} P_g \sigma(t) P_g \int_{-\infty}^\infty d\tau g(\tau) e^{-i\omega_0^{(i)}\tau} \\
& \quad = -\frac{1}{3\epsilon_0 (2\pi)^3 c^3 \hbar} \sum_q \sum_i \frac{|\langle J_g||D||J_e\rangle|^2}{2J_e+1} A_q^{(i)} A_q^{(i)\dagger} P_g \sigma(t) P_g \int d\omega\, \omega^3 \int_{-\infty}^\infty d\tau e^{-i(\omega+\omega_0^{(i)})\tau} \\
& \quad = -\frac{1}{3\epsilon_0 (2\pi)^3 c^3 \hbar} \sum_q \sum_i \frac{|\langle J_g||D||J_e\rangle|^2}{2J_e+1} A_q^{(i)} A_q^{(i)\dagger} P_g \sigma(t) P_g \int d\omega\, \omega^3 \delta(\omega + \omega_0^{(i)}).
\end{aligned}
\tag{B.16}
$$

It is clear that the contributions from the first and third terms of Eq. (B.12) vanish, since the argument of the delta function can never be zero. Physically, this reflects the fact that the atom cannot make a transition from the ground state to the excited state by emitting a photon.

This leaves only the second and fourth terms,

$$\begin{aligned}\dot{\sigma}_{gg}(t) =&\frac{1}{\hbar^2}\sum_q\sum_{i,j}(-1)^q P_g D_q P_{e_i}\sigma(t)P_{e_j}D_{-q}P_g\\ &\times\int_0^\infty d\tau\left(g(\tau)e^{i\omega_0^{(i)}\tau}+g(-\tau)e^{-i\omega_0^{(j)}\tau}\right)\\ =&\sum_q\sum_{i,j}(-1)^q P_g D_q P_{e_i}\sigma(t)P_{e_j}D_{-q}P_g\\ &\times\frac{1}{\hbar^2}\int_0^\infty d\tau\frac{\hbar}{3\epsilon_0(2\pi)^3c^3}\left(\int d\omega\,\omega^3 e^{-i\omega\tau}e^{i\omega_0^{(i)}\tau}+\int d\omega\,\omega^3 e^{i\omega\tau}e^{-i\omega_0^{(j)}\tau}\right)\\ =&\frac{1}{3\epsilon_0(2\pi)^3c^3\hbar}\sum_q\sum_{i,j}(-1)^q P_g D_q P_{e_i}\sigma(t)P_{e_j}D_{-q}P_g\\ &\times\int d\omega\,\omega^3\left(\int_0^\infty d\tau e^{-i\omega\tau}e^{i\omega_0^{(i)}\tau}+\int_0^\infty d\tau e^{i\omega\tau}e^{-i\omega_0^{(j)}\tau}\right).\end{aligned}\tag{B.17}$$

Now, using the fact that $\int_0^\infty d\tau e^{-i\omega\tau}=\pi\delta(\omega)+i\mathcal{P}\frac{1}{\omega}$, where the $\mathcal{P}$ operator indicates that the principal part must be taken when an integration is performed. It is seen from the last equation in Eq. (B.17) that the integrand of the ω integral will consist of two delta functions, on each for $\omega-\omega_0^{(i)}$ and $\omega-\omega_0^{(j)}$, along with two principal-part terms, which combine to be of the form $\mathcal{P}(\frac{1}{\omega-\omega_0^{(i)}}-\frac{1}{\omega-\omega_0^{(j)}})$. The principal-part expression gives the additional energy splitting between the ith and the jth excited-state manifolds due to interaction with the photon reservoir accompanied by the usual pathological divergences which will be ignored in the present case. Neglecting this energy splitting and considering only the delta-function terms, as well as making the approximation that the frequencies $\{\omega_0^{(i)}\}$ are approximately equal,

$$\begin{aligned}\dot{\sigma}_{gg}(t)&\cong\frac{1}{3\epsilon_0(2\pi)^3c^3\hbar}\sum_q\sum_{i,j}(-1)^q P_g D_q P_{e_i}\sigma(t)P_{e_j}D_{-q}P_g\int d\omega\,\omega^3\delta(\omega-\omega_0)\\ &=\frac{{\omega_0}^3}{3\epsilon_0(2\pi)^3c^3\hbar}\sum_q\sum_{i,j}(-1)^q P_g D_q P_{e_i}\sigma(t)P_{e_j}D_{-q}P_g,\end{aligned}\tag{B.18}$$

where ω_0 is the average of the atomic Bohr frequencies $\omega_0^{(i)}$. Expanding the projection-

operator portion,

$$
\begin{aligned}
&(-1)^q P_g D_q P_{e_i} \sigma(t) P_{e_j} D_{-q} P_g \\
&\quad = \sum_{M_g, M_g', M_{e_i}, M_{e_j}} (-1)^q \left|M_g\right\rangle \left\langle M_g\right| D_q \left|M_{e_i}\right\rangle \left\langle M_{e_i}\right| \sigma(t) \left|M_{e_j}\right\rangle \left\langle M_{e_j}\right| D_{-q} \left|M_g'\right\rangle \left\langle M_g'\right| \\
&\quad = \sum_{M_g, M_g', M_{e_i}, M_{e_j}} \left[\left\langle M_g|D_q|M_{e_i}\right\rangle \left|M_g\right\rangle \left\langle M_{e_i}\right|\right] \sigma(t) \left[(-1)^q \left\langle M_{e_j}|D_{-q}|M_g'\right\rangle \left|M_{e_j}\right\rangle \left\langle M_g'\right|\right] \\
&\quad = \frac{-\left\langle J_g||D||J_e\right\rangle \left\langle J_e||D||J_g\right\rangle}{2J_e+1} A_q^{(i)} \sigma(t) A_q^{(j)\dagger} \\
&\quad = \frac{\left|\left\langle J_g||D||J_e\right\rangle\right|^2}{2J_e+1} A_q^{(i)} \sigma(t) A_q^{(j)\dagger},
\end{aligned}
\tag{B.19}
$$

where the fact that $\left\langle J_g||D||J_e\right\rangle^\dagger = (-1)^{J_e - J_g} \left\langle J_e||D||J_g\right\rangle$ has been used. Equation (B.12) finally becomes

$$
\begin{aligned}
\dot{\sigma}_{gg}(t) &= \frac{{\omega_0}^3}{3\epsilon_0 (2\pi)^3 c^3 \hbar} \frac{\left|\left\langle J_g||D||J_e\right\rangle\right|^2}{2J_e+1} \sum_q \sum_{i,j} A_q^{(i)} \sigma(t) A_q^{(j)\dagger} \\
&\cong \gamma \sum_q \sum_{i,j} A_q^{(i)} \sigma(t) A_q^{(j)\dagger},
\end{aligned}
\tag{B.20}
$$

where $\gamma = \gamma_{J_e \to J_g}$ is the transition rate from the J_e excited state to the J_g ground state and which are assumed here to be equal to the transition rate for all of the excited-state hyperfine manifolds. It is clear that the approximation that the various internal atomic frequencies $\omega_0^{(i)}$ are all equal to some average frequency ω_0 amounts to assuming that each excited-state manifold relaxes with the same spontaneous-emission rate.

Turning now to the excited-state sub-density-matrices,

$$
\begin{aligned}
\dot{\sigma}_{e_i e_j}(t) = &-i\delta\omega_{e_i e_j} P_{e_i} \sigma(t) P_{e_j} - \frac{1}{\hbar^2} \int_0^\infty d\tau \sum_q (-1)^q \\
&\times \left\{ g(\tau) \left[\sum_k P_{e_i} D_q P_g D_{-q} P_{e_k} \sigma(t) P_{e_j} e^{i\omega_0^{(k)}\tau} - P_{e_i} D_q P_g \sigma(t) P_g D_{-q} P_{e_j} e^{-i\omega_0^{(i)}\tau} \right] \right. \\
&\left. + g(-\tau) \left[\sum_k P_{e_i} \sigma(t) P_{e_k} D_q P_g D_{-q} P_{e_j} e^{-i\omega_0^{(k)}\tau} - P_{e_i} D_q P_g \sigma(t) P_g D_{-q} P_{e_j} e^{i\omega_0^{(j)}\tau} \right] \right\},
\end{aligned}
\tag{B.21}
$$

where $\delta\omega_{ab} = \omega_a - \omega_b$. The second and fourth terms will combine (having identical projection-operator prefactors) to give two delta functions with arguments of $\omega + \omega_0^{(i)}$ and $\omega + \omega_0^{(j)}$, respectively, which cannot be satisfied and thus give zero upon integration, and also a principal part contribution of the form $\mathcal{P}(\frac{1}{\omega+\omega_0^{(i)}} - \frac{1}{\omega+\omega_0^{(j)}})$, which are neglected as before. What remains is the first term and the third term,

$$\begin{aligned}\dot{\sigma}_{e_i e_j}(t) = &- i\delta\omega_{e_i e_j} P_{e_i}\sigma(t)P_{e_j} \\ &- \frac{1}{\hbar^2}\sum_q\sum_k (-1)^q P_{e_i} D_q P_g D_{-q} P_{e_k}\sigma(t)P_{e_j}\int_0^\infty d\tau g(\tau)e^{i\omega_0^{(k)}\tau} \\ &- \frac{1}{\hbar^2}\sum_q\sum_k (-1)^q P_{e_i}\sigma(t)P_{e_k} D_q P_g D_{-q} P_{e_j}\int_0^\infty d\tau g(-\tau)e^{-i\omega_0^{(k)}\tau}.\end{aligned} \tag{B.22}$$

Simplifying the projection-operator prefactors,

$$\begin{aligned}&(-1)^q P_{e_i} D_q P_g D_{-q} P_{e_k}\sigma(t)P_{e_j} \\ &= \sum_{M_g, M_{e_i}, M_{e_k}} (-1)^q |M_{e_i}\rangle \langle M_{e_i}| D_q |M_g\rangle \langle M_g| D_{-q} |M_{e_k}\rangle \langle M_{e_k}| \sigma(t)P_{e_j} \\ &= \sum_{M_g, M_{e_i}, M_{e_k}} [\langle M_{e_i}|D_q|M_g\rangle |M_{e_i}\rangle \langle M_g|] [(-1)^q \langle M_g|D_{-q}|M_{e_k}\rangle |M_g\rangle \langle M_{e_k}|] \sigma(t)P_{e_j} \\ &= \frac{|\langle J_g||D||J_e\rangle|^2}{2J_e+1} \sum_{M_g, M_{e_i}, M_{e_k}} \alpha_{F_g, F_{e_i}, M_g, M_{e_i}, J_g, J_e, I} |M_{e_i}\rangle \langle M_g| \\ &\qquad\qquad \times \alpha_{F_g, F_{e_k}, M_g, M_{e_k}, J_g, J_e, I} |M_g\rangle \langle M_{e_k}| \sigma(t)P_{e_j} \\ &= \frac{|\langle J_g||D||J_e\rangle|^2}{2J_e+1} A_q^{(i)\dagger} A_q^{(k)} \sigma(t)P_{e_j},\end{aligned} \tag{B.23}$$

and

$$
\begin{aligned}
&(-1)^q P_{e_i}\sigma(t)P_{e_k}D_qP_gD_{-q}P_{e_j} \\
&\quad=\sum_{M_g,M_{e_i},M_{e_k}}(-1)^q P_{e_i}\sigma(t)\left|M_{e_k}\right\rangle\left\langle M_{e_k}\right|D_q\left|M_g\right\rangle\left\langle M_g\right|D_{-q}\left|M_{e_j}\right\rangle\left\langle M_{e_j}\right| \\
&\quad=\sum_{M_g,M_{e_k},M_{e_j}} P_{e_i}\sigma(t)\left[\langle M_{e_k}|D_q|M_g\rangle\left|M_{e_k}\right\rangle\left\langle M_g\right|\right] \\
&\qquad\qquad\times\left[(-1)^q\left\langle M_g|D_{-q}|M_{e_j}\right\rangle\left|M_g\right\rangle\left\langle M_{e_j}\right|\right] \\
&\quad=\frac{\left|\langle J_g||D||J_e\rangle\right|^2}{2J_e+1}\sum_{M_g,M_{e_i},M_{e_k}} P_{e_i}\sigma(t)\alpha_{F_g,F_{e_k},M_g,M_{e_k},J_g,J_e,I}\left|M_{e_k}\right\rangle\left\langle M_g\right| \\
&\qquad\qquad\times\alpha_{F_g,F_{e_j},M_g,M_{e_j},J_g,J_e,I}\left|M_g\right\rangle\left\langle M_{e_j}\right| \\
&\quad=\frac{\left|\langle J_g||D||J_e\rangle\right|^2}{2J_e+1}P_{e_i}\sigma(t)A_q^{(k)\dagger}A_q^{(j)},
\end{aligned}
\tag{B.24}
$$

the excited-state density-matrix equations of motion can be written as

$$
\begin{aligned}
\dot{\sigma}_{e_ie_j}(t) &= -i\delta\omega_{e_ie_j}P_{e_i}\sigma(t)P_{e_j}-\frac{\gamma}{2}\sum_q\sum_k\left(A_q^{(i)\dagger}A_q^{(k)}\sigma(t)P_{e_j}+P_{e_i}\sigma(t)A_q^{(k)\dagger}A_q^{(j)}\right) \\
&= -i\delta\omega_{e_ie_j}P_{e_i}\sigma(t)P_{e_j}-\frac{\gamma}{2}\sum_q\sum_{k,l}P_{e_i}\left(A_q^{(k)\dagger}A_q^{(l)}\sigma(t)+\sigma(t)A_q^{(k)\dagger}A_q^{(l)}\right)P_{e_j},
\end{aligned}
\tag{B.25}
$$

where again the principal-part contributions have been neglected and where in the last line a trivial summation index has been added that will be useful later when combining the various sub-density-matrix decay terms.

The final equations to be considered are the optical-coherence sub-density-matrices,

$$
\begin{aligned}
\dot{\sigma}_{e_ig}(t) &= -i\delta\omega_{e_ig}P_{e_i}\sigma(t)P_g-\frac{1}{\hbar^2}\int_0^\infty d\tau\sum_q(-1)^q \\
&\times\left\{g(\tau)\left[\sum_j P_{e_i}D_qP_gD_{-q}P_{e_j}\sigma(t)P_ge^{i\omega_0^{(j)}\tau}-\sum_j P_{e_i}D_qP_g\sigma(t)P_{e_j}D_{-q}P_ge^{-i\omega_0^{(i)}\tau}\right]\right. \\
&\left.+g(-\tau)\left[\sum_j P_{e_i}\sigma(t)P_gD_qP_{e_j}D_{-q}P_ge^{i\omega_0^{(j)}\tau}-\sum_j P_{e_i}D_qP_g\sigma(t)P_{e_j}D_{-q}P_ge^{-i\omega_0^{(j)}\tau}\right]\right\}.
\end{aligned}
\tag{B.26}
$$

It is important to mention here that the indices on the frequencies in the exponentials are correct in the above equation. The frequency $\omega_0^{(i)}$ (not the summation index) should only appear in the exponential in the second term, while $\omega_0^{(j)}$'s (the summation index) should appear in all of the other terms. The second term and the fourth term are both non-secular, since they involve density-matrix elements σ_{ge_i}, and thus these terms can be neglected. The third term is anti-resonant, i.e., it will contribute delta functions with arguments $\omega + \omega_0^{(i)}$ which cannot be satisfied. Again, principal-part contributions from these terms have been neglected, yielding

$$\begin{aligned}\dot{\sigma}_{e_i g}(t) =& - i\delta\omega_{e_i g} P_{e_i}\sigma(t)P_g - \frac{1}{\hbar^2}\sum_q \sum_j (-1)^q P_{e_i} D_q P_g D_{-q} P_{e_j}\sigma(t)P_g \int_0^\infty d\tau g(\tau) e^{i\omega_0^{(j)}\tau} \\ =& - i\delta\omega_{e_i g} P_{e_i}\sigma(t)P_g - \frac{\gamma}{2}\sum_q \sum_{k,l} P_{e_i} A_q^{(k)\dagger} A_q^{(l)}\sigma(t)P_g.\end{aligned} \tag{B.27}$$

Similarly,

$$\dot{\sigma}_{g e_i}(t) = i\delta\omega_{g e_i} P_g\sigma(t)P_{e_i} - \frac{\gamma}{2}\sum_q \sum_{k,l} P_g\sigma(t) A_q^{(k)\dagger} A_q^{(l)} P_{e_i}. \tag{B.28}$$

Using Eq. (B.9), the equation of motion due to spontaneous emission for the full density operator can be constructed,

$$\dot{\sigma}(t) = \frac{i}{\hbar}[\sigma(t), H_A] + \gamma\sum_q \sum_{i,j} A_q^{(i)}\sigma(t)A_q^{(j)\dagger} - \frac{\gamma}{2}\sum_q \sum_{i,j}\left(A_q^{(i)\dagger}A_q^{(j)}\sigma(t) + \sigma(t)A_q^{(i)\dagger}A_q^{(j)}\right). \tag{B.29}$$

Defining the spontaneous emission relaxation operator,

$$\mathcal{L}_{\rm sp}[\sigma] = \gamma\sum_q \sum_{i,j} A_q^{(i)}\sigma(t)A_q^{(j)\dagger} - \frac{\gamma}{2}\sum_q \sum_{i,j}\left(A_q^{(i)\dagger}A_q^{(j)}\sigma(t) + \sigma(t)A_q^{(i)\dagger}A_q^{(j)}\right), \tag{B.30}$$

the equation of motion can be written as

$$\dot{\sigma}(t) = \frac{i}{\hbar}[\sigma(t), H_A] + \mathcal{L}_{\rm sp}[\sigma]. \tag{B.31}$$

The atomic center-of-mass dependence that was ignored for simplicity in the previous derivation can now be reintroduced. This amounts to adding an integral over

momentum states in 3D that should have been included when the atomic projection operators were inserted. Including this, the full relaxation operator takes the form shown in Eq. (3.4).

Appendix C

Semiclassical Master Equation for Atoms with Complex Internal Structure

Treating the atom's center-of-mass degree of freedom as a classical variable rather than a quantum operator — often referred to simply as the "semiclassical approximation" despite being somewhat ambiguous — yields a set of dynamical equations called the optical Bloch equations. This appendix provides a detailed derivation of the optical Bloch equations corresponding to the situation discussed in Chapter 3: an atom with multiple hyperfine manifolds of arbitrary spacing, interacting with an arbitrary three-dimensional polarization-gradient laser field. These equations are then solved by direct numerical means in Chapter 3 to obtain information such as the friction and diffusion coefficients for laser cooling. This information, although often technically inferior to the solutions of fully quantum equations, is usually much easier to calculate and can provide helpful qualitative insight into the dynamics from the use of the intuitive classical concepts of force, friction, and diffusion.

C.1 Equations without spontaneous decay

C.1.1 Atom-field interaction

The field can be written, in general, as

$$\mathbf{E}(z,t) = \mathbf{E}^{+}(z)e^{-i\omega_L t} + \text{c.c.} \tag{C.1}$$

For the $\sigma_+\sigma_-$ configuration, the positive frequency component is

$$\mathbf{E}^+ = \mathcal{E}_0\hat{\epsilon}e^{ik_Lz} + \mathcal{E}_0'\hat{\epsilon}'e^{-ik_Lz}, \tag{C.2}$$

where $\mathcal{E}_0$ and $\mathcal{E}_0'$ are the amplitudes of the two opposing, circularly polarized beams, respectively, and $\hat{\epsilon}$ and $\hat{\epsilon}'$ are the respective polarization vectors, given by

$$\hat{\epsilon} = \hat{\epsilon}_+ \equiv -\frac{1}{\sqrt{2}}\left(\hat{i} + i\hat{j}\right), \tag{C.3}$$

$$\hat{\epsilon}' = \hat{\epsilon}_- \equiv \frac{1}{\sqrt{2}}\left(\hat{i} - i\hat{j}\right). \tag{C.4}$$

The interaction between the atom and the coherent field in the electric dipole approximations is described by

$$\begin{aligned} V(t) &= -\mathbf{D}\cdot\mathbf{E}(z,t) \\ &= \mathcal{E}_0 D^{(+1)}e^{-i(\omega_L t - k_L z)} + \mathcal{E}_0' D^{(-1)}e^{-i(\omega_L t + k_L z)} \\ &\qquad - \mathcal{E}_0 D^{(-1)}e^{i(\omega_L t - k_L z)} - \mathcal{E}_0' D^{(+1)}e^{i(\omega_L t + k_L z)}. \end{aligned} \tag{C.5}$$

Using the Wigner-Eckart theorem, and noting that $\mathbf{S}$ commutes with $\mathbf{D}$,

$$\begin{aligned} D^{(q)} &= \sum_{j,j',m,m',l,l',s,s'} |j,m,l,s\rangle\langle j,m,l,s|\, D^{(q)}\, |j',m',l',s'\rangle\langle j',m',l',s'| \\ &= \sum_{j,j',m,m',l,l',s} |j,m,l,s\rangle\langle j',m',l',s|\, (-1)^{j-m} \begin{pmatrix} j & 1 & j' \\ -m & q & m' \end{pmatrix} \langle j,l,s\|D\|j',l',s\rangle \\ &= \sum_{j,j',m,m',l,l',s} |j,m,l,s\rangle\langle j',m',l',s|\, (-1)^{j-m+l+s+j'+1} \\ &\qquad \times \sqrt{(2j+1)(2j'+1)} \begin{pmatrix} j & 1 & j' \\ -m & q & m' \end{pmatrix} \begin{Bmatrix} l & j & s \\ j' & l' & 1 \end{Bmatrix} \langle l\|D\|l'\rangle\,. \end{aligned} \tag{C.6}$$

The properties of the 3-j symbol provide the information that the triangle relation must be satisfied between j,j' and 1, and that $m' - m = q$. The 6-j symbol indicates that the following sets must each satisfy triangle relations: $\{j,l,s\}$, $\{j',l',s\}$, $\{j,j',1\}$, and

$\{l, l', 1\}$. The first two are trivial, the third is redundant, and the fourth tells us that l' can equal $l+1$, l, and $l-1$, however, parity considerations rule out the $l' = l$ possibility.

Now specialize to the case, useful to laser cooling, of a ground state j_g coupled to an excited state multiplet $j_e = j_g - 1$, j_g, $j_g + 1$, resulting from a system with $l = l_g$ in the ground state and $l = l_e = l_g + 1$ in the excited state, coupled with a spin of $s = 1$. The dipole matrix element can then be written as

$$\begin{aligned} D^{(q)} = D_{eg} \sum_{j_e, m_g} \Bigg[& |j_e, m_g + q, l_g + 1\rangle\langle j_g, m_g, l_g| \\ & \times (-1)^{j_e + j_g - m_g + l_g - q + 1} \sqrt{(2j_g + 1)(2j_e + 1)} \begin{pmatrix} j_e & 1 & j_g \\ -m_g - q & q & m_g \end{pmatrix} \begin{Bmatrix} l_g + 1 & j_e & 1 \\ j_g & l_g & 1 \end{Bmatrix} \\ & - |j_g, m_g, l_g\rangle\langle j_e, m_g - q, l_g + 1| \\ & \times (-1)^{j_e + j_g - m_g + l_g} \sqrt{(2j_g + 1)(2j_e + 1)} \begin{pmatrix} j_g & 1 & j_e \\ -m_g & q & m_g - q \end{pmatrix} \begin{Bmatrix} l_g & j_g & 1 \\ j_e & l_g + 1 & 1 \end{Bmatrix} \Bigg], \end{aligned} \tag{C.7}$$

which can be further simplified to yield

$$\begin{aligned} D^{(q)} = & D_{eg} \sum_{j_e, m_g} (-1)^{j_e + j_g - m_g + l_g} \sqrt{(2j_g + 1)(2j_e + 1)} \begin{Bmatrix} l_g & j_g & 1 \\ j_e & l_g + 1 & 1 \end{Bmatrix} \\ & \times \Bigg[|j_e, m_g + q, l_g + 1\rangle\langle j_g, m_g, l_g| \, (-1)^{q-1} \begin{pmatrix} j_e & 1 & j_g \\ -m_g - q & q & m_g \end{pmatrix} \\ & - |j_g, m_g, l_g\rangle\langle j_e, m_g - q, l_g + 1| \begin{pmatrix} j_g & 1 & j_e \\ -m_g & q & m_g - q \end{pmatrix} \Bigg], \end{aligned} \tag{C.8}$$

or

$$D^{(q)} = D_{eg}(\mathcal{L}_+^{(q)} - \mathcal{L}_-^{(q)}), \tag{C.9}$$

where the D_{eg} is the reduced dipole matrix element, given by

$$D_{eg} \equiv \langle l_e \| D \| l_g \rangle = - \langle l_g \| D \| l_e \rangle , \tag{C.10}$$

and the raising and lowering operators are defined as

$$\mathcal{L}_{+}^{(q)} \equiv \sum_{j_e,m_g} |j_e, m_g+q, l_g+1\rangle\langle j_g, m_g, l_g|$$
$$\times (-1)^{j_e+j_g-m_g+l_g-q+1}\sqrt{(2j_g+1)(2j_e+1)}\begin{pmatrix} j_e & 1 & j_g \\ -m_g-q & q & m_g\end{pmatrix}\begin{Bmatrix} l_g+1 & j_e & 1 \\ j_g & l_g & 1\end{Bmatrix},$$
$$\mathcal{L}_{-}^{(q)} \equiv \sum_{j_e,m_g} |j_g, m_g, l_g\rangle\langle j_e, m_g-q, l_g+1|$$
$$\times (-1)^{j_e+j_g-m_g+l_g}\sqrt{(2j_g+1)(2j_e+1)}\begin{pmatrix} j_g & 1 & j_e \\ -m_g & q & m_g-q\end{pmatrix}\begin{Bmatrix} l_g & j_g & 1 \\ j_e & l_g+1 & 1\end{Bmatrix}. \tag{C.11}$$

Note that $(\mathcal{L}_{\pm}^{(q)})^{\dagger} = \mathcal{L}_{\mp}^{(-q)}$, as can be seen for the raising operator:

$$
\begin{aligned}
(\mathcal{L}_{+}^{(q)})^{\dagger} &= \sum_{j_e,m_g} |j_g, m_g, l_g\rangle\langle j_e, m_g+q, l_g+1| \\
&\quad \times (-1)^{j_e+j_g-m_g+l_g-q+1}\sqrt{(2j_g+1)(2j_e+1)}
\begin{pmatrix} j_e & 1 & j_g \\ -m_g-q & q & m_g \end{pmatrix}
\begin{Bmatrix} l_g+1 & j_e & 1 \\ j_g & l_g & 1 \end{Bmatrix}, \\
&= \sum_{j_e,m_g} |j_g, m_g, l_g\rangle\langle j_e, m_g+q, l_g+1| \\
&\quad \times (-1)^{j_e+j_g-m_g+l_g-q+1}\sqrt{(2j_g+1)(2j_e+1)}
\begin{pmatrix} j_e & 1 & j_g \\ -m_g-q & q & m_g \end{pmatrix}
\begin{Bmatrix} j_e & l_g+1 & 1 \\ l_g & j_g & 1 \end{Bmatrix}, \\
&= \sum_{j_e,m_g} |j_g, m_g, l_g\rangle\langle j_e, m_g+q, l_g+1| \\
&\quad \times (-1)^{j_e+j_g-m_g+l_g-q+1}\sqrt{(2j_g+1)(2j_e+1)}
\begin{pmatrix} j_e & 1 & j_g \\ -m_g-q & q & m_g \end{pmatrix}
\begin{Bmatrix} l_g & j_g & 1 \\ j_e & l_g+1 & 1 \end{Bmatrix}, \\
&= \sum_{j_e,m_g} |j_g, m_g, l_g\rangle\langle j_e, m_g+q, l_g+1| \, (-1)^{j_e+1+j_g} \\
&\quad \times (-1)^{j_e+j_g-m_g+l_g-q+1}\sqrt{(2j_g+1)(2j_e+1)}
\begin{pmatrix} j_g & 1 & j_e \\ m_g & q & -m_g-q \end{pmatrix}
\begin{Bmatrix} l_g & j_g & 1 \\ j_e & l_g+1 & 1 \end{Bmatrix}, \\
&= \sum_{j_e,m_g} |j_g, m_g, l_g\rangle\langle j_e, m_g+q, l_g+1| \, (-1)^{2(j_e+1+j_g)}(-1)^{-q+1} \\
&\quad \times (-1)^{j_e+j_g-m_g+l_g}\sqrt{(2j_g+1)(2j_e+1)}
\begin{pmatrix} j_g & 1 & j_e \\ -m_g & -q & m_g+q \end{pmatrix}
\begin{Bmatrix} l_g & j_g & 1 \\ j_e & l_g+1 & 1 \end{Bmatrix}, \\
&= \mathcal{L}_{+}^{(-q)},
\end{aligned}
\tag{C.12}
$$

where the fact that $(-1)^{2(j_e+1+j_g)} = 1$ and that $(-1)^{-q+1} = 1$ for $q = \pm 1$ has been used. The procedure for the lowering operator is similar.

Equation (C.5), written in terms of raising and lowering operators, becomes

$$V(t) = D_{eg}\Big[\mathcal{E}_0\left(\mathcal{L}_+^{(+1)} - \mathcal{L}_-^{(+1)}\right)e^{-i(\omega_L t - k_L z)} + \mathcal{E}_0'\left(\mathcal{L}_+^{(-1)} - \mathcal{L}_-^{(-1)}\right)e^{-i(\omega_L t + k_L z)} - \mathcal{E}_0\left(\mathcal{L}_+^{(-1)} - \mathcal{L}_-^{(-1)}\right)e^{i(\omega_L t - k_L z)} - \mathcal{E}_0'\left(\mathcal{L}_+^{(+1)} - \mathcal{L}_-^{(+1)}\right)e^{i(\omega_L t + k_L z)}\Big]. \tag{C.13}$$

In this form, the rotating wave approximation can easily be made by removing terms of the form $\mathcal{L}_\pm^{(q)} e^{\pm\omega_L t}$, and keeping only terms of the form $\mathcal{L}_\pm^{(q)} e^{\mp i\omega_L t}$. The resulting expression for the interaction is

$$V = D_{eg}[\mathcal{E}_0\mathcal{L}_+^{(+1)}e^{-i(\omega_L t - k_L z)} + \mathcal{E}_0'\mathcal{L}_+^{(-1)}e^{-i(\omega_L t + k_L z)} + \mathcal{E}_0\mathcal{L}_-^{(-1)}e^{i(\omega_L t - k_L z)} + \mathcal{E}_0'\mathcal{L}_-^{(+1)}e^{i(\omega_L t + k_L z)}], \tag{C.14}$$

or, if $\mathcal{E}_0 = \mathcal{E}_0'$,

$$V = \frac{\hbar\Omega}{2}\left[\mathcal{L}_+^{(+1)}e^{-i(\omega_L t - k_L z)} + \mathcal{L}_+^{(-1)}e^{-i(\omega_L t + k_L z)} + \mathcal{L}_-^{(-1)}e^{i(\omega_L t - k_L z)} + \mathcal{L}_-^{(+1)}e^{i(\omega_L t + k_L z)}\right], \tag{C.15}$$

where $\Omega \equiv 2D_{eg}\mathcal{E}_0/\hbar$ is the reduced Rabi frequency.

C.1.2 Transformation to moving, rotating frame

C.1.2.1 General properties of time-dependent transformations

For a Hamiltonian H, the equation of motion is given by

$$i\hbar\dot{\rho} = [H, \rho]\,. \tag{C.16}$$

The goal is to find the equation of motion in some other coordinate system, with a time-dependent transformation given by $T(t)$. The density operator in the new coordinate system is given by

$$\tilde{\rho} = T(t)\rho T^\dagger(t), \tag{C.17}$$

which has a time derivative of

$$\begin{aligned} i\hbar\dot{\tilde{\rho}} &= i\hbar\frac{d}{dt}\left(T\rho T^\dagger\right) \\ &= i\hbar T\dot{\rho}T^\dagger + i\hbar\frac{dT}{dt}\rho T^\dagger + i\hbar T\rho\frac{dT^\dagger}{dt} \\ &= i\hbar T\dot{\rho}T^\dagger - [H,T]\,\rho T^\dagger - T\rho\left[H,T^\dagger\right] \\ &= i\hbar T\dot{\rho}T^\dagger - [H,\tilde{\rho}] + \left[THT^\dagger,\tilde{\rho}\right]. \end{aligned} \tag{C.18}$$

The above result can then be used in Eq. (C.16) with a transformation applied,

$$i\hbar T\dot{\rho}T^\dagger = T\,[H,\rho]\,T^\dagger, \tag{C.19}$$

giving

$$i\hbar\dot{\tilde{\rho}} = \left[THT^\dagger,\tilde{\rho}\right] - [H,\tilde{\rho}] + T\,[H,\rho]\,T^\dagger. \tag{C.20}$$

The second two terms can be manipulated,

$$\begin{aligned} T\,[H,\rho]\,T^\dagger - [H,\tilde{\rho}] &= TH\rho T^\dagger - T\rho HT^\dagger - HT\rho T^\dagger + T\rho T^\dagger H \\ &= -T\rho\left[H,T^\dagger\right] - [H,T]\,\rho T^\dagger \\ &= i\hbar\left[T\rho\frac{dT^\dagger}{dt} + \frac{dT}{dt}\rho T^\dagger\right] \\ &= i\hbar\left[\tilde{\rho}T\frac{dT^\dagger}{dt} + \frac{dT}{dt}T^\dagger\tilde{\rho}\right], \end{aligned} \tag{C.21}$$

resulting in

$$i\hbar\dot{\tilde{\rho}} = \left[THT^\dagger,\tilde{\rho}\right] + i\hbar\left[\tilde{\rho}T\frac{dT^\dagger}{dt} + \frac{dT}{dt}T^\dagger\tilde{\rho}\right]. \tag{C.22}$$

Also, noting that

$$\begin{aligned} T\frac{dT^\dagger}{dt} &= T\left(-\frac{1}{i\hbar}\right)\left[H,T^\dagger\right] \\ &= -\frac{1}{i\hbar}\left(THT^\dagger - H\right) \\ &= \frac{1}{i\hbar}\left(H - THT^\dagger\right) \\ &= \frac{1}{i\hbar}\,[H,T]\,T^\dagger \\ &= -\frac{dT}{dt}T^\dagger, \end{aligned} \tag{C.23}$$

yields

$$\begin{aligned} i\hbar\dot{\tilde{\rho}} &= \left[THT^{\dagger}, \tilde{\rho}\right] + i\hbar\left[\frac{T^{\dagger}}{dt}T\tilde{\rho} - \tilde{\rho}\frac{dT}{dt}T^{\dagger}\right] \\ &= \left[THT^{\dagger}, \tilde{\rho}\right] + \left[i\hbar\frac{dT}{dt}T^{\dagger}, \tilde{\rho}\right], \end{aligned} \tag{C.24}$$

or

$$i\hbar\dot{\tilde{\rho}} = \left[\tilde{H}, \tilde{\rho}\right], \tag{C.25}$$

$$\tilde{H} \equiv THT^{\dagger} + i\hbar\frac{dT}{dt}T^{\dagger}. \tag{C.26}$$

C.1.2.2 Application to an atom in the $\sigma_+\sigma_-$ laser configuration

Since the coupling of the atom to the vacuum field is being ignored for the time being, the total Hamiltonian is

$$H = H_0 + V(t), \tag{C.27}$$

where H_0 is the internal atomic Hamiltonian and $V(t)$ represents the interaction between the atom and the coherent external laser field. If the transformation to the center-of-mass frame of an atom moving with velocity v is made, z must be replaced with vt. In this moving frame, the interaction term is of the form

$$V(t) \sim \mathbf{d} \cdot \hat{\epsilon}_y = d_x \sin kvt + d_y \cos kvt. \tag{C.28}$$

It is useful to transform to a rotating coordinate system in order to simplify the interaction term. Consider a transformation operator given by

$$T(t) = \exp(-ikvtJ_z/\hbar). \tag{C.29}$$

Using the commutation relations $[J_z, d_x] = i\hbar d_y$ and $[J_z, d_y] = -i\hbar d_x$, the transformed interaction operator takes the simplified form

$$\tilde{V}(t) = T(t)\left[d_x \sin kvt + d_y \cos kvt\right]T^{\dagger}(t) = d_y. \tag{C.30}$$

The time-independent form of the interaction operator in the rotating frame allows steady-state solutions to be obtained when working in this reference frame. With the results of the previous section, the equation of motion is

$$i\hbar\dot{\tilde{\rho}} = \left[\tilde{H}, \tilde{\rho}\right]. \tag{C.31}$$

The inertial term in Eq. (C.26), with the transformation operator given in Eq. (C.29), becomes

$$i\hbar\frac{dT}{dt}T^{\dagger} = kvJ_z, \tag{C.32}$$

and so

$$\tilde{H} = H_0 + kvJ_z + \tilde{V}(t), \tag{C.33}$$

since H_0 commutes with J_z. In the rotating frame, the interaction operator from Eq. (C.15) becomes

$$\begin{aligned}\tilde{V}(t) &= \frac{\hbar\Omega}{2}T(t)\Big[\mathcal{L}_{+}^{(+1)}e^{-i(\omega_L t - k_L z)} + \mathcal{L}_{+}^{(-1)}e^{-i(\omega_L t + k_L z)} \\ &\qquad + \mathcal{L}_{-}^{(-1)}e^{i(\omega_L t - k_L z)} + \mathcal{L}_{-}^{(+1)}e^{i(\omega_L t + k_L z)}\Big]T^{\dagger}(t) \\ &= \frac{\hbar\Omega}{2}\Big[\mathcal{L}_{+}^{(+1)}e^{-i(\omega_L t + k_L v t - k_L z)} + \mathcal{L}_{+}^{(-1)}e^{-i(\omega_L t - k_L v t + k_L z)} \\ &\qquad + \mathcal{L}_{-}^{(-1)}e^{i(\omega_L t + k_L v t - k_L z)} + \mathcal{L}_{-}^{(+1)}e^{i(\omega_L t - k_L v t + k_L z)}\Big].\end{aligned} \tag{C.34}$$

Here it is useful to compare to the form of the interaction term obtained by Cohen-Tannoudji and Dalibard [16], in which cooling is performed on a $J = 1$ ground state (with sublevels $|g_i\rangle$) and a $J = 2$ excited state (with sublevels $|e_i\rangle$). For this situation, Eq. (C.34) becomes

$$\begin{aligned}\tilde{V}(t) = \frac{\hbar\Omega}{2\sqrt{3}}\Bigg[&\left(|e_{+2}\rangle\langle g_{+1}| + \frac{1}{\sqrt{2}}|e_{+1}\rangle\langle g_0| + \frac{1}{\sqrt{6}}|e_0\rangle\langle g_{-1}|\right)e^{-i(\omega_L t + k_L v t - k_L z)} \\ &+ \left(|e_{-2}\rangle\langle g_{-1}| + \frac{1}{\sqrt{2}}|e_{-1}\rangle\langle g_0| + \frac{1}{\sqrt{6}}|e_0\rangle\langle g_{+1}|\right)e^{-i(\omega_L t - k_L v t + k_L z)} \\ &+ \left(|g_{+1}\rangle\langle e_{+2}| + \frac{1}{\sqrt{2}}|g_0\rangle\langle e_{+1}| + \frac{1}{\sqrt{6}}|g_{-1}\rangle\langle e_0|\right)e^{i(\omega_L t + k_L v t - k_L z)} \\ &+ \left(|g_{-1}\rangle\langle e_{-2}| + \frac{1}{\sqrt{2}}|g_0\rangle\langle e_{-1}| + \frac{1}{\sqrt{6}}|g_{+1}\rangle\langle e_0|\right)e^{i(\omega_L t - k_L v t + k_L z)}\Bigg],\end{aligned} \tag{C.35}$$

or, in the notation of Cohen-Tannoudji and Dalibard,

$$\begin{aligned}\tilde{V}(t) =& \frac{\hbar\Omega}{2\sqrt{3}}\left[|g_{+1}\rangle\langle e_{+2}| + \frac{1}{\sqrt{2}}|g_0\rangle\langle e_{+1}| + \frac{1}{\sqrt{6}}|g_{-1}\rangle\langle e_0|\right]e^{i(\omega_+ - k_L z)} + \text{h.c} \\ &+ \frac{\hbar\Omega}{2\sqrt{3}}\left[|g_{-1}\rangle\langle e_{-2}| + \frac{1}{\sqrt{2}}|g_0\rangle\langle e_{-1}| + \frac{1}{\sqrt{6}}|g_{+1}\rangle\langle e_0|\right]e^{i(\omega_- + k_L z)} + \text{h.c},\end{aligned} \tag{C.36}$$

where

$$\omega\pm = \omega_L \pm k_L v. \tag{C.37}$$

From Eq. (C.36), it appears that Eq. (5.1) of Ref. [16] is missing a factor of $1/\sqrt{3}$ and the $\omega_\pm$ should be reversed. Furthermore, Eq. (5.1) of Ref. [16] is misleading because the transformation to the moving frame has not been made. In applying this transformation ($z \to vt$) to my Eq. (C.34), the velocity terms in the exponentials cancel exactly, resulting in

$$\tilde{V}(t) = \frac{\hbar\Omega}{2}\left[\mathcal{L}_+^{(+1)}e^{-i\omega_L t} + \mathcal{L}_+^{(-1)}e^{-i\omega_L t} + \mathcal{L}_-^{(-1)}e^{i\omega_L t} + \mathcal{L}_-^{(+1)}e^{i\omega_L t}\right]. \tag{C.38}$$

C.2 Optical Bloch equations

The equations of motion developed up to this point can now be extended to include spontaneous emission. The form of the spontaneous-emission relaxation operator is derived in detail in Appending B and the results will be used here, with the center-of-mass degree of freedom neglected due to the semiclassical nature of the current equations. There will be three classes of equations:

$$i\hbar\dot{\tilde{\rho}}\left(e_i^{(m)}, g_j\right) = \left[\tilde{H}, \tilde{\rho}\right]_{\left(e_i^{(m)}, g_j\right)}, \tag{C.39}$$

$$i\hbar\dot{\tilde{\rho}}\left(g_i, g_j\right) = \left[\tilde{H}, \tilde{\rho}\right]_{(g_i, g_j)}, \tag{C.40}$$

$$i\hbar\dot{\tilde{\rho}}\left(e_i^{(m)}, e_j^{(n)}\right) = \left[\tilde{H}, \tilde{\rho}\right]_{\left(e_i^{(m)}, e_j^{(n)}\right)}. \tag{C.41}$$

The first class describes optical coherences, the second describes ground-state populations and ground-state coherences, and the third describes excited-state populations and excited-state coherences.

C.2.1 Class I: optical coherences

Redefining the density matrix elements corresponding to optical coherences as

$$\tilde{\rho}\left(e_i^{(m)}, g_j\right) \rightarrow \tilde{\rho}\left(e_i^{(m)}, g_j\right) e^{i\omega_L t}, \tag{C.42}$$

$$\tilde{\rho}\left(g_i, e_j^{(m)}\right) \rightarrow \tilde{\rho}\left(g_i, e_j^{(m)}\right) e^{-i\omega_L t}. \tag{C.43}$$

All other elements are unchanged. This results in a change to the optical-coherence equations of motion of

$$\dot{\tilde{\rho}}\left(e_i^{(m)}, g_j\right) = i\omega_L \tilde{\rho}\left(e_i^{(m)}, g_j\right) + \dot{\tilde{\rho}}^{(\text{old})}\left(e_i^{(m)}, g_j\right) e^{i\omega_L t}, \tag{C.44}$$

$$\dot{\tilde{\rho}}\left(g_i, e_j^{(m)}\right) = -i\omega_L \tilde{\rho}\left(g_i, e_j^{(m)}\right) + \dot{\tilde{\rho}}^{(\text{old})}\left(g_i, e_j^{(m)}\right) e^{-i\omega_L t}. \tag{C.45}$$

$$\begin{aligned}
\dot{\tilde{\rho}}\left(e_i^{(m)}, g_j\right) &= i\omega_L \tilde{\rho}\left(e_i^{(m)}, g_j\right) - \frac{i}{\hbar} e^{i\omega_L t}\left[H_0 + k_L v J_z + \tilde{V}, \tilde{\rho}\right]_{\left(e_i^{(m)}, g_j\right)} \\
&= i\left[\omega_L - \omega_{e^{(m)}} + \omega_g - k_L v(i-j)\right]\tilde{\rho}\left(e_i^{(m)}, g_j\right) - \frac{i}{\hbar} e^{i\omega_L t}\left[\tilde{V}, \tilde{\rho}\right]_{\left(e_i^{(m)}, g_j\right)} \\
&= i\left[\delta\omega^{(m)} - \Delta - k_L v(i-j)\right]\tilde{\rho}\left(e_j^{(m)}, g_i\right) - \frac{i}{\hbar} e^{i\omega_L t}\left[\tilde{V}, \tilde{\rho}\right]_{\left(e_i^{(m)}, g_j\right)}.
\end{aligned} \tag{C.46}$$

$$\begin{aligned}
\dot{\tilde{\rho}}\left(g_i, e_j^{(m)}\right) &= -i\omega_L \tilde{\rho}\left(g_i, e_j^{(m)}\right) - \frac{i}{\hbar} e^{-i\omega_L t}\left[H_0 + k_L v J_z + \tilde{V}, \tilde{\rho}\right]_{\left(g_i, e_j^{(m)}\right)} \\
&= i\left[-\omega_L - \omega_g + \omega_{e^{(m)}} - k_L v(i-j)\right]\tilde{\rho}\left(g_i, e_j^{(m)}\right) - \frac{i}{\hbar} e^{-i\omega_L t}\left[\tilde{V}, \tilde{\rho}\right]_{\left(g_i, e_j^{(m)}\right)} \\
&= i\left[\Delta - \delta\omega^{(m)} - k_L v(i-j)\right]\tilde{\rho}\left(g_i, e_j^{(m)}\right) - \frac{i}{\hbar} e^{-i\omega_L t}\left[\tilde{V}, \tilde{\rho}\right]_{\left(g_i, e_j^{(m)}\right)}.
\end{aligned} \tag{C.47}$$

$$
\begin{aligned}
e^{i\omega_L t}\left[\tilde{V},\tilde{\rho}\right]_{(e_i^{(m)},g_j)} &= e^{i\omega_L t}\left[\left\langle e_i^{(m)}\right|\tilde{V}\tilde{\rho}\left|g_j\right\rangle - \left\langle e_i^{(m)}\right|\tilde{\rho}\tilde{V}\left|g_j\right\rangle\right] \\
&= \frac{\hbar\Omega}{2}e^{i\omega_L t}\Bigg[\left\langle e_i^{(m)}\right|\mathcal{L}_+^{(+1)}e^{-i\omega_L t}\tilde{\rho}\left|g_j\right\rangle + \left\langle e_i^{(m)}\right|\mathcal{L}_+^{(-1)}e^{-i\omega_L t}\tilde{\rho}\left|g_j\right\rangle \\
&\qquad - \left\langle e_i^{(m)}\right|\tilde{\rho}\mathcal{L}_+^{(+1)}e^{-i\omega_L t}\left|g_j\right\rangle - \left\langle e_i^{(m)}\right|\tilde{\rho}\mathcal{L}_+^{(-1)}e^{-i\omega_L t}\left|g_j\right\rangle\Bigg] \\
&= \frac{\hbar\Omega}{2}\Bigg[\left\langle e_i^{(m)}\right|\mathcal{L}_+^{(+1)}\tilde{\rho}\left|g_j\right\rangle + \left\langle e_i^{(m)}\right|\mathcal{L}_+^{(-1)}\tilde{\rho}\left|g_j\right\rangle \\
&\qquad - \left\langle e_i^{(m)}\right|\tilde{\rho}\mathcal{L}_+^{(+1)}\left|g_j\right\rangle - \left\langle e_i^{(m)}\right|\tilde{\rho}\mathcal{L}_+^{(-1)}\left|g_j\right\rangle\Bigg].
\end{aligned}
\tag{C.48}
$$

The raising operators in the four matrix elements above will produce terms of the form $\langle g_i|\tilde{\rho}|g_j\rangle$ and $\langle e_i|\tilde{\rho}|e_j\rangle$, both of which are not redefined according to Eqs. (C.42) and (C.43). Similarly, in the equation of motion for $\dot{\tilde{\rho}}(g_i, e_j^{(m)})$, an exponential of $e^{-i\omega_L t}$ will multiply the interaction commutator, and this time will cancel the $e^{i\omega_L t}$ exponentials in the lowering operator portions of the interaction operator.

At this point, further confirmation can be made of the error in Ref. [16]. E.g., if Eq. (C.46) is used to determine the coefficient of $\tilde{\rho}\,(g_0, g_0)$ in the equation of motion for $\dot{\tilde{\rho}}\,(e_1, g_0)$, one finds that Cohen-Tannoudji and Dalibard's result differs by lacking a factor of $1/\sqrt{3}$, as we noted before. Using the paper by Bambini and Agresti (Ref. [43]), Eq. (2.8b), agreement with my result is found. (Note: Bambini and Agresti define their reduced dipole matrix element as $\langle l_g\|d\|l_e\rangle$, which differs from mine by a sign.)

C.2.2 Class II: ground-state populations and ground-state coherences

$$
\dot{\tilde{\rho}}\,(g_i, g_j) = -ik_L v(i-j)\tilde{\rho}\,(g_i, g_j) - \frac{i}{\hbar}\left[\tilde{V},\tilde{\rho}\right]_{(g_i,g_j)}. \tag{C.49}
$$

C.2.3 Class III: excited-state populations and excited-state coherences

$$\begin{aligned}\dot{\tilde{\rho}}\left(e_i^{(m)}, e_j^{(n)}\right) &= i\left[\omega_{e^{(n)}} - \omega_{e^{(m)}} - k_L v(i-j)\right]\tilde{\rho}\left(e_i^{(m)}, e_j^{(n)}\right) - \frac{i}{\hbar}\left[\tilde{V}, \tilde{\rho}\right]_{\left(e_i^{(m)}, e_j^{(n)}\right)} \\ &= i\left[\delta\omega^{(m)} - \delta\omega^{(n)} - k_L v(i-j)\right]\tilde{\rho}\left(e_i^{(m)}, e_j^{(n)}\right) - \frac{i}{\hbar}\left[\tilde{V}, \tilde{\rho}\right]_{\left(e_i^{(m)}, e_j^{(n)}\right)}.\end{aligned} \tag{C.50}$$